

# **AALTO UNIVERSITY**

School of Engineering

Department of Civil and Structural Engineering

Structural Engineering

**Andreas Limnell**

## **A COLD-FORMED STEEL ELEMENT AS A ROOF OF A POWER PLANT IN ARCTIC CLIMATE.**

Thesis submitted in partial fulfilment of the requirements for the degree of Master  
of Science in Engineering,  
Espoo November 30<sup>th</sup> 2015

Supervisor: Professor Jari Puttonen, Aalto University

Instructor: Wei Lu, D. Sc. (Tech.), Aalto University  
Kaj Grön, M. Sc. (Eng.), Citec Oy



---

<b>Author</b> Andreas Linnell		
<b>Title of thesis</b> A cold-formed steel element as a roof of a power plant in arctic climate.		
<b>Department</b> Department of Civil and Structural Engineering		
<b>Professorship</b> Structural Engineering and Building Physics	<b>Professorship</b> RAK.thes	
<b>Thesis supervisor</b> Professor Jari Puttonen		
<b>Thesis advisor</b> Dr. Wei Lu (D. Sc.), Mr. Kaj Grön (M. Sc.)		
<b>Date</b> 30.11.2015	<b>Number of pages</b> 91+39	<b>Language</b> English

---

### **Abstract**

This Master Thesis is a development work on the roof structure used in Wärtsilä power plants. Wärtsilä uses conceptually orientated design and focuses on developing their products to improve their competitiveness.

The main objective was to develop a new roof element for Wärtsilä power plants in arctic climate. The roof element needs to fulfil the normal requirements of a roof structure for a power plant in several different countries, but also be fast, easy and cost efficient to assemble, both in the workshop and at site.

Secondary objective was to determine the maximum allowable characteristic loads for the roof elements of two different spans. This was done for different purlin thicknesses.

Focus was put on the structural capacity of light weight thermal steel purlins including experimental testing, analytical analysis and FEM-design. The initial FEM-results deviated a great deal from the experimental test results, which put focus on the analytical analysis.

The power plant is a working environment for several people, which sets acoustical requirements, while the arctic climate sets high thermal and moisture requirements on the element. These things are all analysed in thesis.

---

**Keywords** Structural, Engineering, Product, Development, Cold-formed steel, Roof, Element, Thermal, Arctic, Power plant, FEM, Distortional, Lateral, Torsional, Local, Buckling, EN 1993

---

---

**Tekijä** Andreas Limnell

---

**Työn nimi** Kylmämuovattu teräselementti voimalaitoksen kattorakenteeksi pohjoisissa olosuhteissa.

---

**Laitos** Rakennustekniikan laitos

---

**Professuuri** Talonrakennustekniikka

**Professuurikoodi** RAK.thes

---

**Työn valvoja** Professori Jari Puttonen

---

**Työn ohjaaja** Tekniikan tohtori Wei Lu, Diplomi-insinööri Kaj Grön

---

**Päivämäärä** 30.11.2015

**Sivumäärä** 91+39

**Kieli** Englanti

---

## Tiivistelmä

Tämä diplomityö käsittelee Wärtsilän voimalaitoksen kattorakenteen kehittelyä. Wärtsilä käyttää konseptiorientoitunutta suunnittelua keskittyään kehittämään tuotetta mahdollisimman pitkälle kilpailukyvyyn parantamiseksi.

Pää tavoite oli kehittää Wärtsilän voimalaitoksiin uusi kattoelementtityyppi, joka soveltuu pohjoisiin olosuhteisiin. Tämän kattoelementin pitää täyttää yleiset vaatimukset kattorakenteille voimalaitoksissa useissa eri maissa. Sen pitää myös olla nopea ja helppo asentaa, mutta myös sekä valmistuksen ja asennuksen suhteen kustannustehokas.

Toissijainen tavoite oli määrittää suurimmat sallittavat kuormat kyseisille kattoelementeille kahdelle eri jänneväleille ja kolmella eri profiilipaksuudella.

Tässä työssä keskityttiin ohut-uumaisten termo-orsien rakenteelliseen kestävyYTEEN sisältäen kokeelliset kuormitukset, analyttiset laskelmat ja FEM-analyysi. Ensimmäiset FEM-tulokset poikkesivat niin paljon kokeellisista tuloksista, joten pääpaino keskittyi analyttisiin laskelmiin.

Pohjoiset olosuhteet tuovat rakennusfysikaalisia vaatimuksia kattorakenteille ja voimalaitos on usealle ihmiselle työpaikka, joten siinä on tietyt ääniteknisii vaatimuksia. Nämä asiat ovat käsitelty tässä työssä.

---

**Avainsanat** Rakennetekniikka, Tuote, Kehitys, Kylmämuovattu, Teräs, Katto, Elementti, Lämpö, Voimalaitos, FEM, Lommahdus, Kiepahdus, Nurjahdus, EN 1993

---



---

**Författare** Andreas Limnell

---

**Arbetets titel** Ett kallformat stålelement som takkonstruktion för kraftverk i nordiska förhållanden. A cold-formed steel element as a roof of a power plant in arctic climate.

---

**Institution** Institutionen för byggteknologi

---

**Professur** Byggnads konstruktion

**Kod för professuren** RAK.thes

---

**Övervakare** Professor Jari Puttonen

---

**Handledare** Doktor Wei Lu, Diplomingenjör Kaj Grön

---

**Datum** 30.11.2015

**Sidantal** 91+39

**Språk** Engelska

---

## Sammandrag

Detta diplomarbete behandlar produktutvecklingen av en takkonstruktion för Wärtsiläs kraftverk. Wärtsilä använder konceptbaserad design som baserar sig på en långt utvecklad produkt för att öka konkurrenskraften.

Huvudmålet var att utveckla en ny typ av takelement för Wärtsiläs kraftverk som är anpassat för nordiska förhållanden. Detta innebär att takelementet måste uppfylla allmänna krav på takkonstruktioner i flera olika länder runt om i världen. Takelementet måste också vara snabbt och lätt att tillverka samt installera.

Sekundära målet var att bestämma de högsta tillåtna lasterna för denna takelement-typ för två olika spännvidder och tre olika profiltjocklekar.

Detta diplomarbete fokuserar på slitsade tunnplåtsreglars böjhallfasthet. Detta omfattar provtryckningar, analytiska uträkningar samt FEM-analys, med huvudvikt på provtryckningarna och de analytiska uträkningarna enligt Eurokoderna.

Byggnadsfysikaliska krav ställs även på takkonstruktioner för kraftverk. De nordiska förhållandena ställer fukttekniska krav på taket och kraftverket som arbetsmiljö ställer ljudtekniska krav. Dessa behandlas också i detta diplomarbete.

---

**Nyckelord** Byggnadsteknik, Produkt, Utveckling, Kallvalsad, Stål, Tak, Element, Värme, Kraftverk, FEM, Buckling, Vippning, Knäckning, EN 1993

---

## Preface

This Master's thesis has been ordered by Wärtsilä and has been a collaboration between Wärtsilä, Citec and Ruukki. I want to thank everyone involved in this project for all the help and guidance I've received.

This work has been a long process, as development projects usually are. When I was first presented with this opportunity back in 2012, I was much excited, as this was something I had some experience of from before and I also liked development work. It took a while before the project got up and running and before the final subject was locked and narrowed down, however it was interesting to follow the development.

Along the way there were a few bumps, which set me back in the schedule and I really had to get a deeper understanding of the difficulties involved with thin-walled structures and the dangers of trusting blindly on the output of a computer software. The experimental part was very educational for me and has helped understanding and interpreting the different types of buckling occurring in thin-walled structures. It also showed me that the final product is not always exactly as planned and this might have significant impact on the structural capacity of a structure.

I want to especially thank the following persons for their help and guidance along the way: Jari Puttonen, Wei Lu, Kaj Grön, Nicklas Holmqvist, Stefan Björkgren, Markus Sandås, Jyrki Kesti, Jani Matintupa, Simon Nyman, Arto Rokkanen, Jari Pitkänen, Jussi Pitkänen, Jukka Sammi, Arto Sivili, Juha Kutvonen and everyone at the Sheet Metal Centre at HAMK University of Applied Sciences who helped me with the experimental tests.

Last but not least I want to thank my lovely family for their understanding and support. I have spent a lot of time in the office, away from them, trying to get to this point, where I finally can consider it complete. Thanks to my wife and two children, my mother, father, brother and mother-in-law for their support and understanding.

Espoo November 30<sup>th</sup> 2015



Andreas Limnell

# Table of contents

Abstract.....	i
Tiivistelmä .....	ii
Sammandrag .....	iii
Preface .....	iv
Table of contents .....	v
Symbols .....	viii
Acronyms.....	ix
Definitions .....	x
1 Introduction .....	1
1.1 Objectives .....	1
1.2 Outline of the Thesis .....	1
2 Background of research .....	3
2.1 Wärtsilä power plants.....	3
2.1.1 Main frame .....	5
2.1.2 Roof structures for tropic climate .....	7
2.2 Development of a roof element for arctic climate .....	11
2.3 Design details, manufacturing, transportation and erection .....	17
2.3.1 Product description .....	17
2.3.2 Design process.....	19
2.3.3 Manufacturing process .....	20
2.3.4 Manufacturing tolerances .....	22
2.3.5 Transportation.....	23
2.3.6 Site erection .....	24
3 Structural theory and design codes .....	26
3.1 Failure modes for thin-walled beams .....	26
3.2 Failure modes of slotted member in bending .....	29
4 Experimental studies .....	31
4.1 Introduction.....	31
4.1.1 Objectives .....	32
4.1.2 Primary FEM-model .....	32
4.1.3 Primary FEM analysis and observations .....	33
4.2 Test programme .....	35
4.3 Test specimens .....	37

4.3.1	Deviations and imperfections .....	38
4.4	Set-up of test apparatuses and testing procedures.....	43
4.5	Test results .....	48
4.5.1	Load capacities .....	48
4.5.2	Deformation and failure modes .....	48
4.5.3	Displacements and strains measured.....	54
4.6	Discussion of test results .....	58
4.6.1	Effects of deviations and imperfections .....	58
4.6.2	Rotational stiffness of top flange joint .....	58
4.6.3	Local buckling .....	61
4.6.4	Distortional buckling and local transverse load.....	61
4.6.5	Lateral-torsional buckling .....	61
4.6.6	Shear forces at support .....	63
4.6.7	Discussion of failure modes .....	63
4.7	Conclusions of the test.....	65
5	Structural capacity .....	66
5.1	Boundary conditions and assumptions .....	68
5.2	Calculations according to EN 1993.....	69
5.2.1	Section parameters of LPT-C250x50x1.2 .....	69
5.2.2	Spring stiffness of web .....	70
5.2.3	Effective cross-section parameters.....	72
5.2.4	Support reactions .....	74
5.2.5	Fire resistance .....	75
5.2.6	Discussion and comparison of calculated and test results.....	76
5.3	Optimization for projects.....	77
6	Building physical properties.....	78
6.1	Boundary conditions.....	79
6.2	Thermal properties .....	80
6.3	Moisture analysis .....	84
6.4	Acoustic properties.....	86
7	Conclusions and discussions .....	88
7.1	Further studies.....	89
	References.....	90

## Appendices

- Appendix 1     Analytical calculations of section properties of LPT-C250x50x15x1.2, S350GD+Z according to EN 1993-1-3:2006 /AC:2009. 11 pages
- Appendix 2     Local transverse force calculations according to EN 1993-1-3:2006 /AC:2009. For thin-walled cross-sections with a single web. 6 pages
- Appendix 3     Insulation thickness for fire resistance - Standard fire. 2 pages
- Appendix 4     Manufacturing details & drawings for experimental test. 16 pages

# Symbols

## *Latin upper case letters*

$E_d$	Dimensional load
$F$	Point load
$G$	dead load
$K$	spring stiffness for displacement
$M_{y,Rd}$	bending moment capacity around y-axis
$Q_k$	Characteristic load
$R_k$	Load bearing capacity

## *Latin lower case letters*

$e$	eccentricity
$m$	mass
$q_k$	characteristic line load
$u$	unit load
$t$	thickness

## *Greek lower case letters*

$\delta$	deflection
$\varepsilon$	strain
$\sigma$	stress
$\chi_d$	reduction factor for the distortional buckling resistance

## Acronyms

ARE	Arctic roof element
BIM	Building Information Model
CAD	Computer Aided Design
FEM	Finite Element Method
HAMK	Hämeen ammattikorkeakoulu
LPT	Lightweight thermal purlin
LTB	Lateral torsional buckling
MD	Manufacturing detail
TS	Tekla Structures,

## Definitions

Cassette	Is a thin-walled steel section with two webs, connected by a wide bottom flange. Also referred to as linear tray in some literature.
Dividing beams	Beams that are used in the experimental testing to spread the load on the test specimen.
Eurocodes	The Structural Eurocode programme, which consists of several parts and are harmonized technical rules for the structural design of construction works in the European Union.
Linear tray	See cassette.
Thermal slots	Several intermitted rows of holes that increases the thermal resistance of a steel purlin.



# 1 Introduction

This Master's Thesis focuses on a specific type of roof element used for multi-fuel power plants, such as oil and gas engine halls with a steel frame, external roof trusses and radiators above the roof structure. It is developed for arctic weather conditions, and this has set specific building physical requirements on the structure. There is an existing product that is used for similar power plants, but in tropic climate conditions, which is not as such suitable for arctic conditions.

Since 2009 the customer Wärtsilä, has used prefabricated roof elements made out of cold-formed thin-walled steel as their main type of roof structure. These roof elements have proven to be better than the prior roof structure built on site. In arctic climates the roof structure is still usually built on site, as the roof element for tropic climate conditions is not suitable for arctic conditions.

The roof elements that are used in tropical climates have a perforated steel sheet on the lower surface with insulation mainly for acoustical purpose, but for arctic climates there is a need for a vapour barrier and more thermal insulation. There are also other types of loads on the roof elements depending on the climate.

Wärtsilä has developed roof elements to save manufacturing time and cut costs. The product is used in several power plants over the world in tropic climates. Now they want to have a product which can be used in arctic climates as well.

## 1.1 Objectives

The primary objective of this thesis is to help develop a fully functional roof element for power plants in arctic climate conditions. This includes reassuring the structural integrity, building physical properties that are suited for the climate and making sure the roof element is possible to manufacture and erect.

## 1.2 Outline of the Thesis

The scope of this work includes technical solutions, such as support principal and other changes needed due to the change in climate, but not other detailed design. The basic functionality has been taken into account, so that the product will be fully functional and all critical requirements are met. In an arctic environment both thermal conductivity and moisture analysis are required. The acoustical environment in an engine hall is also challenging, and is considered as well.

The main focus is put the structural part, as this is one of the most critical things. If the structural capacity is exceeded, it may have heavy consequences. Due to the arctic climate, the web of the section is thermally slotted, to increase thermal resistance. The thermally slotted main purlins are very prone to local, distortional and global buckling as the stiffness of the thin web is reduced. This is why experimental tests and thorough analytical analysis were done. Finite element method calculations have also been used

to some degree to determine the structural capacity and primary FEM-analysis were done to assist the experimental testing.

This thesis will not focus on any other roofs of buildings or connecting buildings that may be present at a power plant site. It is only the roof of the engine hall of the power plant, where these specific requirements and boundary conditions are present. Material costs are not compared, but material optimization and manufacturing aspects are considered to provide a cost-efficient solution.

To begin with, some light will be shed on what a multi-fuel power plant may look like and what buildings you may find on site. You will also get an understanding of why the roof structure is done as it is today and how it has been done earlier. This you can read about in Chapter 2. In Chapter 3 the theory behind the structural behaviour of the roof element and the design code used is presented. The experimental studies are presented and the results analysed in Chapter 4. The structural analysis is presented in Chapter 5.

Chapter 6 focuses on building physics presenting specific boundary conditions, which are typical for a power plant in arctic weather conditions are presented. The thermal properties of the roof element will be examined and also the moisture properties will be taken into account. In power plants the acoustical environment is always challenging, and this is also investigated in the end of this chapter. Last but not least some conclusions are presented and a summary of what the results of this work has added up to.

## 2 Background of research

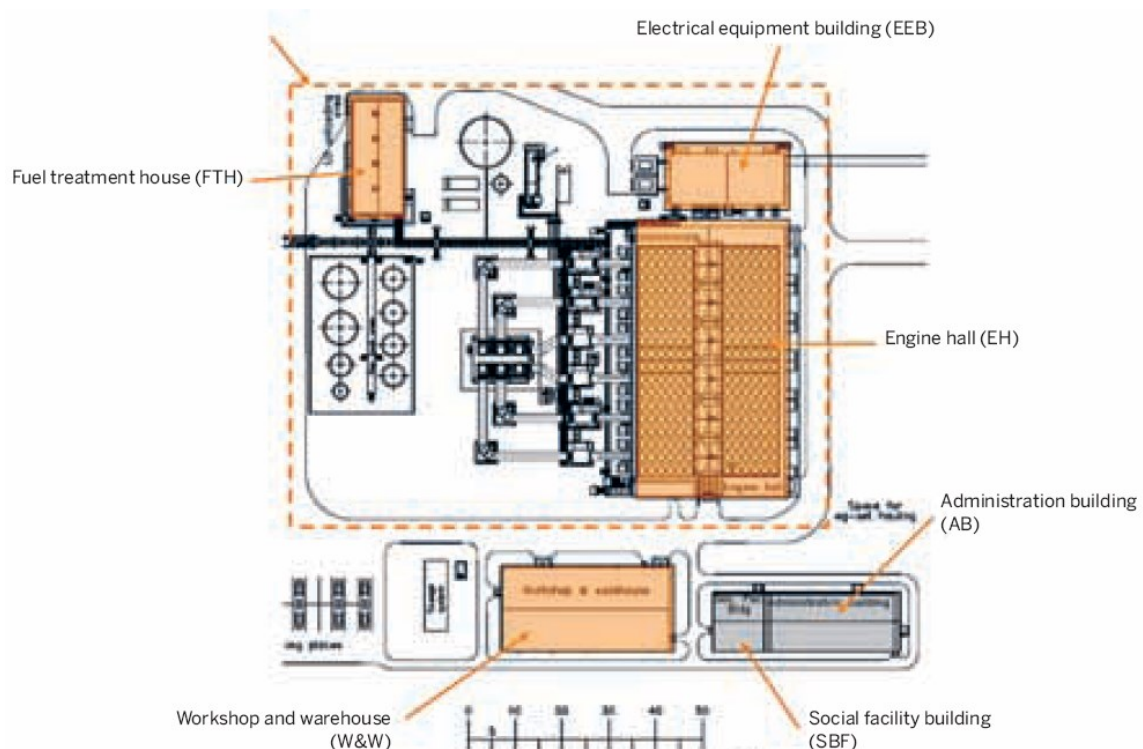
In this chapter the basics of a Wärtsilä power plant and the background of the roof structure used in Wärtsilä power plants is explained. Both the development work, which has been done before this thesis, as well as the development, which has continued as a part of this thesis is all included in this chapter.

It is clear that some projects may be very different from what is described here, but we will take a look at the common solutions and situations that can be expected of the structure in most cases.

### 2.1 Wärtsilä power plants

Wärtsilä is a supplier of multi-fuel power plants. A power plant consists of several separate or combined buildings, each serving a purpose. These are all located near each other on the same premises, which is referred to as a site. On a site you usually find one or several engine halls and several other buildings. There is usually a fuel treatment house, electrical equipment building, administration building and workshop & warehouse besides the engine hall as shown in Figure 2-1. Sometimes there might be other buildings as well or there might be existing facilities, which may replace some of these buildings. (Wärtsilä Corporation, 2014)

What people normally think of, when talking of a power plant is the engine hall. This is where the resource is transformed from one form of energy to another. In this case from oil or gas to kinetic energy and then the kinetic energy is generated into electricity. The effect of these power plants ranges from 2 MW to 700 MW and above. The effect of the power plant depends on the amount of engines located in the engine hall and the type of engines used.



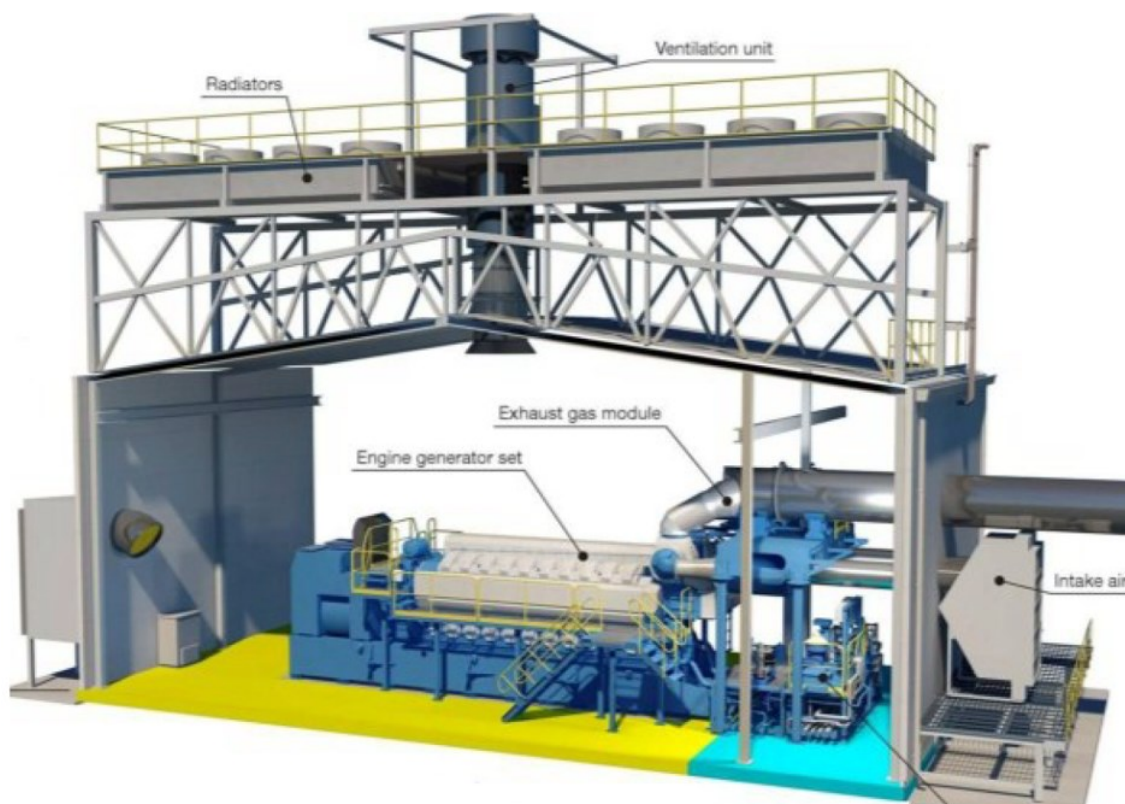
**Figure 2-1.** Site layout example of a 6 x 20V46F power plant solution. (Lindqvist, et al., 2009)

There are four standard engine types with different size. The engine type defines the standard module lengths, which is the spacing between the main frames, used in the engine hall or halls. The number of engines may vary from one to several dozen and each module contains one engine and other auxiliary equipment as shown in Figure 2-2.

Wärtsilä uses standardized design to maximize efficiency and lower costs. This means that everything that can be, should be standardized. The same types of units, parts and equipment can be used in the same type of power plants again and again, with only minor changes to suite the specific project and location. This saves design time and makes it easier to serve, when the same solutions are used in several power plants.

A key concept which Wärtsilä has strongly implemented on many of today's power plants, is placing the radiators on the roof as shown in Figure 2-2. This is something which has several advantages. The air flow to the radiators is always optimal, regardless of wind direction and they do not require any additional support structure, as the roof truss is modified to support the radiators at the top chord. The roof elements are supported at the bottom chord of the roof truss. (Lindqvist, et al., 2009)

Typical spacing's between roof trusses are 5.4 m and 7.2 m, although others are also used in some projects. Spacing's up to 8.2 m have also been used with the 46F-engine type, but these types of power plants are no longer that common. This is why focus will be put on two spacing's: 5.4 m and 7.2 m. Table 2-1 shows the typical spans for each engine type.



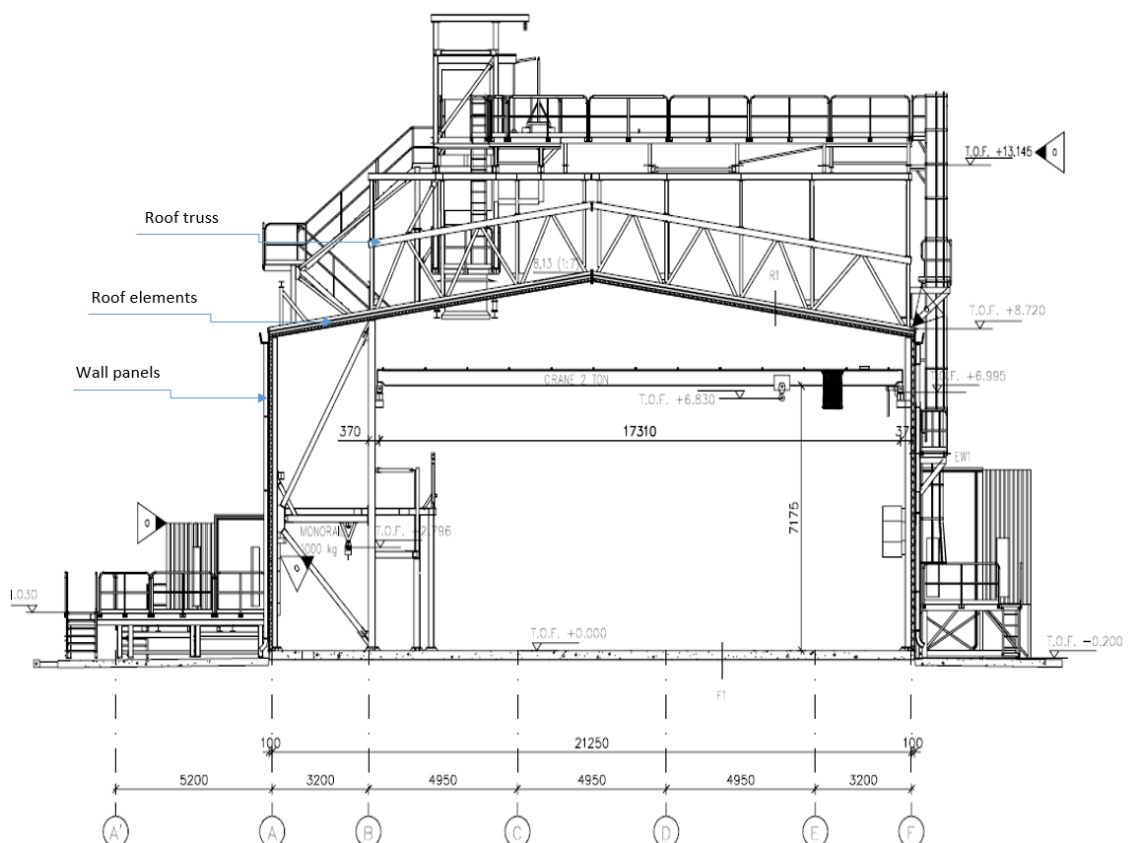
**Figure 2-2.** Section of one engine hall module. (Wärtsilä Corporation, 2014)

**Table 2-1.** Typical module span of engine types.

Engine type	Spacing between trusses [mm]
32GD	5400
46GD	7200
34DF	5400
50DF	7200
46F	8200

The envelope of the engine hall consists of wall panels and roof elements. The wall panels are light-weight sandwich panels with thin steel sheet on both sides of a mineral wool core. The roof elements are made of cold-formed thin-walled steel sheets and are supported by the bottom chord of the external roof truss. See Figure 2-3.

The roof elements need to adapt to the spacing of the external roof trusses, as this may vary from project to project. The solutions should however be such that the structure can easily be adjusted to fulfil the structural requirements without affecting any other parts too much.



**Figure 2-3.** Section of a Wärtsilä 34DF-engine power plant (Grande Cote, Senegal).

### 2.1.1 Main frame

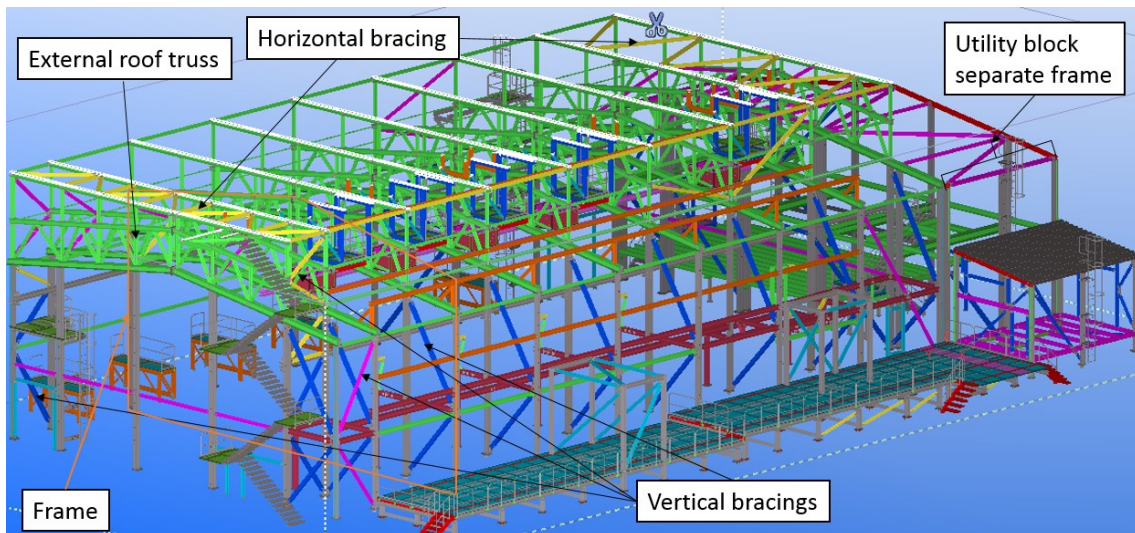
The most commonly used building frame by Wärtsilä in a power plant is a braced steel frame structure with an external roof truss supporting both the roof structure and



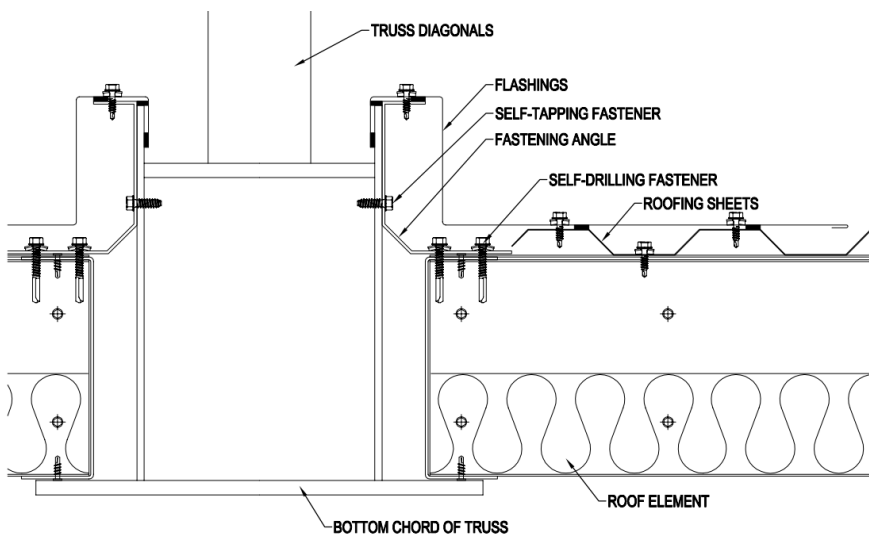
radiators above the roof. Structurally it not optimal to have additional weight high up, especially in earthquake conditions, but the advantages mentioned in the previous section are greater than the increased material costs.

Each truss and steel frame is either braced with steel bracings in the direction of the truss or a portal frame is used to stabilize it, depending mostly on the engine type. The steel structure is also braced at one or several locations between the main columns in the other direction, depending on the size of the building. There is also vertical bracing at both gables, but none along the long sides, as every frame is rigid. Some projects might be extended with a utility block, but these have separate steel frames. The scope of this thesis does not include the utility block. A typical steel frame of the 34DF-engine hall can be seen in Figure 2-4.

The bottom chord and roof beam are WQ-beams with webs that extend above the top flange to create a sort of gutter. The truss diagonals are welded to the top flange and holes are made in stiffeners and connection plates, so that the water can drain out. See Figure 2-5.



**Figure 2-4.** 3D-model of steel structure of a Wärtsilä Power Plant (Grande Cote, Senegal).



**Figure 2-5.** Section detail of the tropical roof element attached to bottom chord of external truss.

### **2.1.2 Roof structures for tropic climate**

The main purpose of the roof structure is to protect the equipment inside from the outside climate, but also to reduce and absorb the noise produced by the engines. Visually it is also more pleasing to the eye if there is a roof covering all the pipes and cables attached to the engines.

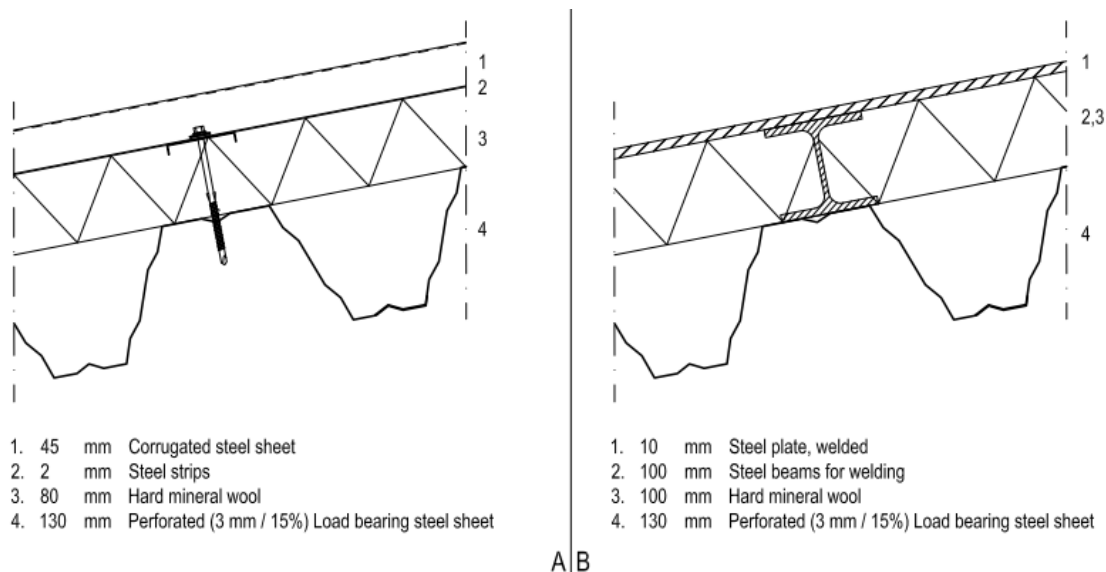
The slope of the roof on a Wärtsilä power plant is in general around 6° to 8°, which is not so steep. In very windy conditions there is a risk that the water is pushed upwards and through joints in the roofing sheets. This is why it is important to have overlapping joints with sufficient sealing between the roofing sheets, which prevents the water from pushing through. If there happens to be a leak somewhere, the steel sheets or membrane on the roof elements should direct the water out another way and prevent any water from entering the structure and creating moisture problems in the structure. (Nevander & Elmarsson, 1994)

#### **Earlier solutions for the roof structure**

Before the radiators were placed on the roof the most commonly used roof structure in a Wärtsilä power plant consisted of a load bearing sheet, which was supported by the main frame. The sheet was perforated to allow the 80 mm thick insulation to absorb sound. This is critical to lower the sound intensity in the power plant. The insulation sheets were fixed to the load bearing sheet with steel strips on top that were fastened through the insulation to the load bearing sheet. A corrugated steel sheet was then fastened to the steel strips. See type A in Figure 2-6. This roof structure contains several work phases, which consume quite a lot of time. Another problem is that the roof insulation is exposed for a long period, until the roofing sheets are installed. This solution is still used in some cases, when there is no external roof truss.

Another roof structure that was used in the beginning when Wärtsilä started placing the radiators on the roof to achieve better efficiency of the power plant is a similar structure as the one mentioned above, but with 10 mm thick welded steel sheet as roofing sheet. The load bearing sheet is placed in between the flanges of the lower cord of the roof trusses. The sheets are a bit shorter than the spacing of the roof beams or truss, so that they can be installed after the steel frame. This also required additional steel beams to support and provide a surface to weld to. All the sheets need to be assembled and welded on site, and this requires a lot of welding and work on site. See type B in Figure 2-6.

There is also a third roof structure that has been used on the power plant site, but this roof structure is not used on the engine hall. It is a structure based on thin-walled Z-purlins that are attached to the roof truss on site.



**Figure 2-6.** Earlier roof structures used in tropical climate.

### **Roof element for tropic climate**

Citec together with Wärtsilä and Ruukki developed a more efficient roof structure, which was made of roof elements, for the power plants in tropic climate conditions in 2009. The first type of roof element was built up from cold-formed lightweight steel purlins and steel sheets. The load bearing structure consisted of eight C-purlins with a centre to centre distance of 300, forming a 2150 mm wide element. The height of the purlins typically varied from 150 - 200 mm and thickness of 1.2 - 2 mm, depending on the span and the loads. See type C in Figure 2-7.

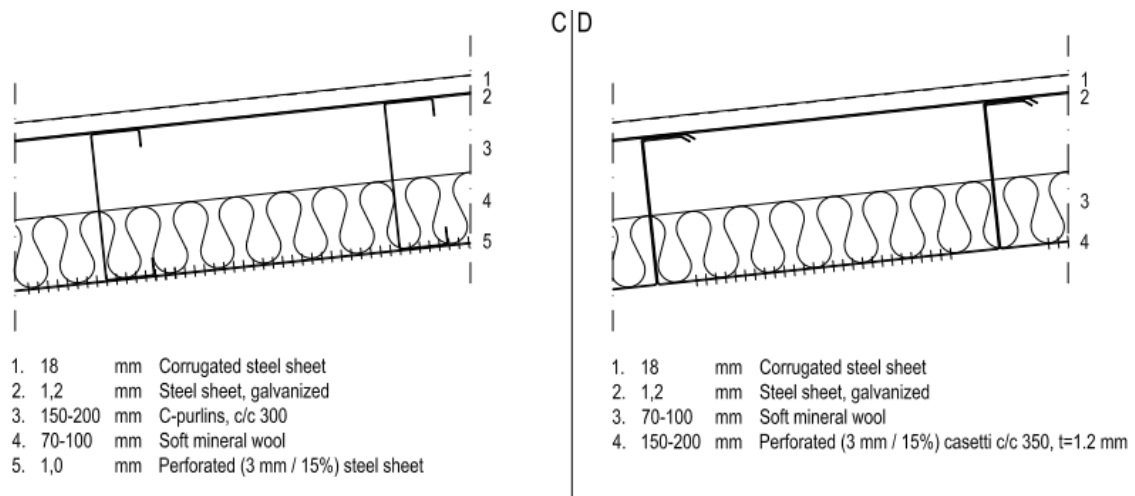
The main purlins were fastened with steel angles and self-drilling fasteners to a U-purlin at the support. A perforated steel sheet was fastened to the bottom side of the element and a 70 mm thick insulation sheet was placed on top of that acted as a sound absorber. On the outside of the element a 1,2 mm thick steel sheet was fastened with self-drilling fasteners, stiffening the element and forming a water tight surface.

Using this roof element instead of the load bearing roof structure provided several benefits at the building site. First of all there were fewer working phases involved in the installation. This meant easier and faster installation, which is crucial at site. After installing the roof elements there was already a basic water ceiling even before installing the roofing sheets or other final water sealing on top of the element. This was also a big benefit compared to the earlier type A structure, as the load bearing direction was perpendicular to the slope and this did not allow for the water to drain of the load bearing sheets in the same way. When installing the insulation on the load bearing sheets, it would also had to be protected against rain until the final roof sheets were in place.

The roof element was further developed a couple of years later. The C-purlins and the inner perforated steel sheet were replaced with linear trays with a perforated bottom flange. See type D in Figure 2-7. This made manufacturing much easier and faster, as there was no need for a special rig to set up the C-purlins and there was no longer a



need of turning the element to fasten the steel sheets on the other side. The inner surface was also found to be smoother without fasteners and dents in the sheet.



**Figure 2-7.** Earlier roof elements used in tropical climate.

The roof elements for tropic climate are fastened to the bottom chord with specific fastening angles and self-drilling and self-tapping fasteners. The modified WQ-beam, which is used as bottom chord for the truss allows for the elements to rest on the bottom flange while the elements are fastened. The flange will also take the downward load that the element is subjected to. The fastening angles will take horizontal and vertical upwards loads.

After the elements are fastened, the roofing sheets can be installed on top of the elements. To make all connections and joints tight flashings, sealing strips and compounds are installed according to specific assembly details. Figure 2-5 showed a typical detail on how the roof element is attached to the bottom chord of the external truss.

### **Common equipment on the roof**

When the roof structure with load bearing sheets was still used the most common equipment on the roof was a roof monitor along the roof ridge of the engine hall. This was a time when the radiators were usually located beside the engine hall on a separate steel frame.

Placing the radiators on the roof brought some challenges, as to getting the roof watertight, while having columns and bracings going through the roof. In the first projects they solved this by placing the roof structure in between the roof truss and beams. To the top of the flange they welded the roofing sheets. See Figure 2-6 B.

This required a lot of welding and was a relatively expensive solution, which lead to that not very many power plants were designed with the radiators on the roof until 2009. This was when the first power plant using the roof element for tropic climate was designed. The detailing had been developed so that it was possible to ensure a

watertight connection between the roof truss and the element using cover flashings, sealing strips and compound. This was a much easier and faster way than welding.

Today the radiators are usually on the roof on an external roof truss. The truss verticals and diagonals are welded to the bottom chord, which works as sort of a gutter. The elements are then placed in between the bottom chords and sealed properly using flashings, sealing strips and compound. The roof monitors had been replaced with roof fans that are placed in the joint between two elements on the ridge or near to the ridge allowing for watertight detailing with the corrugated roofing sheets and flashings. Other equipment penetrating the water sealing are very uncommon but may occur in some projects and are project specific.

## 2.2 Development of a roof element for arctic climate

This thesis focuses on only a small part of the main product. The power plant may be considered the main product. The engine hall is the core of the power plant and without it there would not be any need for an envelope or other structures. The roof element is only a part of the envelope of the engine hall. There are also several other buildings on the site and the scope might also include service agreements among other things. These can be seen more as separate products, but are usually sold together. The power plant may sometimes also be sold without any civil scope. Increasing the efficiency and lowering the costs of the civil work, not to mention increasing added value, will increase the probability for Wärtsilä to get orders that include a wider set of products.

In product development, there are usually several stages. Usually it starts with gathering ideas, which then are evaluated. Some ideas are discarded and some are further developed until the decision is made to continue the development one idea into a product. Even though the decision is made to develop an idea to a product, sometimes the idea does not make it all the way to the market. In this thesis we experienced this phenomenon, which is common within product development.

Although the work spent on an idea that is rejected at some point is a bit of wasted time, some parts of the work may sometimes still be benefited from. It can give insights, which can be further developed using another approach. The longer you have developed the idea before it is disregarded, the more work may be wasted. With an efficient screening process, it is possible to minimize the setback. An efficient screening process requires experience and a variety of knowledge from manufacturing, development, designer and customer interfaces to be able to take into account all requirements, restrictions and expectations.

In the beginning of the development project it is impossible to know the outcome. That is why it is good to have some milestones set up, when the work and the ideas can be evaluated. It is important to evaluate if it is worth to continue on the path or explore other alternatives.

This development project started with an interest from Wärtsilä to optimize the structural capacities for a linear tray roof element. They had only recently back in 2012 started using this type of roof element, as the previous one was based on a C-purlin frame. There was not much talk about product development at this point, but as time passed several new ideas were developed.

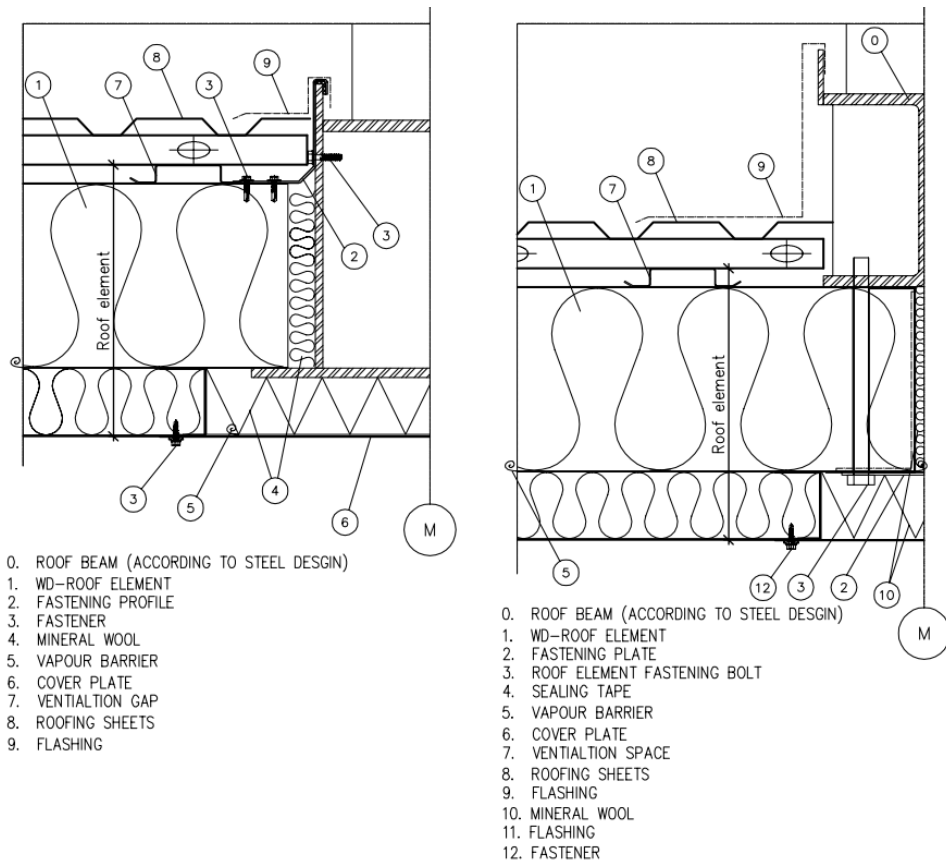
About a year later the project had not yet started due to lack of time, but now the linear tray element was already implemented in some projects in tropical climates. The problem was that the same solution was not very good in arctic climates. At this point the development of an arctic climate roof element started, although no financial decision was made for this thesis. Ideas started evolving and some initial discussions were held.

At this point the main idea was to develop the roof element solution for tropical climate so that it would be suitable for the arctic climate. The main challenge was the poor thermal resistance of steel and the structural height, which determines how thick the thermal insulation layer can be. This has been solved in similar elements with a thermally slotted web, which reduces the area and increases the distance, through which

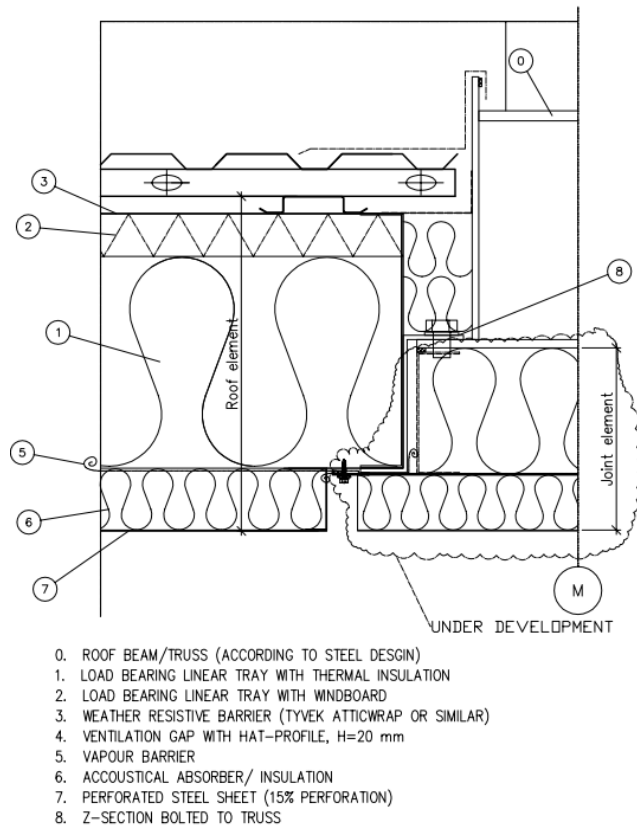
the heat flows. Another problem was that the inner sheet of the element was perforated to provide better acoustical absorption, but this meant that there was not an air and vapour tight layer on the inside. This could result in that humid air can condensate inside the insulation, as the air cools down. This could lead to mould, which is a health risk. Below the main challenges at this point are listed.

1. Thermal resistance
2. Condensation of humidity
3. Acoustical absorption
4. Structural capacity
5. Installation

It was not until a half year later when the first milestone was reached. This was a meeting between Citec and Wärtsilä, where it was agreed that one of the presented solutions could be further developed with some minor changes. At this meeting, where Detail 1 and Detail 2 were presented, which are shown in Figure 2-8. Detail 1 was very much like the tropic climate element, only with additional insulation inside the linear tray and acoustical absorber on the inside and a vapour barrier. Compare Detail 1 with Figure 2-5. In Detail 2, the element was suspended below the bottom chord with bolts. This was not a good solution, as it would require installation from inside the building and this would affect the installation of other equipment inside. The outcome from this meeting was a third solution, which was a combination of the both and is shown in Figure 2-9. The main purlins were half-way suspended with a Z-section at the support. This reduced the cold bridge, which was dominant in Detail 1 and still allowed for an installation from the outside.



**Figure 2-8.** From the left, Detail 1 and Detail 2.



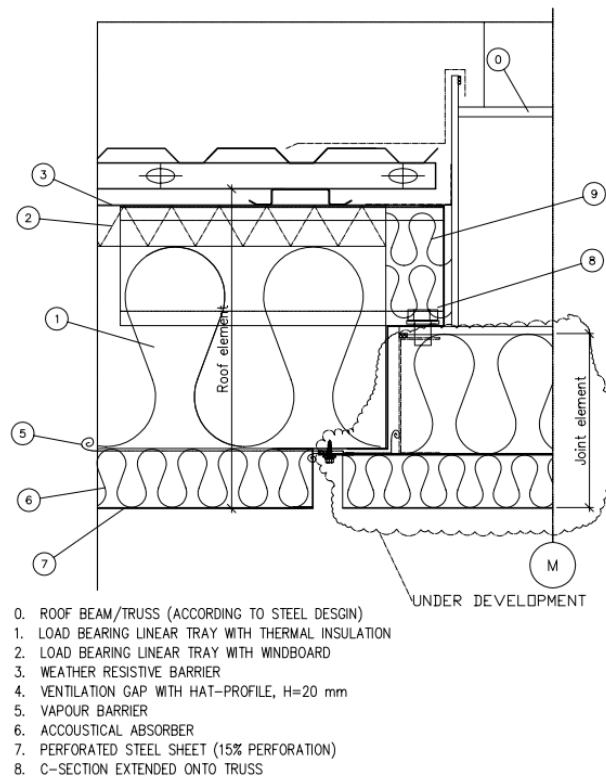
**Figure 2-9.** Detail 3 was a combination of Detail 1 and Detail 2. Element suspended by Z-section.

It was also agreed to do some research into the existing markets, to see if there are existing products that can be used. Both the Finnish and the international market were researched for already existing solutions. There are some products quite similar to the roof element Wärtsilä uses in the tropic climates that are used in arctic climate conditions. Ruukki, for example, have a roof element solution based on thermal steel purlins.

Most roof elements in arctic climates are anyhow wood frame products, as wood has much smaller thermal conductivity than steel. The thermally slotted purlin is however comparable to a wooden stud. In some countries there are regulations on combustible materials in certain structures, which can be problematic for wooden structures. There are also some hollow core slabs of concrete that come pre-fabricated with thermal insulation on the inside. Some roof element products are also based on the same principal as the light weight sandwich panels, with steel sheets on the outer and inner surfaces and only an insulation core of either mineral wool or polyurethane in between. Some manufacturers have even developed purlins with a mineral wool web and steel sheet flanges glued to the web. The load bearing capacity of these insulation core products are usually smaller than a wood or steel purlin element of the same height. The hollow core slabs have a good load bearing capacity, but are much heavier and require more work at site.

From a structural point of view the weight of the concrete hollow core slabs would be problematic in earthquake areas. The cold formed steel element was found to be a good competitor to the wood frame elements as long as the web is slotted to increase the thermal resistance. It was also seen as beneficial to have similar roof element solutions in both tropic and arctic climates. As a result the linear tray solution was further developed.

Figure 2-10 shows the next step in the development process. Instead of the Z-purlin at the support the linear trays were suspended by attaching C-purlins to the web to avoid the multiple non-slotted purlins at the support and decrease the cold bridge. This also had a structural benefit, as the local transverse compressive forces on the thermal slotted main linear trays were transferred to the thicker C-sections, which are considerably stiffer. The solution in Detail 3 would surely have required additional strengthening at the support to avoid crippling and shear failure.



**Figure 2-10.** Detail 4. Element suspended by C-sections attached to main purlins.

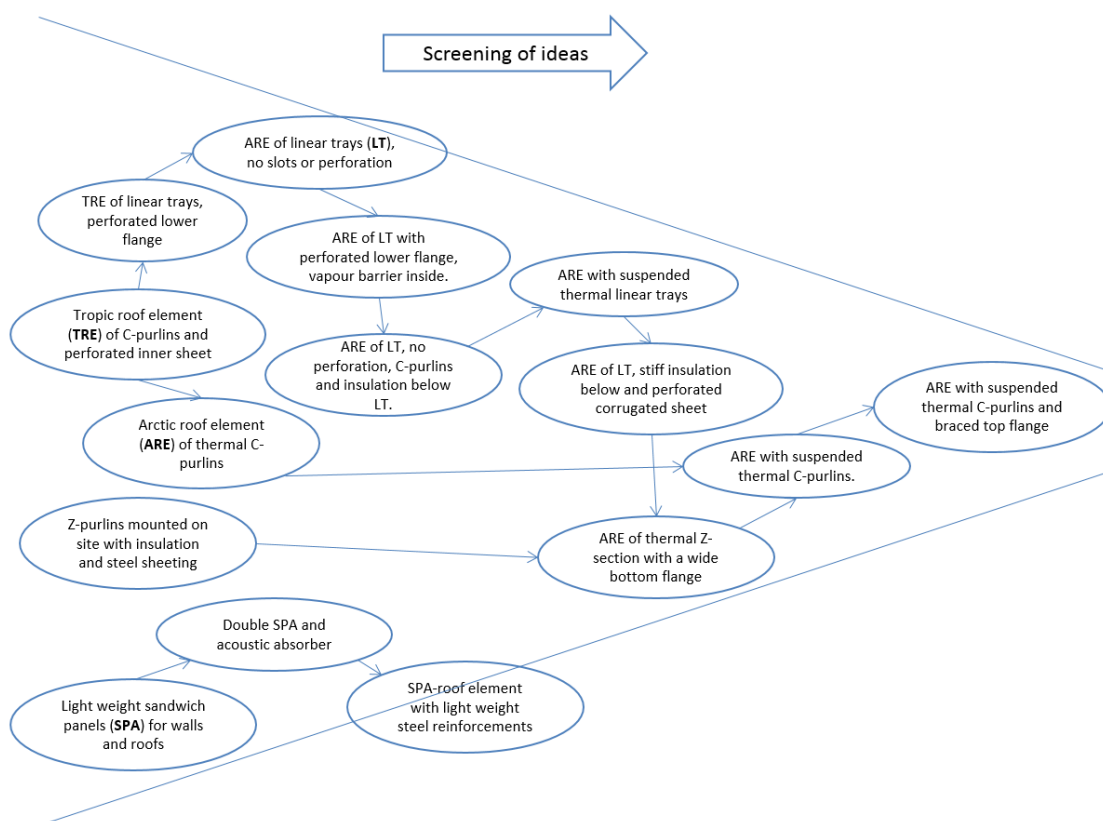
Laboratory bending tests were set as the next milestone. These would be carried out at the Sheet Metal Centre at HAMK University of Applied Sciences together with the manufacturer Ruukki. Ruukki had been involved in the development of the roof element for tropic climate using linear trays earlier and the element was originally proposed by them. For the development work it was important to have the feedback from the manufacturer as well. The idea of a thermally slotted linear tray element had been discussed with them on several occasions, and there had been some concerns on how to avoid the contact between the slotted webs, as the contact would reduce the thermal resistance. It was not however until the manufacturing drawings for the experimental tests were sent to the manufacturer, when they informed that they do not have the equipment to manufacture these thermally slotted cassettes. The problem was that the thermal slot line is made only for a plate width up to 580 mm. The linear tray, which was planned for the experimental test had a width of approximately 950 mm. Due to this the frame had to be changed.

Preliminary FEM analysis done for the experimental tests showed that the effective width of the linear trays could be increased, as the load bearing capacity was exceeding the expected loads. In the roof element with the linear trays, there are two webs with a 359 mm interval. The possibility to cut the other web of the linear tray was assessed, and by reducing the effective width a little, the 580 mm wide steel sheet would be sufficient. This would still allow for the linear tray, or maybe a Z-sections with a wider bottom flange would be a more appropriate name for the section, to be connected to each other in a similar way as the linear trays.

This modification was suggested to the manufacturer, but it turned out that there was another restriction in the production line. The slotting area could only be in the middle of the sheet. This was not the case for the Z-section, as the lower flange was considerably wider than the upper flange making it impossible to place the slotted holes in the middle of the sheet.

Due to these restrictions the load carrying structure changed from thermally slotted linear trays to thermally slotted C-purlins. These C-purlins are commonly used in wall structures. The roof structure changed to a solution much like the prefabricated roof element solution that Ruukki offers to other customers. These roof elements differ, as they have a plywood sheet on the cold side of the C-purlins. Most of the solutions developed for the linear tray could still be implemented in this element, especially the support arrangement. It is still clear that there was a big amount of work that could not be utilized.

The development process has been quite long and several ideas were considered along the way. Some parts of some ideas have been further developed in a new idea. The process and how these ideas have developed and been screened out is shown in Figure 2-11.



**Figure 2-11.** The product development process and screening of ideas.

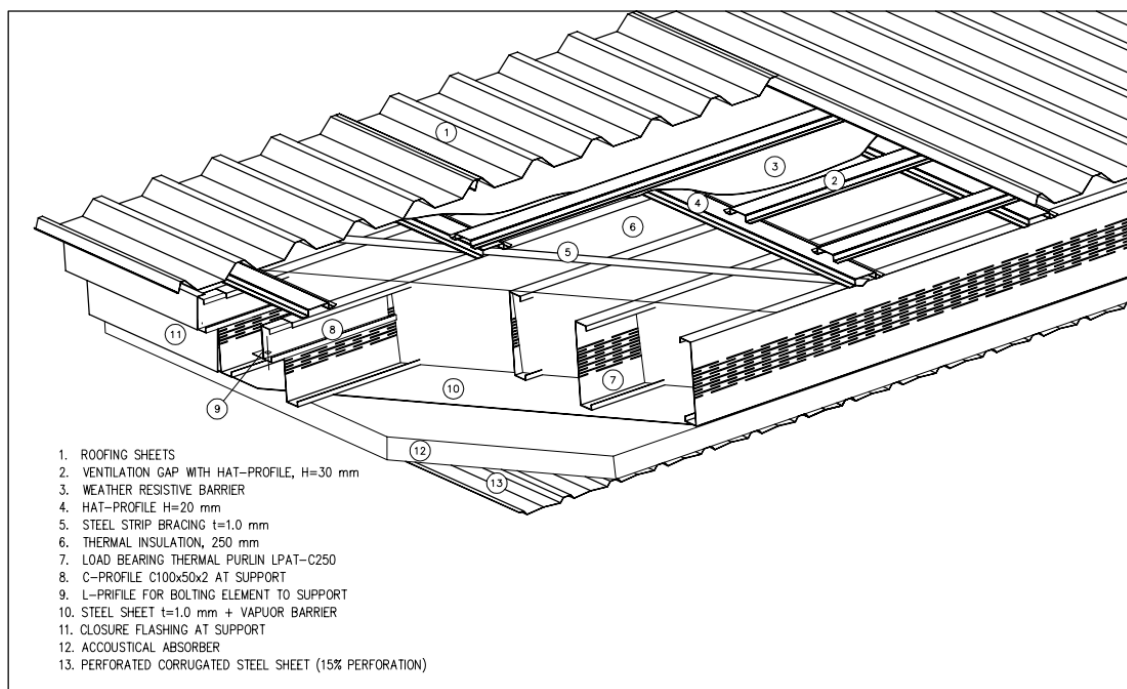


## 2.3 Design details, manufacturing, transportation and erection

When designing a new type of product there are several things that need to be considered. If a product cannot be manufactured or does not work in the environment, the design is not worth much.

In this section the final product is described so you get an understanding of which components it contains. The design process is also presented, including every aspect that has been looked at, as well as the project specific design that is needed. As already stated the manufacturing process also plays a big part, and it is also presented in the end of this section.

The finalized roof structure requires some work at site, but the goal is to make as much as possible ready in the workshop and minimize the work at site. Figure 2-12 shows all parts and layers that the arctic roof element structure contains. The roofing sheets and top layer of hat-profiles are installed on site, the rest are assembled in the workshop and come as an element.

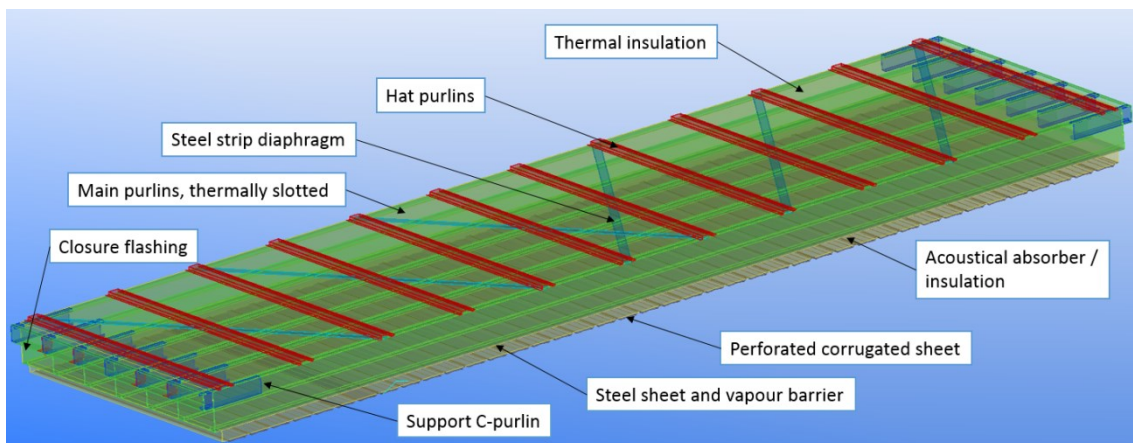


**Figure 2-12.** Arctic roof element with roofing sheets and hat profiles attached.

### 2.3.1 Product description

The roof element for arctic climate consists of cold-formed thin-walled steel purlins, insulation, steel sheets, a vapour barrier and a weather resistive barrier, which lets humid air through. These components are assembled using self-drilling fasteners. The web of the main purlins has slotted holes to increase the thermal resistance. The 250 mm high main purlins have a centre to centre distance of 300 and between them there are 100 mm + 150 mm thick soft mineral wool slabs. The purlins are tied together with a steel sheet at the bottom and hat profiles placed perpendicularly at the top with a

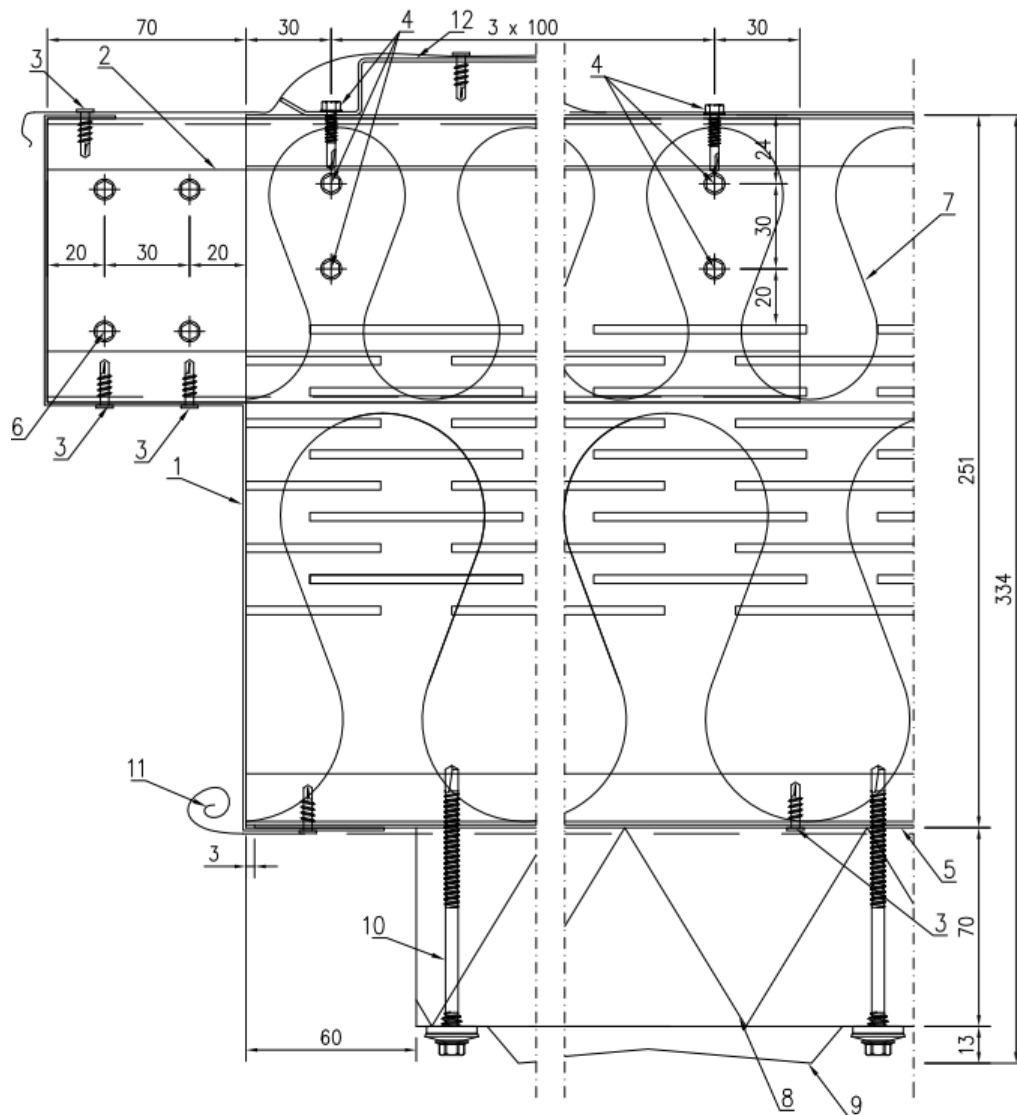
spacing of 600 mm. The experimental tests showed that the hat profiles alone cannot reliably prevent lateral-torsional buckling, so to prevent this, the top flanges are also stiffened with a steel strip forming a diaphragm. Beneath the steel sheet there is a vapour barrier and another layer of hard mineral wool that is 70 mm thick. This layer acts as both a thermal insulation, an acoustical absorber and protects the load bearing purlins from fire. The mineral wool is fastened to the purlins through a corrugated sheet with self-drilling fasteners. The corrugated sheet has a 15 % perforation to allow for the sound waves to pass through it and be absorbed by the mineral wool. Figure 2-13 shows the complete roof element apart from the weather resistive barrier on top.



**Figure 2-13.** 3D-model of a single roof element.

At the support ends of the element there are additional C-purlins in the same direction as the main purlins. These are 100 mm high and 2.0 mm thick purlins that are attached to the upper part of the web, below the upper flange. They are extended 70 mm out from the main purlins. These are designed to lower the element compared to the lower cord of the roof truss, so that it is easier to insulate the element joint at the roof truss and the cold bridge is reduced. As the C-purlins are thicker and have a lower web than the main purlins, they also increase the local transverse load capacity at the support. They suspend the main purlins, creating tension instead of compression in the web, preventing it from crushing the main purlin.

To close the element at the support, there is a 1.0 mm thick steel sheet or flashing, which has been cold-formed to fit the profiles. It is attached to the top and bottom flange of the 100 mm high purlins, preventing them from rotating around the length axis. It is also attached to the bottom flange and bottom steel sheet. See Figure 2-14.



1. FLASHING 50\*152\*70\*102\*25\*1.0
2. PURLIN C100\*38\*2.0
3. SCREW SL4-F-4,8\*16, c/c 300
4. SCREW SD6-5.5\*28, c/c 100
5. STEEL SHEET, 1.0
6. SCREW SD6-5.5\*25, 4 pcs

7. INSULATION SHEETS 150 + 100
8. HARD MINERAL WOOL 70 mm
9. CORRUGATED SHEET, 15% PERFORATED
10. SCREW SDT5-S19-5,5\*97, c/c 300
11. VAPOUR BARRIER, OVERLAP 100 mm
12. HAT PROFILE, H20\*1.2

**Figure 2-14.** Manufacturing detail ARE-MD-1.

### 2.3.2 Design process

The things, which affect the design the most is of course the boundary conditions. There are some loads on the element, such as self-weight, snow and wind load, and it has certain other requirements, which it needs to fulfil. The structural capacity is further studied in Chapter 5. The acoustical, moisture and thermal design aspects are studied in Chapter 6.

There are also manufacturing issues to be solved in details and drawings. Transportation has to be accounted for, and this usually put some restraints on the maximum size of the elements. The elements need to be designed in such a way that they are intact when

arriving at site. On site the erection has to work as smoothly and without any interfering with other disciplines. These are all things which need to be considered in the early stages of the design, as changes to the erection method might affect the core system. In this Thesis most of these aspects have been designed, so that the project specific changes will not affect the main system.

The design of most Wärtsilä power plants is based on the engine type, which determines the standard module width for the engine hall. The main steel frame does not vary much from project to project if the radiators are on the roof and the engine type is the same. The profile sizes vary depending on the external conditions, but this does not impact the roof element design. This makes it possible to start the roof element design as soon as the basic design of the main steel frame is ready.

The spacing of the roof trusses determines the length of the roof element and the external loads, usually wind and snow load, determine the section and/or centre to centre distance of the main purlins. More about structural aspects can be read in the Chapter 5. As the structural measures are clear the modelling can start. The good thing with elements is that the whole element can be copied and elements with the same dimensions can be produced with the same drawing. Small changes, such as stretching, copying or removing parts are easily done. The first element should be modelled with care before copying, otherwise the same mistakes will be transferred everywhere. At the eaves and at the ridge, there is usually a modified element.

The manufacturing and assembly details can be used in several projects over and over again and only project specific additions need to be done. This makes the producing complete drawings much more efficient than making all drawings from scratch.

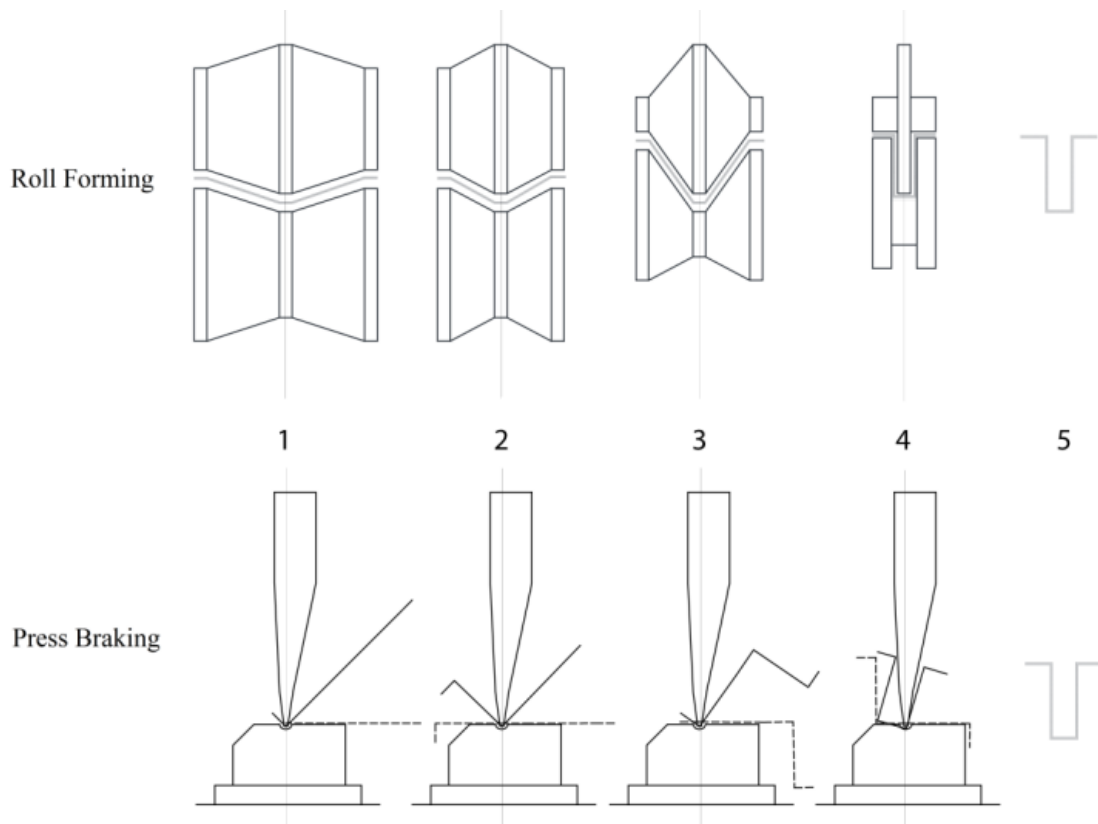
### **2.3.3 Manufacturing process**

The manufacturing process is a wide concept. Basically it starts from the mines and producing steel, but in this chapter the focus will mainly be on the part starting with cutting the steel sheets and producing the sections and parts needed for the roof element leading up to the finalized roof structure.

The raw material used for the roof elements comes in big coils of steel sheet. The sheets are of a certain thickness and usually pre-coated with either a zinc coating or some type of polyester coating depending on the corrosion resistance expected from the sheet and the esthetical requirements. The polyester coatings come in a large variety of colours as well. This is an important aspect to take into account, as the factory does not usually have every material in stock. By choosing only a few materials, it is also easier for the manufacturer to keep those materials in stock, which results in shorter delivery times, as the material does not need to be ordered weeks upfront.

To make the purlins and other profiles, the sheets are cut to specific widths. After this the sheets that need to be slotted are either slotted by cutting or punching out the holes. Then the sheets are cold-formed in to the desired profile either by roll forming or press breaking as shown in Figure 2-15. Roll forming gradually modify the sheet as it passes through various rolls. The press breaking bends each corner of the profile to the desired

angle one at a time. The roll forming method usually allows for making longer profiles at a time, and is only economical when large amounts of the same profile shape is produced, as each profile requires a new set of rolls. Press breaking is better suited for project specific profiles, which are only produced in smaller amounts.



**Figure 2-15.** Cold-forming methods for thin-walled steel profiles. (Grey, 2011)

When all the profiles and parts are slotted and formed in to shape the assembling starts. This is usually manual work, where each profile and part needs to be measured in to place and fastened to each other. The time it takes to assemble an element is dependent on the number of parts and connections in the element. The type of fastener and material thickness also plays a role as well as the number of work phases involved. The manufacturing drawing show the distances between the parts and critical measures such as bolthole distances and cross dimensions, which need to fulfil the tolerances in order for the element to fit in place. The centre of gravity should also be marked along with measures so that lifting and erection of the element can be carried out safely.

The manufacturing details show distances between fasteners. It is important to emphasize measures that are critical. This can be done by adding allowed tolerances to the measures, so that the manufacturer understands that these need to be followed. All measures should of course be followed, but experience shows that this is not always the case. A good example of this was the experimental tests carried out in this Thesis. In Appendices 4 you can find the manufacturing drawings and details for the test specimen used in the experimental tests.

The basic idea of a pre-fabricated element is to reduce the amount of work required at site, where the working conditions are varying and sometimes very difficult. By using

elements produced in a workshop, most of the work can be done in a controlled environment where the ergonomics are better. This often reduces both construction time and total costs.

It is much easier to assemble a roof element on a turning table in a workshop, than 10 meters up in the air. In the workshop all parts may be pre-cut and ready for assembling right next to the table, as on site some parts need to be cut and fitted in places, which are hard to reach. It is also easier to estimate and re-use spare material in a workshop, than it is on site.

### **2.3.4 Manufacturing tolerances**

Manufacturing tolerances are required to achieve a product, which fulfils the design assumptions for the structure in terms of mechanical resistance and stability, but also functionality. These tolerances may be specified on the manufacturing drawings or specified in a standard or guideline and referred to on the manufacturing drawing. The tolerances specified on the drawing always replace any value given in the standard. If no specific tolerances are given, the values specified in the standard or guideline referred to are to be followed.

EN 1090-2 gives tolerances for the manufacturing of steel parts. It separates between essential tolerances and functional tolerances, where the essential tolerances are stricter. This is to satisfy the design assumptions for the structure in terms of resistance and stability. Functional tolerances make sure that the parts are within the limits for e.g. assembling and appearance. The Finnish manufacturers usually follow RunkoRYL 2010, and these guidelines may be used if the manufacturing is carried out in Finland. (Rakennustieto Oy, 2010)

Another aspect which may increase the accuracy in the workshop is ergonomics. If the person fixing the parts to each other needs to stretch or kneel to get the screw in the right place, it might be more difficult to reach the required tolerances. Appropriate tools and technique may save both time and money in the end, as the amount of rework is reduced. (Karwowski, 2012).

The roof element based on linear trays had several benefits for the workshop. It had less fasteners that were only fastened from one side and did not require so much measuring, as the trays may be placed next to each other. These were all reasons, why this thesis started with this principal.

However, compromises had to be done. The important thing is to ensure a certain quality, by making sure that the manufacturing environment and quality control is at a level, which reaches the design criteria's. The elements used in the experimental tests are a good example how many things can differ from the actual manufacturing drawings, when proper quality control is not sufficient. It also shows how big difference the deviations may have on the capacity. More about the deviations from the drawings can be found in Section 4.3.

### 2.3.5 Transportation

Transportation is always something that needs to be considered, when building with elements. The transportation method gives some restrictions on element size and protection. In this case, when the project can be located on the other side of the globe, it is even more important to plan the transportation. Wärtsilä usually loads all material in containers, which are shipped over sea to the location. The containers can be loaded with elements up to 12 m in length.

The roof element should come as pre-fabricated as possible, but not take up any unnecessary space in the container. The roofing sheets have to be installed on site so that they can be installed as full length sheets. The upper layer of hat-purlins are also installed on site, even though they could be part of the element. The benefit is that the structural height of the element is less, which will reduce the container volume. The upper layer would also extend a bit over the element, which increases the risk for both personal and structural injuries.

It is also important that the inner surface of the element is not injured during transportation. Feedback from both the manufacturer, from site and from the end user is always important to achieve a good product. It may be difficult to get the feedback if it is not given first hand. It is not always possible to ask the end user directly, and this is where the importance of project follow-up comes in. It is seldom that all disciplines get feedback, but in a big project there are so many things that have been done, that it is not reasonable to ask about every little detail. Problems tend to be presented if they are noticed, and these should be addressed as swiftly as possible. When introducing a new product, it is suggested that feedback is gathered for that specific product during the pilot project to allow for adjustments and improvements for the following project.

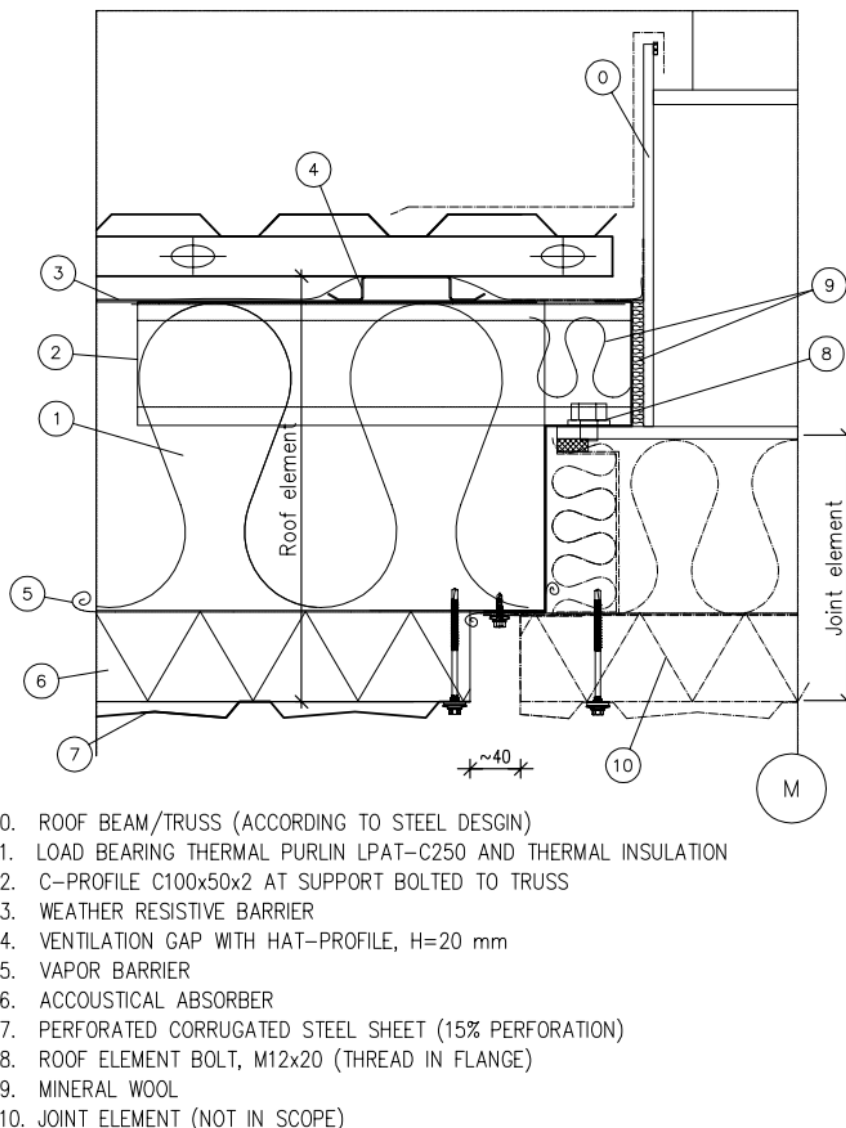
The most common feedback for the envelope is usually that some kind of injury to the surface has occurred. For this type of elements, where the inner surface has a significant risk for getting injured, it would be good to provide a number of perforated sheets along with the ready elements. This allows for small repairs at site without having to wait for the spare parts and possibly delaying the erection.

Transporting the perforated sheets separately could also be an option. They would have to be fixed to the elements on site. This would have the benefit of taking up less volume in the container and reduce the likelihood for them to get injured during transport. It is also possible to have the sheets assembled to the roof elements on site, while the elements are still on the ground, before erecting the elements. This ensures a more ergonomic working position and reduces the risk of injuring the surface of the sheets.

If the sheets and wool is attached to the roof element in the workshop and transported to site, there should be some sort of spacers at the end, which keeps the elements apart, so the hat-profiles do not rub against the perforated sheets, when the elements are stacked upon each other.

### 2.3.6 Site erection

The roof elements arrive on site in containers and they are well protected from weather and wind. After the steel frame is erected, each roof element can be lifted in place from the outside. It does not matter if the engines are already in place or if they will come later, as the installation is done from the outside. As all roof elements are installed, they already provide some protection against the rain and/or snow, but as soon as possible the second layer of hat profiles and the roof sheets should be installed. If it is rainy, it is of course better to do this quickly, as the membrane on the outside of the element is not 100 % waterproof nor are the joints, it only provides a temporary protection. When the sheets are installed all flashings need to be fitted according to the details to get the roof fully waterproof. Figure 2-16 shows the typical assembly detail for the arctic roof element.



**Figure 2-16.** Assembly detail 6. Final version for the arctic roof element.

The required tolerances for assembly are always a bit hard to estimate. When assembling steel frames, the tolerances are small, compared to in-situ concrete for



example. 3D-design is a huge factor in achieving small tolerances. Usually all connections are pre-fabricated and bolted with small tolerances.

However we still need to have some tolerances, as there is always some variance in lengths, thickness, curvature and cross-dimensions. Temperature differences also affect the length, and should be accounted for during erection. Some connections may require sliding connections with increased tolerances in one direction, but it also means that the connection is not able to transfer forces in that direction.

The roof elements are bolted to predrilled threaded holes in the bottom flange of the bottom chord of the roof truss. In case the tolerances are not enough, the elements may also be fastened with 4 self-drilling or self-tapping fasteners instead of each bolt. If possible, one end of the roof element should always be bolted, to allow for some movement in the connection, otherwise a slotted hole in the element should be done in one end of the element. Both the bolts and the self-drilling fasteners should be provided just in case.

There has been a lifting hook developed for the roof elements in tropic climate conditions, and the same solution can be used for the arctic elements. It consists of a steel plate with a lifting hole in one end that is bolted to the element in the other end. The plate can be rotated around the bolt, so that it can be pushed down in the element joint, when installed. This is a fast and easy solution, as no lifting eye bolts need to be attached or removed.

### 3 Structural theory and design codes

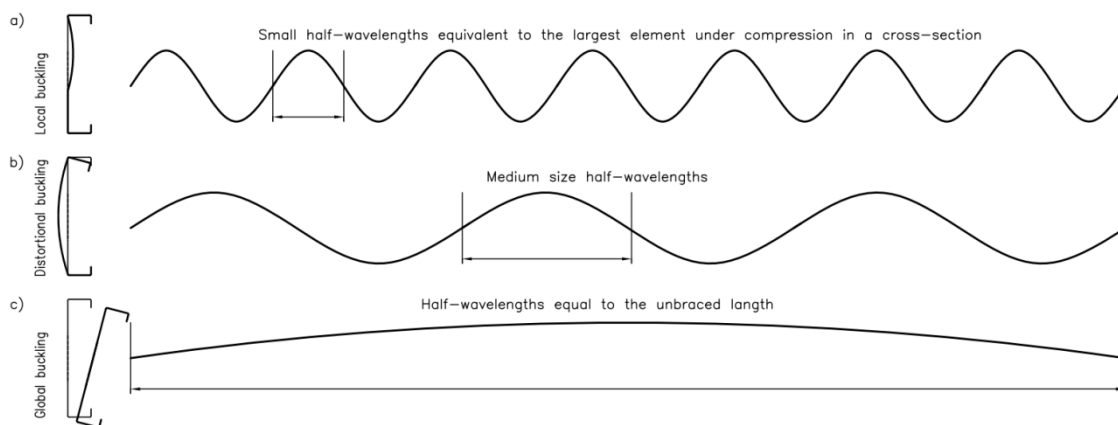
This chapter covers the structural behaviour of the roof element. It is strongly based on the Eurocodes and especially EN 1993-1-3, which is specific for cold-formed members and sheets. There are some things, which the Eurocodes do not cover, such as the thermally slotted purlins and how the slotted web effects the section properties of a member. To understand how this effects the structure other literature and publications have been used along with the experimental testing, which also support the calculations.

In order to understand how the structural capacity is calculated, a deeper understanding of the different failure types is needed. This chapter begins with examining the typical failure modes of cold-formed beams and how these are included in the Eurocodes. The effects a slotted web has on a thin-walled section and how this can be accounted for is presented in the following section.

#### 3.1 Failure modes for thin-walled beams

For a long thin-walled cross-section the typical failure is usually some type of buckling. Even shear failures may be some sort of local buckling of the web. It is of course possible to have other failures as well, for example tearing, but buckling is clearly the governing failure mode.

There are several different types of buckling modes, which may occur on a thin-walled purlin subjected to transverse loading. These can be categorized in different ways but are usually divided in to three main categories: a) local buckling, b) distortional or c) global buckling as shown in Figure 3-1. These are characterized by the half-wave lengths and the deformation of the cross-section.



**Figure 3-1.** Three main buckling modes and their half-wavelengths for beams subjected to transverse loading.

Individual plate elements in a cross-section, which are exposed to compressive stress, may buckle independent from each other and this type of buckling is called local buckling. Local buckling is characterized by a short half-wave length, which is not

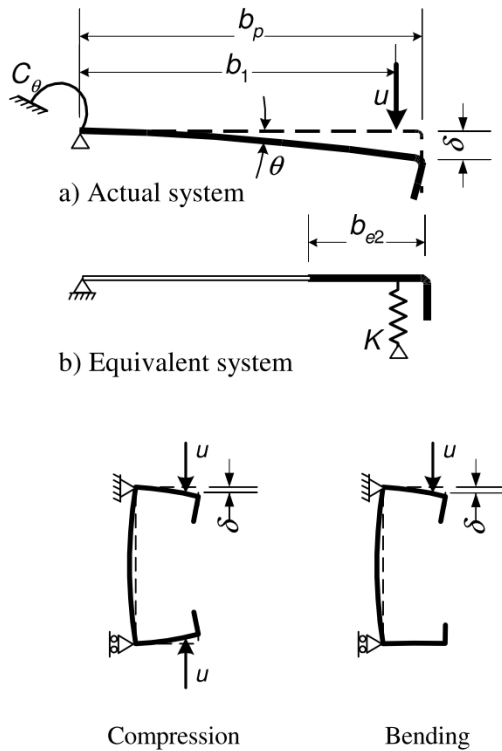
longer than the largest element under compression. Local elastic buckling is very common in thin-walled cross-sections and is not always critical as the post buckling strength is usually much bigger than the critical local buckling stress. The Eurocode accounts for local buckling by neglecting the parts of the cross-section which buckles due to the compressive stress, which is usually the upper parts of the web and part of the upper flange of simply supported beams under gravity loading. The partial gross cross-section areas are reduction to effective partial cross-section areas and these are then used to calculate the effective cross-section properties for the specific load case. Local buckling may also occur under a concentrated load, but this type of local buckling has to be checked separately and it may also be the ultimate failure mode for the structure.

Distortional buckling is also very common in cold-formed sections. It is distinguished by a medium half-wave length and a distorted cross-section. Distortional buckling occurs as the stiffness of the web, flanges and stiffeners is not big enough to keep the shape of the section from deforming when under compression. The effect of distortional buckling can be reduced by adding stiffeners that reduce the buckling length or providing torsional restraint to the flange(s) in compression.

The effect of distortional buckling is also taken into account by reducing the effective cross-section area of the flange stiffener. The reduction factor for distortional buckling is based on the flexural stiffness of the web. EN 1993-1-3 gives two formulas for calculating the spring stiffness  $K$  for a C-section, formulas (5.9) and (5.10b). Formula (5.9), also shown in Equation 3-1, is a general formula in which the unit load is divided by the deformation at the loading point. Formulas given in (5.10a) allows you to calculate the deflection for an edge stiffener, but to calculate the rotation a rotational spring stiffness coefficient  $C_\theta$  is needed. Determining the rotational spring stiffness analytically for a section with a slotted web is very complicated. Formula (5.10b) is specific for lipped C- and Z-sections, but without a slotted web. It is also possible to determine the spring stiffness by numerical methods. This may be done by inserting a unit load  $u$  on the section at the distance  $b_l$  and calculating the deformation according to Figure 3-2. The unit load and deflection may then be inserted into Equation 3-1.

**Equation 3-1**

$$K = \frac{u}{\delta}$$



c) Calculation of  $\delta$  for C and Z sections

**Figure 3-2.** Determining the flange spring stiffness of C-purlin according to EN1993-1-3 Figure 5.6.

When the whole cross-section buckles over the entire span, without the cross-section changing shape, it is called global buckling. Global buckling can be sub-categorized and global buckling of a beam is usually lateral-torsional buckling, if there is not any axial loads present. There are also flexural, torsional and flexural-torsional buckling modes, but these occur only on axially loaded members. Axially loaded members are not covered in this Thesis. Lateral-torsional buckling can be prevented by bracing or providing sufficient rotational restraint to the compressed flange. EN 1993-1-3 also provides several alternatives for determining the lateral-torsional buckling capacity for different cold-formed structures with different types of restraints or for a free compressed flange.

Flange induced buckling is sort of a local buckling mode, as the wave length is usually short. It is not however independent of other plate elements. As a beam member with a thin web is subjected to a transverse load, there is also compression induced in the web. This web supports the flange, but buckling occurs in the web, the already curved flange will lose the transverse support in the weaker axis and may also buckle. EN 1993-1-5 gives a criterion for plated structural elements, but it assumes that the web has a uniform thickness over the height and is not slotted. (Ivanyi & Skaloud, 2014)

Shear buckling may also occur in sections with a thin web. This usually occurs close to the support. Continuous multiple span beams are especially prone to shear buckling. EN 1993-1-3 section 6.1.7 analyses how the thin-walled cross-section can resist local transverse loads. It takes into account crushing, crippling and buckling of the web. It is

not however suitable for sections with a slotted web. The additional C-section, which has been used at the supports to suspend the main thermal purlins can be analysed with the formulas provided in EN 1993-1-3 section 6.1.7. (EN 1993-1-3, 2009)

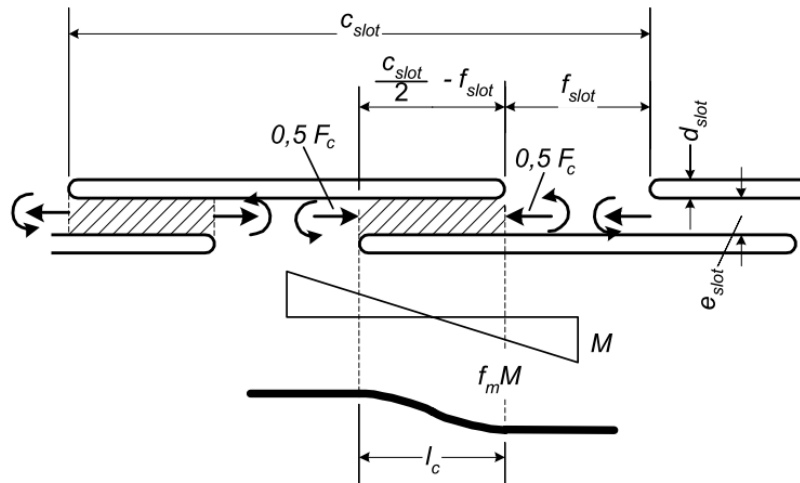
### 3.2 Failure modes of slotted member in bending

There are some failures which are specific for thermally slotted sections. The holes in the slotted web reduce the flexural stiffness of the web. This reduces the critical stress for distortional buckling and the maximum local transverse load the section can resist. The slotted web also changes the shear buckling mechanism. (Kesti, 2000)

As already explained in the previous section, the occurrence of buckling does not automatically indicate failure of the complete system. Local buckling occurs at a very early stage, but the cross-section might be able to carry several times the critical buckling load for local buckling. Local buckling for instance means that the local area, which has buckled, has reached the critical stress level and the additional stress will be distributed on to other areas in the cross section. The ultimate load bearing failure occurs when it is no longer possible to increase the load upon the system. At this point there might be several types of buckling occurring at different locations in the system. One type of local failure might not be a failure of the element, but it might encourage another type of failure and lead to an accelerated occurrence of another type of failure. For instance if the connection between the hat purlins and the main purlins exceeds the rotational capacity the rotation of the main purlin will accelerate and this might result in either distortional or lateral-torsional buckling of the main purlin at a lower load, than with an element with higher rotational capacity in this connection. (Yang & Liu, 2012)

The slotted web reduces the stress level at which buckling occurs in the web. This is due to the fact that the bending stiffness, especially across the web is greatly reduced. Since the shear buckling stress is low the post buckling range is large. Shear failure of a thermally slotted purlin may also be seen as a type of plastic buckling. As the web consists of several connected steel strips, which will take both tensile and compressive stress. If the critical buckling force is less than the shear capacity of the part connecting the strips the shear failure will be a form of flexural or lateral buckling failure. Figure 3-3 shows how the shear force  $F_c$  creates both a bending moment on the strip along with an axial force, which is negative on every second and positive on every other strip. The ultimate shear failure is usually governed by yielding at the sharp ends of cut slots, as these act as stress concentrators.

Crippling is still more common in thin-walled sections than shear failure. The Eurocodes do not provide design rules taking into account crippling for sections with slotted web. This is something, which can be avoided by either adding stiffeners at the support or arranging the support so that transverse compression is avoided. (Thöyryä, 2001)



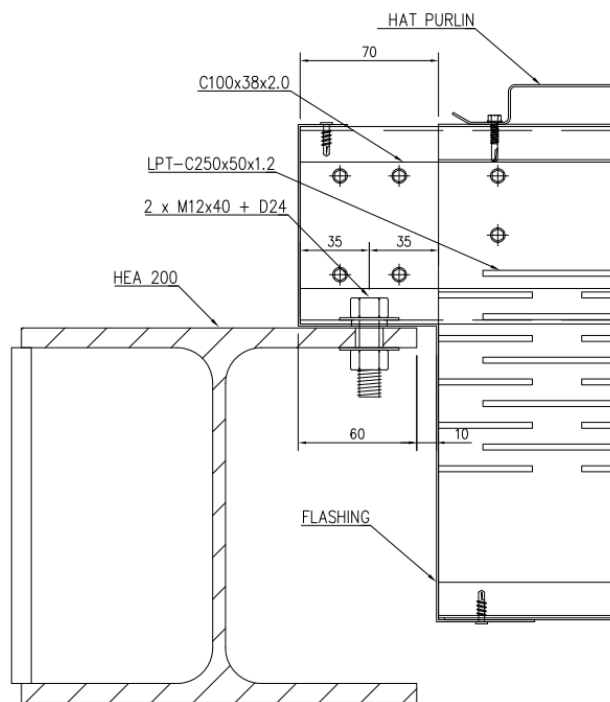
**Figure 3-3.** Forces acting upon the strips (cross hatched) between the slots in the web. (Thöyrä, 2001)

## 4 Experimental studies

### 4.1 Introduction

These experimental studies were done on four prototype elements, half the width of the intended element width. The test specimen were manufactured with certain assumptions and after the results were analysed some improvements were done to the roof element type. What is explained below is how the test specimen were manufactured and tested.

What made this type of roof element special was that the support was different from other types of roof elements. There a smaller non-slotted C-section out of thicker steel ( $t=2.0$  mm), which are placed inside the thermally slotted main section and fastened through the web. The thicker C-section, C100x38x2.0, suspends the thinner and higher main thermal purlin, LPT-C250x50x1.2, from the upper flange and upper part of web. This creates tension instead of compression in the web of the main thermal purlin and the support reactions are transferred to the thicker and stiffer C-section. Another thing, which was special for the test specimen was that the upper flange of the thermally slotted cold-formed sections was not directly restrained by any sheet, only by the hat-sections at a certain interval. Only the last test specimen was modified to reduce the buckling length of the upper flanges. Both the upper the C-sections at the support and the lower flange of the main thermal purlins are connected by a flashing, which prevents rotation around the length axis of the main purlins. See Figure 4-1. This arrangement is similar to the actual support, apart from the HEA200 beam substituting the WQ-beam, which is normally used as bottom chord on the roof truss. The HEA200 beams had a plate welded between the flanges on the opposite side of the fixation to simulate the double webs on the WQ-beam.



**Figure 4-1.** Support arrangement for experimental tests.

### 4.1.1 Objectives

The main objective for the experimental studies was to give a realistic idea of which failures might occur for this type of roof element. Secondary objectives were to check if the calculated capacities and deflections received from the primary FEM-model were close to the test results. Another secondary objective was to see if there were any unexpected problems at the support. The test was only planned to assist the dimensioning and not to dimension the actual elements. The snow load was considered dimensioning, which is why the specimens only were subjected to downward loading and not uplift loading.

### 4.1.2 Primary FEM-model

The initial idea was to create an FEM-model of the roof element and validate the results with the experimental tests. A primary FEM-model was created to assist the experimental testing and assess the maximum deflection before failure as well as the critical load. It was also to provide an understanding on what will occur during the testing, so that it would be easier to decide where to place gauges and help observe the right things.

The primary FEM-models were modelled using Dlubal's RFEM software version 4.10.1920 (hereafter referred to as RFEM). RFEM is a 3D structural engineering program, where you can model members, surfaces and solid elements. There were two models, one for each span. The elements were modelled with all the same structural parts as the test specimen.

The main purlins were made out of surfaces, both rectangular and quadrangular shape, taking into account corner radius of the cross-section. Openings were inserted, where the thermal slots were in the web. The surfaces were connected through members with the cross-section "Dummy Rigid". The member type was chosen based upon if it was only a contact point or if it represented a fastener. If it was a contact point, "Compression" was chosen and if it was a fastener, "Beam" was chosen. No node releases are set for either member.

All other profiles were also modelled as surfaces. This forms a small problem, as the surfaces are very thin, the stresses at a point may get very high if a contact area is only connected at one node. These areas are better modelled using several nodes, so that the stresses will be distributed more evenly over the whole contact area. The mesh size can also be smaller in these parts, and it is recommended that the surfaces are divided into smaller parts, so that only the required areas have finer mesh size and the areas with more uniform stress can have larger mesh size. Otherwise it will take longer for the calculations to run.

At the supports it was clear that the stresses will be concentrated, so there several nodal supports have been used. Most of these supports are only taking compressive vertical forces to simulate the contact surface between the supporting beam flange and the element. The only pinned support was where the bolts were located, which were released in the length-axis in one end of the element.



Vertical surface loads were applied on the hat-sections, where the dividing beams would be placed. All surface loads were equally big, assuming the dividing beams would distribute it equally on to the hat-sections. Only gravitational loading was applied in the primary FEM analysis.

RFEM gives the possibility to choose the plate bending theory. The options are either Mindlin or Kirchhoff. The difference between the two theories is that the Mindlin theory (also known as Reissner-Mindlin theory), which is based on the Timoshenko beam theory, takes into account the shear deformation. The Kirchhoff theory (also known as Poisson-Kirchhoff or Kirchhoff-Love theory), which is based on the Euler-Bernoulli theory, does not take into account the shear deformation. The Kirchhoff theory is applicable for thin plates, as transverse shear strains are usually very small in thin plates. The Mindlin theory is applicable for both moderately thick and thin plates.

As the structure was made of thin plates, either theory could be used. A comparison calculation was made with the same parameters apart from the theory, and the differences were basically not noticeable. The theory which was chosen for these analyses was the Kirchhoff theory as it was faster. (Aalto, 2009) (Hughes, 2000).

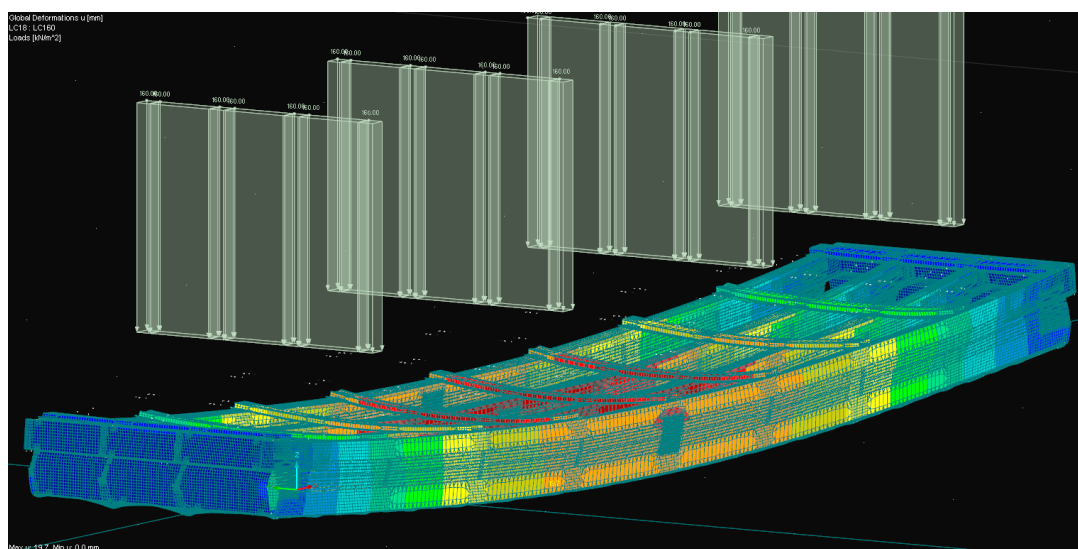
Nonlinear calculations in RFEM are based on two methods. There is an option that allows setting the percentage of load increments should be calculated with either method. The first load increments, assuming the percentage is not 0, are calculated according to the relatively strong Picard method. It helps avoiding instability problems, but the calculations are slower.

After the chosen percentage of load increments have been calculated the calculations are based on the Newton-Raphson method. There is no exact value or optimal percentage for switching from Picard to Newton-Raphson, but this switching should be performed when the first search direction for the Newton scheme is such that quadratic convergence is soon achieved. (Bergamaschi & Putti, 1999).

There is also an add-on module in RFEM, which is named RF-Stability. This module analyses the stability of the structure according to Eigenvalue Calculation Method. It checks the stability modes and critical load factors of the structure. This module was not used in the primary calculations. (Dlubal Software GmbH, 2013).

### **4.1.3 Primary FEM analysis and observations**

The deformation results from the primary FEM analysis seemed realistic as well as the equivalent stress distribution according to von Mises. The global deformation results can be seen in Figure 4-2.



**Figure 4-2.** Global deformation results for 5058 mm element span.

The maximum global deformation calculated for each span at the critical load is listed in Table 4-1. The maximum deformation is vertical and the load is converted to an evenly distributed surface load over the whole element. The surface load, which was used in the FEM-analysis was distributed on the hat-sections.

**Table 4-1.** Maximum global deformation and load for given span.

Span	Max. load	Max. deformation
[mm]	[kN/m <sup>2</sup> ]	[mm]
5058	11,7	27,9
6858	7,5	48,4

According to the primary FEM analysis, concentrated stress would arise at the corners of the slots, which would reach the yielding point. The out of plane deformation was also relatively big at both ends of the main purlins due to this stress. The supports were chosen as one of the main things of interest during the testing, especially for the shorter span, due to the assumed higher shear forces.

It was also of interest to see if the failures would be brittle or ductile. Ductile failure is preferred, as brittle failure is sudden and usually occurs without warning. Brittle failure in this type of structure is usually caused by shear failure in fasteners, as metal is a ductile material. The biggest risk for a brittle failure was at the support, where high stress levels were concentrated and transferred through self-drilling fasteners. According to the FEM-analysis, the shear forces at any given fastener near the support did not exceed the shear capacity of the fastener.

For thin-walled cold-formed steel there are some specific areas, which are more critical, than for hot-rolled steel cross-sections. Due to the small material thickness of the cold-formed steel the slenderness ratios are bigger. Cross-sections, which are thin, wide and exposed to compressive load, may buckle under fairly low loads, if they are not stiffened in any way. The occurrence of buckling was observed and recorded both by still pictures and video.

## 4.2 Test programme

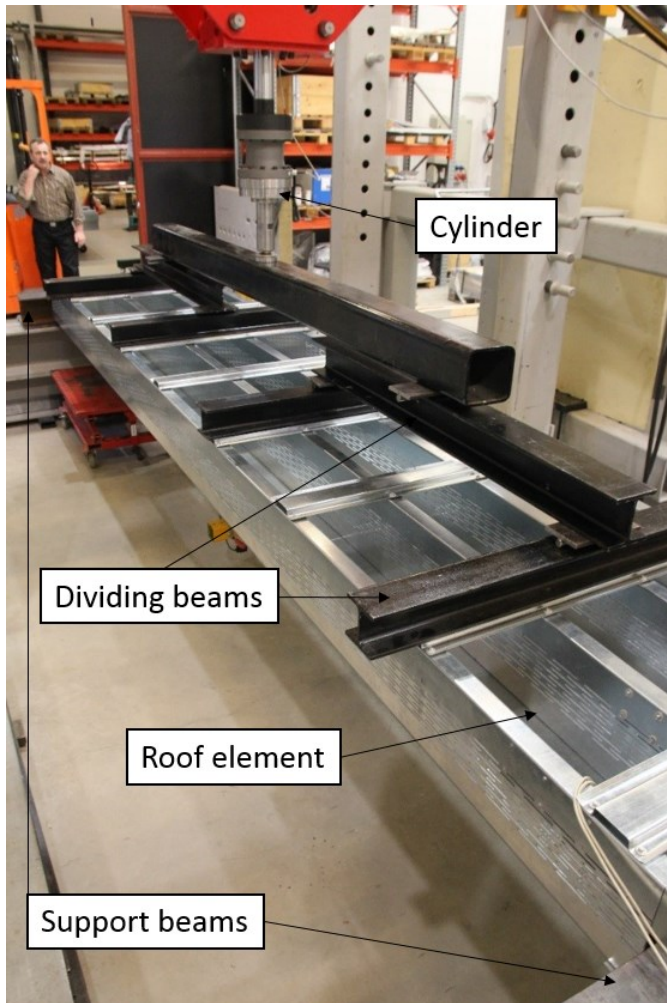
Experimental studies were carried out at the Sheet Metal Centre at HAMK University of Applied Sciences. A series of tests were done on elements with only half the width of an actual roof element, reducing the main purlins from seven to four. The tested elements did not contain any non-structural part, such as insulation or vapour barriers. The hat purlins on top of the element were also adjusted to the suit the loading arrangement and not the realistic conditions. EN 1993-1-3 Annex A was used to provide guidelines, but was not followed in every aspect.

The experimental studies started with two tests on elements for a 5.4 m structural module span. The latter two tests were carried out on elements for a 7.2 m structural module span. The structural module span is the centre to centre distance between the roof trusses. Some modifications to the tests were done after getting the results from the first tests.

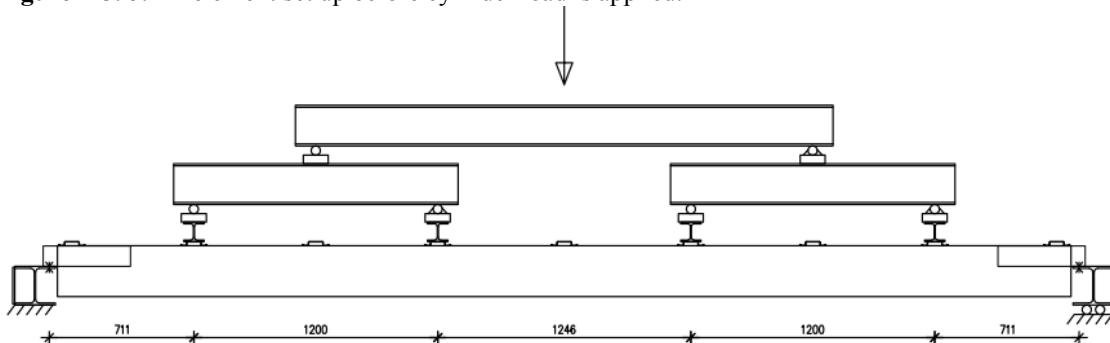
Bending tests were performed on all in all four elements under laboratory conditions. The load was applied by a cylinder as a point load and it was distributed using dividing beams to simulate an evenly distributed surface load. See Figure 4-3. For the shorter elements, 4 beams were applying load to the hat-purlins on the elements and for the longer elements, 8 beams were applying the load. The hat-purlins were placed to match the loading beams, but at a reasonable interval as shown in Figure 4-4 and Figure 4-5.

The length of each test took about 5-10 minutes, from applying the load through the cylinder to failure. The speed, which the cylinder extended itself, was chosen based on the assumed deflection before failure. At each interval of 0.5 s, the cylinder registered the amount of force applied by the cylinder and the displacement of the cylinder.

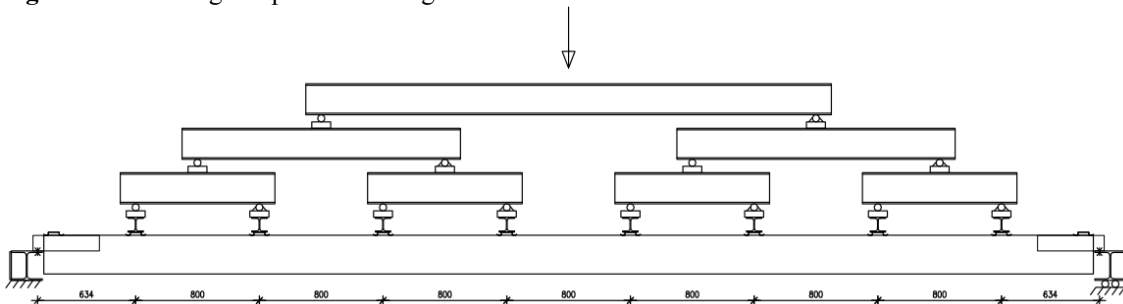
Initial measurements were taken at each gauge, before any of the dividing beams were placed on the element, as these also introduced a load on the element. The roof elements were subjected to their self-weight before these measurements could be taken. The load from the dividing beams and the load produced by the cylinder resulted in the total external load on the element.



**Figure 4-3.** 5.4M element set up before cylinder load is applied.



**Figure 4-4.** Loading setup with dividing beams on the 5.4M elements.



**Figure 4-5.** Loading setup with dividing beams on the 7.2M elements.

### 4.3 Test specimens

There were two types of elements. Each type has a different structural module span, but all elements consisted of the same parts as listed in Table 4-2, Table 4-3 and Table 4-4, apart from the additional top flange bracing of test specimen 7.2M-B2. The steel grade for all parts is S350GD+Z. The element span is shorter from the structural module span. The 5.4 m structural module span equals a 5058 mm element span (referred to as 5.4M hereafter) and 7.2 m structural module span equals a 6858 mm element span (referred to as 7.2M hereafter). The main purlins are 70 mm shorter than the element span. The width of each element was 950 mm. Test specimen 7.2M-B2 was braced with two additional steel strips at the top flange.

**Table 4-2.** Components of test specimens 5.4M-B1 and 5.4M-B2 (without top flange lateral bracing).

Components	Dimensions		Amount
Main purlin	Thermal purlins LPT-C250x50x1.2, 10 rows L = 4988 mm		4 pcs
Support profiles	C-sections C100-38x2.0, L = 430		8 pcs
	Closure flashing 1.0, L = 950		2 pcs
Upper flange restraint	Hat purlin, h=20 mm, t=1.2 mm, L= 950 mm, c/c ~600 mm		9 pcs
Lower sheeting	PL1.0x950x1250		c/c 1200
Self-drilling fasteners	Purlin-lower sheet	4.8x16	4 pcs/ c/c 300
	Purlin-hat purlin	5.5x28	2 pcs / joint
	Purlin-support profile	5.5x28	2 pcs/ c/c 100

**Table 4-3.** Components of test specimen 7.2M-B1 (without top flange lateral bracing).

Components	Dimensions		Amount
Main purlin	Thermal purlins LPT-C250x50x1.2, 10 rows L = 6788 mm		4 pcs
Support profiles	C-sections C100-38x2.0, L = 430		8 pcs
	Closure flashing 1.0, L = 950		2 pcs
Upper flange restraint	Hat purlin, h=20 mm, t=1.2 mm, L= 950 mm, c/c ~800 mm		10 pcs
Lower sheeting	PL1.0x950x1250		c/c 1200
Self-drilling fasteners	Purlin-lower sheet	4.8x16	4 pcs/ c/c 300
	Purlin-hat purlin	5.5x28	2 pcs / joint
	Purlin-support profile	5.5x28	2 pcs/ c/c 100

**Table 4-4.** Components of test specimen 7.2M-B1 (with top flange lateral bracing).

Components	Dimensions		Amount
Main purlin	Thermal purlins LPT-C250x50x1.2, 10 rows L = 6788 mm		4 pcs
Support profiles	C-sections C100-38x2.0, L = 430		8 pcs
	Closure flashing 1.0, L = 950		2 pcs
Upper flange restraint	Hat purlin, h=20 mm, t=1.2 mm, L= 950 mm, c/c ~800 mm		10 pcs
	Steel strip PL50x1.0, L1140		2 pcs
Lower sheeting	PL1.0x950x1250		c/c 1200
Self-drilling fasteners	Purlin-lower sheet	4.8x16	4 pcs/ c/c 300
	Purlin-hat purlin	5.5x28	2 pcs / joint
	Purlin-support profile	5.5x28	2 pcs/ c/c 100

The theoretical self-weight of the 5.4M elements was 138.3 kg and 178.6 kg for the 7.2M elements. This equals a line load of 0,267 kN/m for the 5.4M elements and 0,255 kN/m for the 7.2M elements.

### 4.3.1 Deviations and imperfections

Even though each type of element was manufactured based on the same manufacturing drawings, (see Appendix 4) the elements were not identical and there were deviations from the manufacturing drawings.

Test specimen 5.4M-B1 had a total length of 5139 mm, which was 9 mm longer than specified on the erection drawing. It seemed that the C-sections and L-angles at the support were too long and had been cut after installation, cutting the self-drilling fastener even. See Figure 4-6.

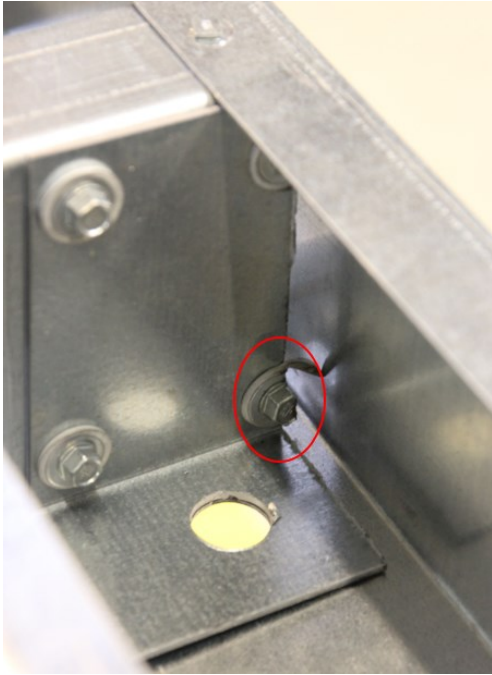
Test specimen 5.4M-B2 had a total length of 5150 mm, which was 20 mm longer than the specified length. The end flashing should have been 70 mm wide at the support, but was measured to 78 mm. This resulted in that the total height was less than 253 mm and when the element was tightened to the support it created pre-stress in the web. This caused an initial horizontal displacement of the webs of approximately 10-20 mm at the support. See Figure 4-7.

Both 7.2M test specimens had a total length of approximately 6940 mm, which was 10 mm longer than specified on the erection drawing. It seemed that there had been problems with the tolerances of the end flashings and each end was 5 mm too long.

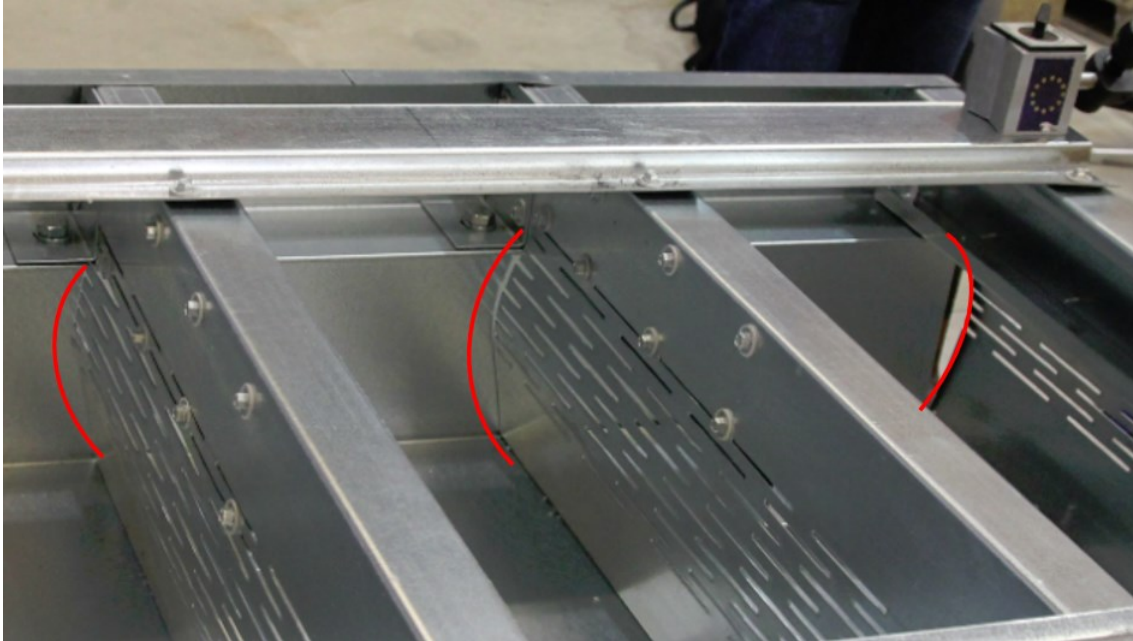
Some fasteners that were on the erection details were also missing at the support. There should have been four fasteners through the flange of the main purlins to the C-sections, but only 2 were present where the hat profiles were fastened and not in the other end where they would have taken tension. Instead the moment was only transferred through the shear resistance of the fasteners in the web.

The C-sections at the support were also mostly missing fasteners through the end flashing on the lower side. In one or two corners there were fasteners, but not at each corner and without any consistency. Edge distances for fasteners were not according to details, they were considerably less in most places.

Both 5.4M elements had only 5 out of 9 hat purlins in the correct locations. The deviations were approximately 45 mm. The hat purlins, which were subjected to the line load, were moved to the correct position according to Figure 4-4. This left eight old fastener holes in the top flange of both elements. The width of the elements varied from 945-950 mm.



**Figure 4-6.** L-angle fastened to C-section at the support.



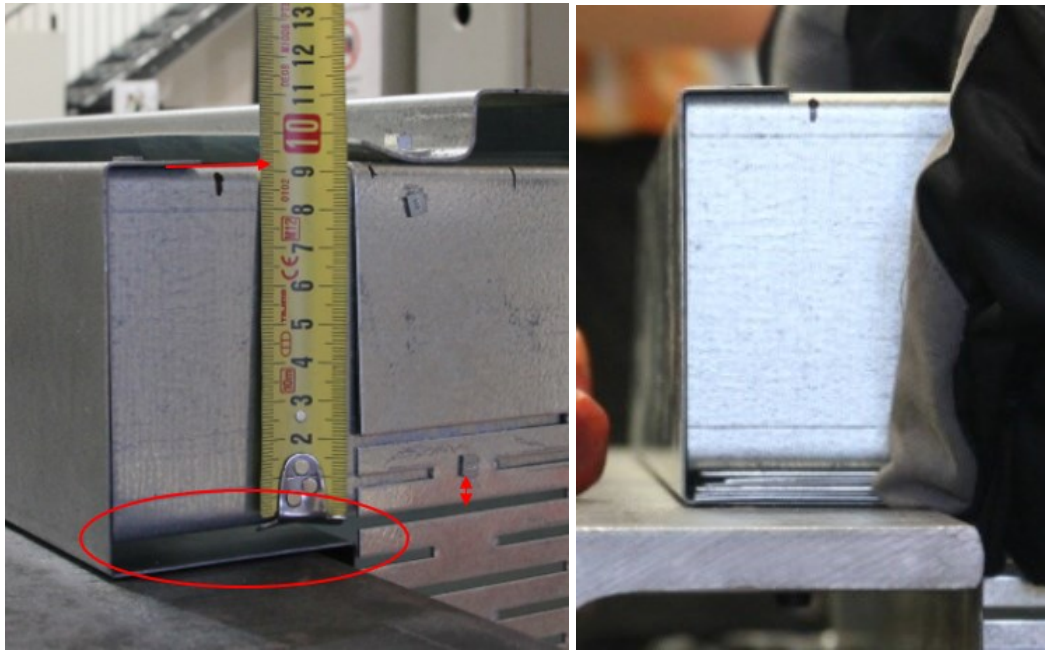
**Figure 4-7.** Pre-stress and deformation after tightening the 5.4M-B2 element to the support. No load applied.

On element 7.2M-B1, there was one C-section at the support that had a height of almost 10 mm less than the rest. To avoid having this interfering with the results, thin slices of metal sheets were stacked in between the support profile and the end flashing. See Figure 4-8.

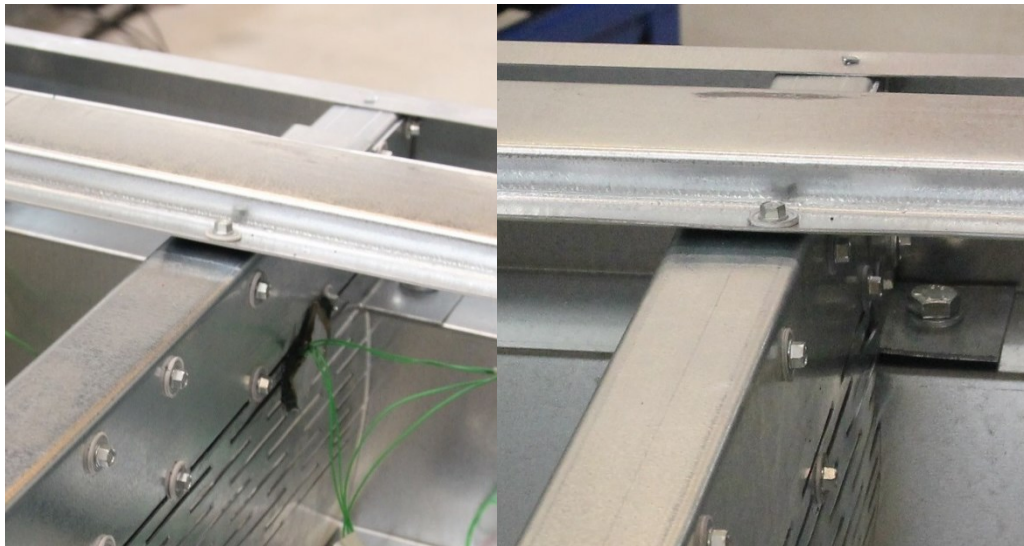
Another notice was that test element 5.4M-B1 had the fasteners between the hat purlins and the main purlins relatively centred on the main purlin flange according to manufacturing details, while on test elements 5.4M-B2, 7.2M-B1 and 7.2M-B2 the fasteners were much closer to the web. See Figure 4-9. This created a much smaller moment capacity of the joints between the hat purlins and the main purlins. As the results from the second and third test indicated that this had a significant impact on the ultimate load, the top flange of the last element, 7.2M-B2, was braced to reduce the buckling length and prevent lateral torsional buckling.

The edge distances for fasteners were also neglected in the manufacturing phase and fasteners were placed in between the slotted holes, as shown in Figure 4-8 and Figure 4-9. According to the manufacturing details the lower row of fasteners between the slotted web and the web of the support C-section should have been 20 mm.





**Figure 4-8.** C-section at support on element 7.2M-B1. Metal sheets were stacked under the profile.



**Figure 4-9.** Fasteners at support. 5.4M-B1 to the left and 5.4M-B2 to the right.

After the loading of both 5.4M elements a few fasteners between the bottom flange and steel sheet were removed and it became apparent that the sheets had been glued to the main purlins at some locations. The glue was only spread out on small areas, and should not have big influence on the results. The bottom sheet was made out of several sheets, which were overlapped. See Figure 4-10.

All the deviations and imperfections are listed in Table 4-5. The ones that may have significant impact on the structural capacity are items c, d and g. The primary FEM-model had also a continuous metal sheet attached to the bottom flange of the main purlins and has some impact on the results. The pre-stress at the support will affect the stress distribution, but should not have significant impact on the ultimate capacity. Some deviations were corrected before the tests were started. Other deviations and

inaccuracies should have very small impact on the ultimate capacity of the test specimen. The element length deviation is less than 0.5% on all elements



**Figure 4-10.** Overlap of bottom sheets on 5.4M-B1.

**Table 4-5.** Deviations and imperfections

- a. Total length of element
- b. Pre-stress at support
- c. Missing fasteners
- d. Small or no edge distance for fasteners
- e. Placement of hat-sections, corrected
- f. Support C-section 10 mm to low, shim plates inserted
- g. Hat-section to main purlin fasteners placed too close to main purlin web
- h. Bottom steel sheet not continuous over span and glued to the main purlins

#### 4.4 Set-up of test apparatuses and testing procedures

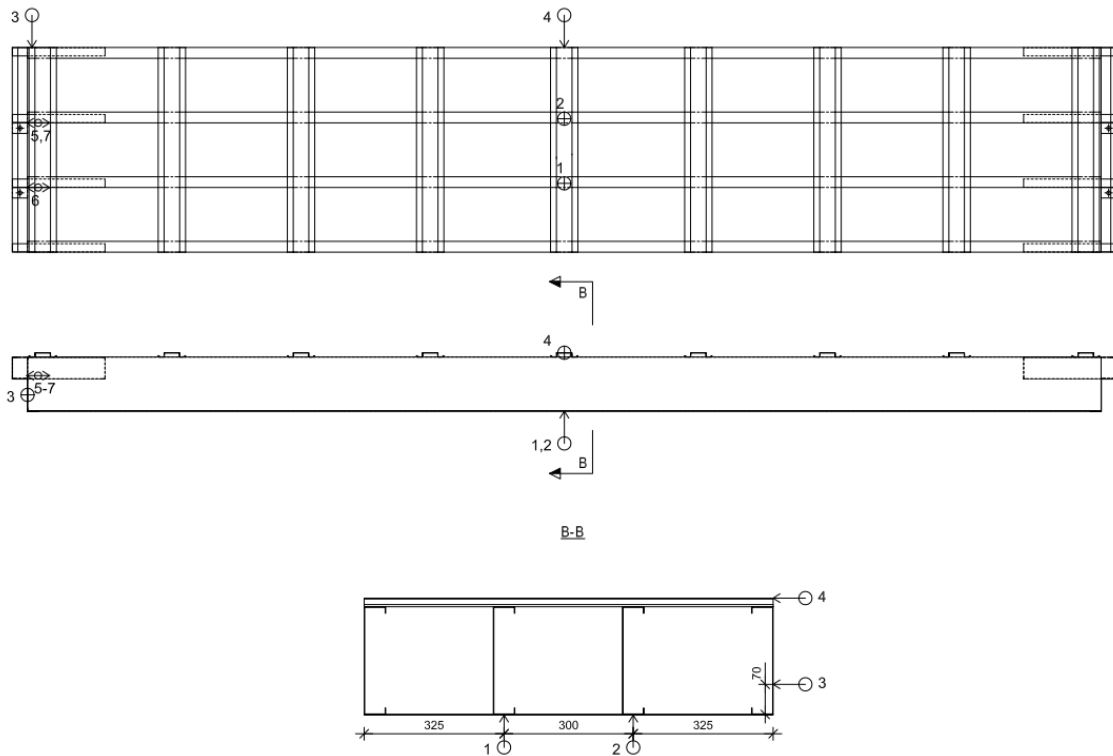
Each element was bolted with grade 8.8 M12 bolts, snug tight, to a HEA200 beam at each support. The HEA200 beams were fixed to the concrete slab, but the bolts were placed in the centre of the oversized holes in the element, allowing for a relative horizontal movement.

As each element was fixed between the supports the displacement transducers and strain gauges, shown in Figure 4-11, were positioned according to Figure 4-12, Figure 4-13 and Figure 4-14. Displacement transducers measured the vertical displacement in the middle of the span and the difference between the displacements indicated if the element was level or not (see Figure 4-11). Transducer #3 measured the horizontal displacement of the web at the support. This gave an indication of the stress level at the support based on the preliminary FEM model. The global horizontal displacements of the elements near the middle of the span were measured with a fourth transducer. The transducer was placed on top of the hat profile for the 5.4M elements, and on a transverse dividing beam for the 7.2M elements to reduce the effect of any local rotation at the measurement point.

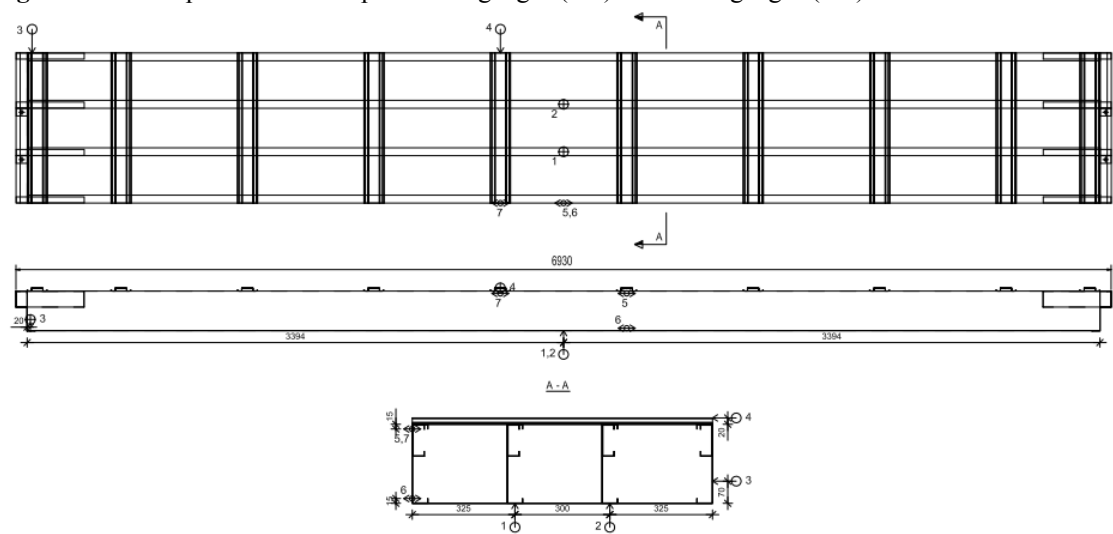
The strain gauges, #5, #6 and #7, were only placed on the first of the 5.4M elements and on both 7.2M elements. The positions of the strain gauges were adjusted in between the tests to get results, which were useful. On the first 5.4M element, the strain gauges were placed close to the support as shown in Figure 4-12 and Figure 4-15. They were to give a better indication of the stresses at the support, but due to the complexity of the slotted web, the major axis of the stresses change within millimetres, so the results were not conclusive. Due to this the strain gauges were shifted towards the middle of the span, where the stresses are more evenly distributed. In test 7.2M-B1, the gauges were placed beneath the two most centred hat-purlins as shown in Figure 4-13 and Figure 4-16. For the last test, 7.2M-B2, two of the gauges were moved to the centre of the span, to avoid interference from the local transverse force from the dividing beam, but the last gauge was kept in the same location as in the previous test for comparison. See Figure 4-14 and Figure 4-17.



**Figure 4-11.** Displacement transducers 1-2 to the left, 3-4 in the centre and strain gauges 5-7 to the right on test specimen 5.4M-B1.

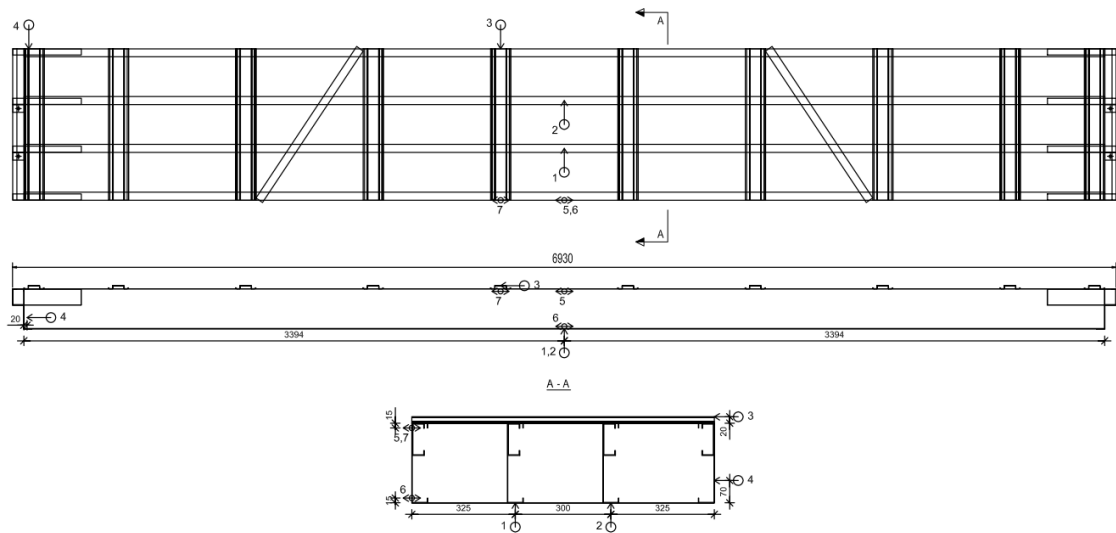


**Figure 4-12.** The placement of displacement gauges (1-4) and strain gauges (5-7) on 5.4M elements.

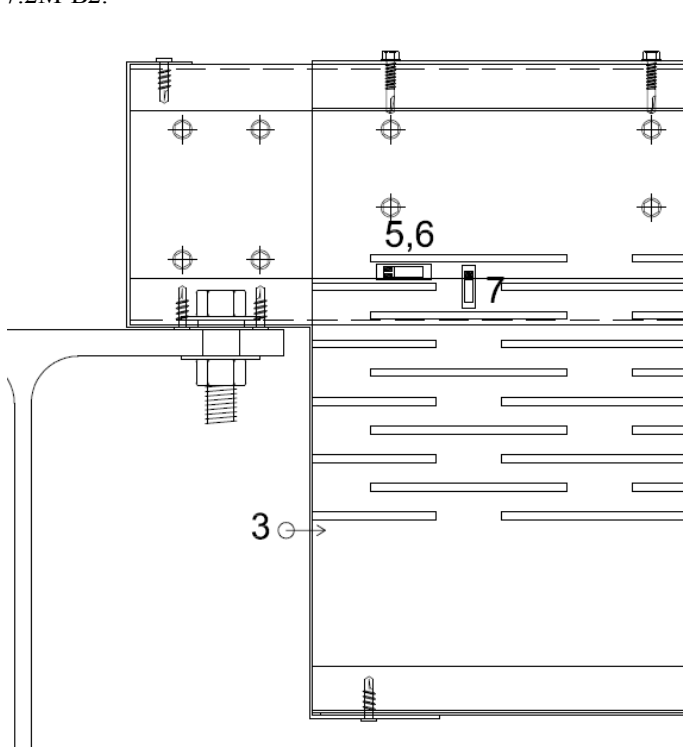


**Figure 4-13.** The placement of displacement gauges (1-4) and strain gauges (5-7) on element 7.2M-B1.

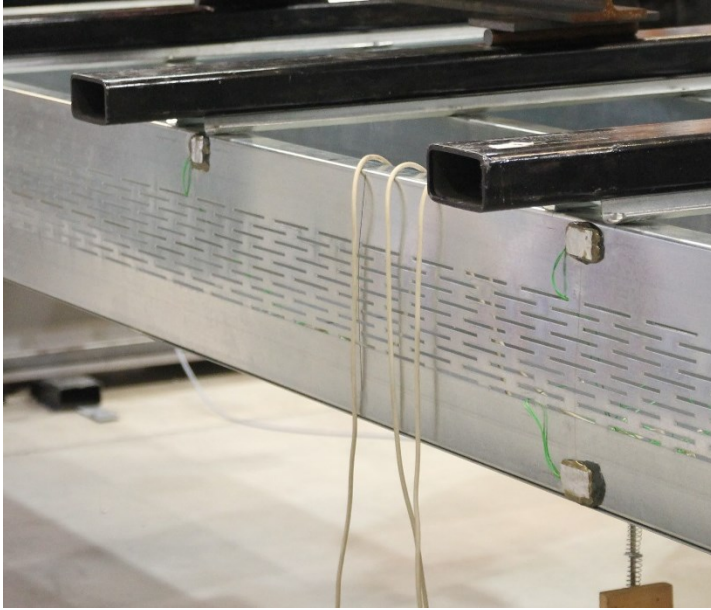




**Figure 4-14.** The placement of displacement gauges (1-4) and strain gauges (5-7) on braced element 7.2M-B2.



**Figure 4-15.** Strain gauges placed below the first row of slots from the top on test specimen 5.4M-B1.



**Figure 4-16.** Three strain gauges placed below the hat profiles closest to the centre of the span, two 15 mm from the upper and lower flanges on the right and one 15 mm below the upper flange on test specimen 7.2M-B1.

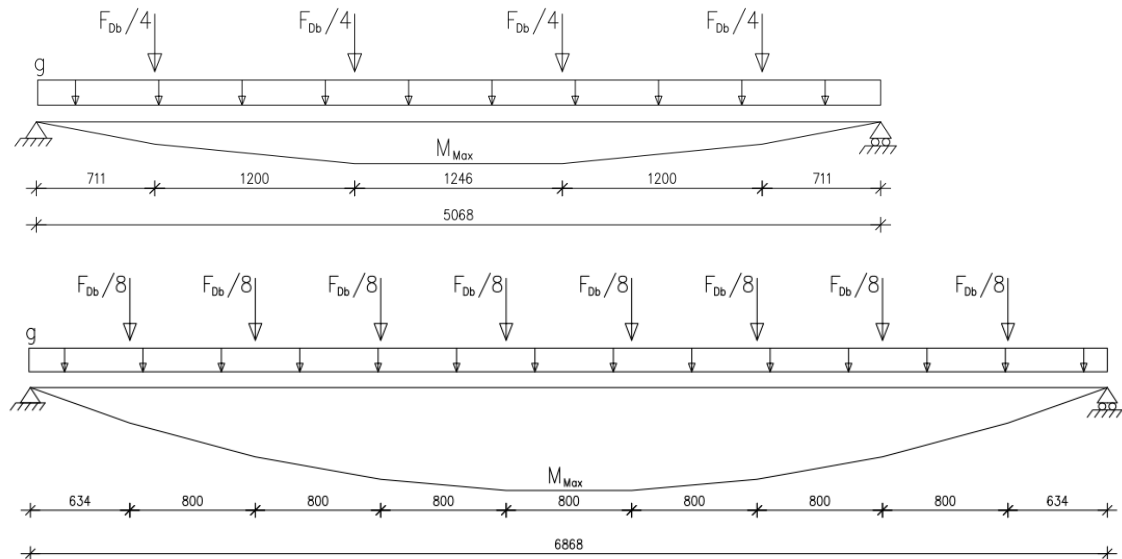


**Figure 4-17.** Two strain gauges placed in the middle of the span, 15 mm from the upper and lower flanges on test specimen 7.2M-B2. One strain gauge was also placed below one of the hat profiles closest to the centre of the span 15 mm from the upper flange as on test specimen 7.2M-B1.

The self-weight were 137.3 kg for the 5.4M roof elements and 178.6 kg for the 7.2M elements. The self-weight has been assumed as an evenly distributed load  $g$  over the span, even though more material was concentrated near each support. The impact of the self-weight is very small, and this is why the concentration of the self-weight has been ignored. The total weight of the dividing beams on the 5.4M-elements were 263.5 kg, adding an initial load  $F_{Db} = 2.585$  kN on the elements before the cylinder load was applied. For the 7.2M-elements the weight of the dividing beams was 564.2 kg, adding an initial load  $F_{Db} = 5.53$  kN. Each dividing beam was carefully placed one by one on the elements and the measured and adjusted in to place.

The initial loading and the moment distribution before the cylinder load was applied can be seen from Figure 4-18. The initial moment in the middle of the span was 2.55 kNm for the 5.4M elements and 6.58 kNm for the 7.2M elements.

Each test was recorded on video for later playback. The video camera was set up so that it shows the element from the side at the middle of the span. During the first test the support was also recorded on video with a handheld camera.



**Figure 4-18.** Initial loading and moment distribution. 5.4M on top, 7.2M below.

## 4.5 Test results

### 4.5.1 Load capacities

The ultimate load applied on each test specimen is shown in Table 4-6. It was assumed that the load was distributed equally on each purlin, as the dividing beams were much stiffer than the cold-formed sections. The maximum moment was calculated at the centre of the span as a result of the point loads on the purlins.

**Table 4-6.** Applied loads before failure on each test specimen and maximum bending moment per purlin.

Element	Self-weight g	Dividing beams F <sub>Db</sub>	Cylinder load P	Total load	Max bending moment per purlin	Point load under hat purlin
Nr.	[kN/m]	[kN]	[kN]	[kN]	[kNm]	[kN]
5.4M-B1	0,268	2,585	30,520	34,462	5,640	2,069
5.4M-B2	0,268	2,585	26,380	30,322	4,962	1,810
7.2M-B1	0,255	5,530	14,540	21,822	4,977	0,627
7.2M-B2	0,255	5,530	18,300	25,582	5,839	0,745

### 4.5.2 Deformation and failure modes

During the experimental testing, each test was observed and recorded using still photo and video camera. The ultimate failure mode was analysed based on what was observed right before the load on the test specimen did not increase any further and what could be observed on the test specimen after failure. The results of the displacement gauges were also analysed before determining the ultimate failure mode. Other observations were also made before and after ultimate failure, but as long as the test specimen has been able to take increased load post-buckling, this mode has not been considered as the ultimate failure mode, instead this has been called a deformation mode. Table 4-7 shows the deformation modes that occurred on each test specimen with a lower case “x” and the ultimate failure modes for each test specimen are marked with a capital “X”. A failure, which was a result of an ultimate failure has been marked with an “(X)”. The observations are also explained below.

**Table 4-7.** Deformation and failure modes observed during testing on each test specimen.

Deformation modes	Buckling				Shear		Crippling
	Local	Transverse load	Distortional	Lateral torsional	Elastic	Plastic	
5.4M-B1	x	(X)	X		x	x	
5.4M-B2	x		x	X <sup>(*)</sup>	x	x	
7.2M-B1	x		x	X <sup>(*)</sup>	x		
7.2M-B2	x	(X)	X		x		

<sup>(\*)</sup> The upper flange was not braced with a diaphragm and differs from the final product.



#### 4.5.2.1 Local buckling

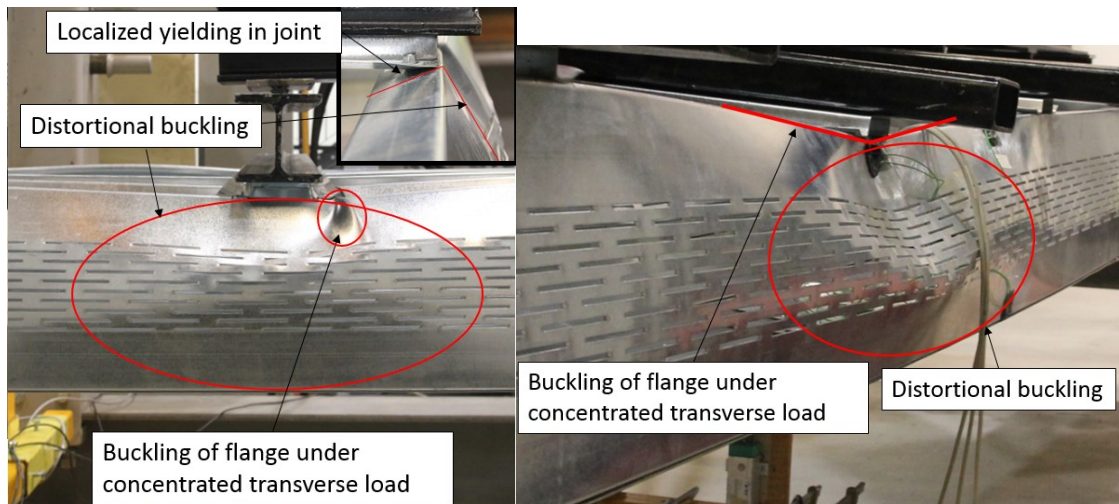
Local elastic buckling was visible on each of the test specimens at a very small load. Local buckling was not visible after the dividing beams were set up, but the shorter elements showed first signs of local buckling at a cylinder load of 5-7 kN. On the longer elements it was visible even earlier. The upper part of the web, which was compressed, shows small half-wave lengths as can be seen in Figure 4-19. The local buckling occurs on several places along the length of the profile with an interval which was much smaller than the centre to centre distance of the hat profiles. These were not as easy to notice as the distortional waves, which occurred at the same location at higher loads, but with clearly longer wave-lengths.



**Figure 4-19.** Local elastic buckling of upper parts of web in the middle of span of test specimen 7.2M-B1 at a cylinder load of 2-3 kN.

#### 4.5.2.2 Buckling of flange under concentrated transverse load

The top flange of two test specimen buckled vertically, while rotating around the length axis as a result of distortional buckling of the cross-section under the hat profiles nearest to mid span. The buckling of the web reduces the vertical support of the flange and increased the rotation. It also increased an eccentricity of the load. This lead to a buckling failure of both the web and the top flange. This occurred at the same time as the load carrying ability of the test specimen decreased. Figure 4-20 shows how the web has a buckling half-wave length greater than the height of the section and how the flange has buckled with a relatively sharp angle where the load was applied. The figure also shows that the hat-section to main purlin joint has failed on test specimen 5.4M-B1, as yielding has occurred. This means that the rotational restraint of the main purlin also has reached its limit. This again has induced the distortional buckling of the main purlin.



**Figure 4-20.** Buckling of top flange after failure on the distorted cross-section on test specimen 5.4M-B1 to the left and 7.2M-B2 to the right.

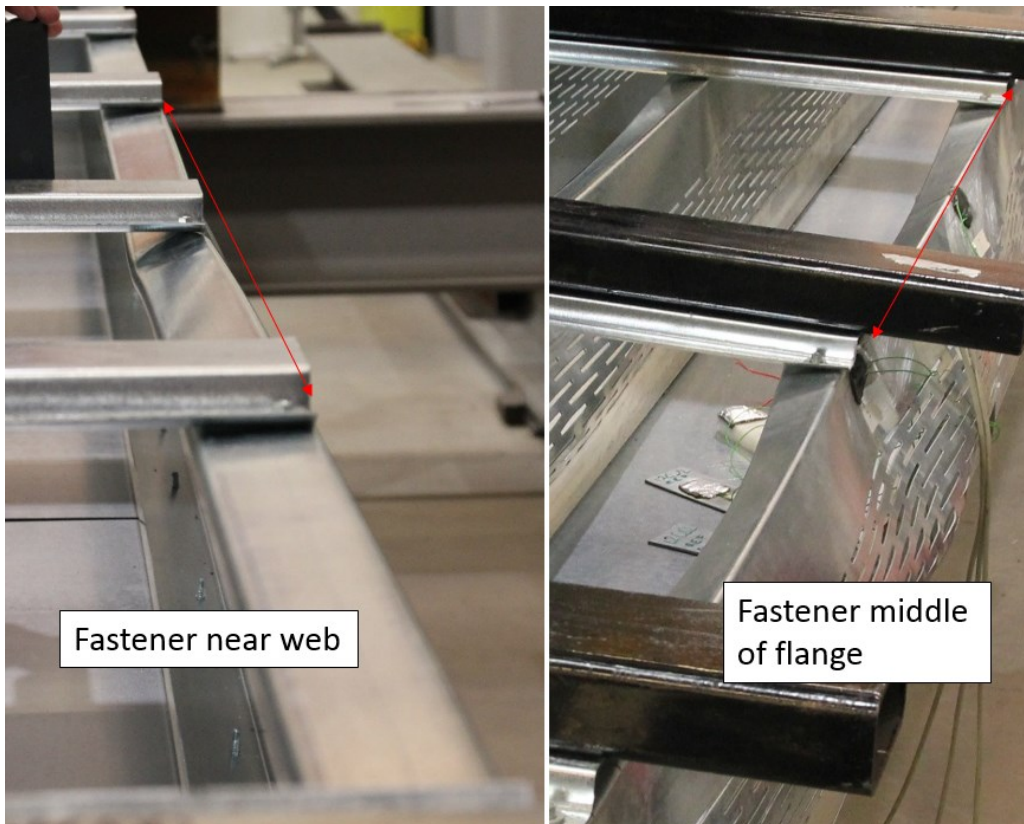
#### 4.5.2.3 Distortional buckling

Distortional buckling occurred on all test specimens in the mid span and can be considered the main failure mode for two of the test specimen. The distorted area was clearly shorter on the 5.4M elements, consisting of only one half-wave and confined to only approximately 1.2 m, whereas the 7.2M elements showed several distortional waves over a longer area as can be seen in Figure 4-21.

The half-wave length of the distortional buckling seemed to be very dependent on the rotational restraint at the upper flange of the main purlins. This can be seen in Figure 4-22, where the red arrow indicates the half-wave buckling length.



**Figure 4-21.** Distortional buckling waves in web and top flange on test specimen 7.2M-B1 nearing ultimate failure.

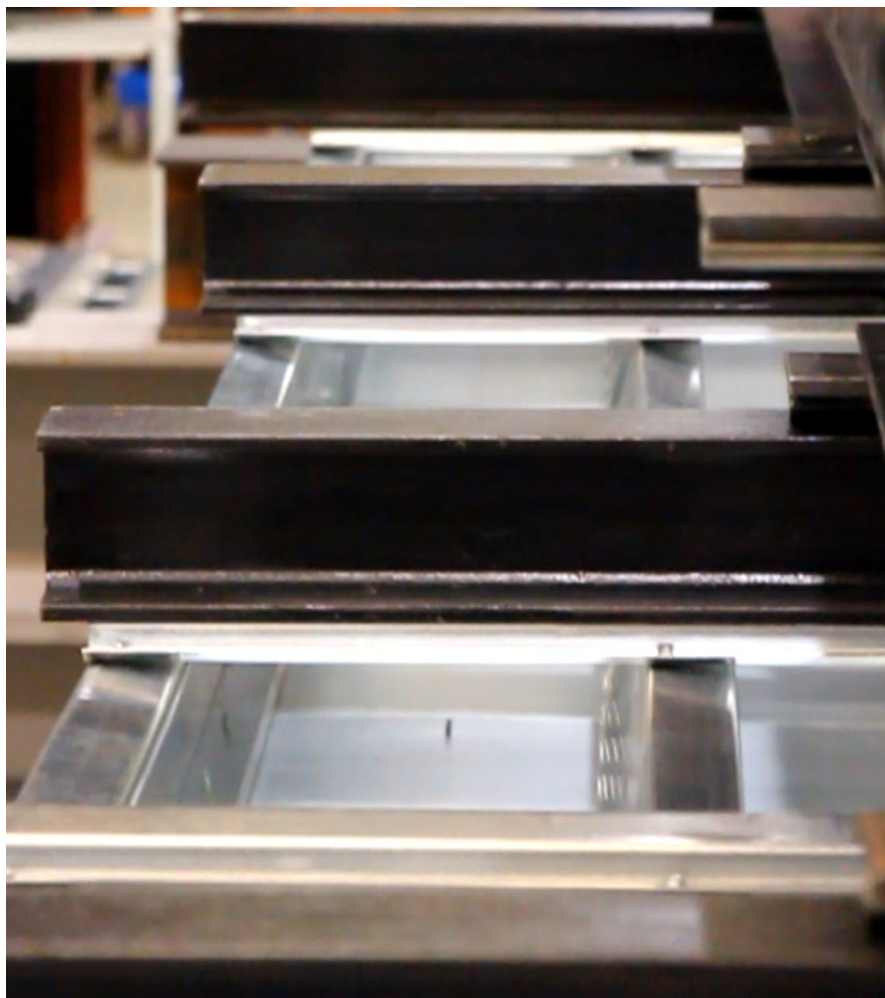


**Figure 4-22.** Distortional buckling half-wave length of top flange depending on fastener position in top flange. From the left test specimen 5.4M-B2 and 7.2M-B2 after failure.



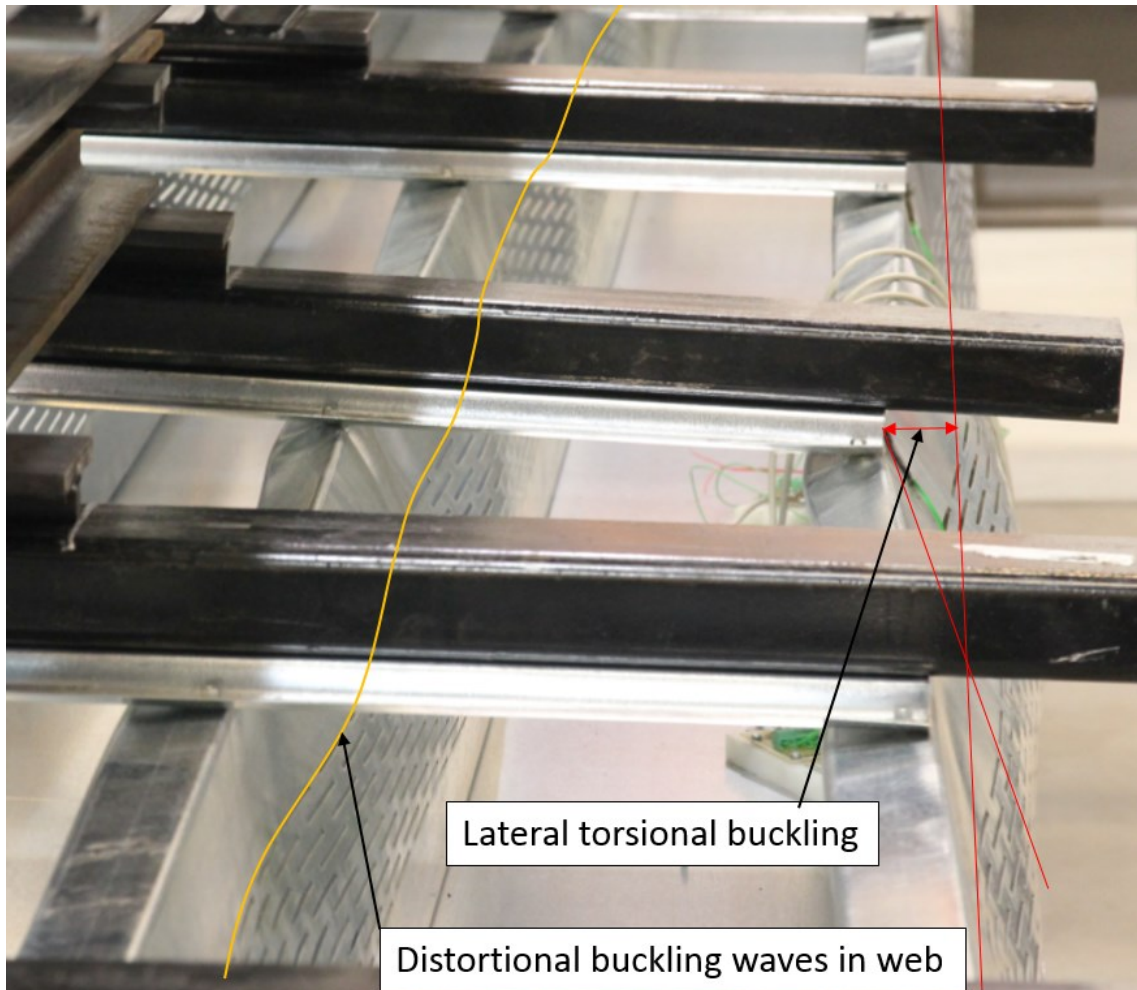
#### 4.5.2.4 Global buckling

Global buckling occurred on two test specimen in form of lateral torsional buckling (LTB). As the load was applied on element the top flanges showed clear torsional buckling with a half-wave length equal to the element span. The cross-section twisted around the length axis, apart from the bottom flange, which was restrained by the bottom sheeting. The failure was not sudden, but the load slowly decreased, even though the cylinder displacement was still increasing. At the same time there were distortional buckling visible in the upper parts of the web, but the half-wave length of the top flange shows that LTB was the ultimate failure mode. See Figure 4-23.



**Figure 4-23.** LTB of main purlins. Buckling half-wave length equal to the element span of test specimen 5.4M-B2.

One of the specimens showed some interaction between LTB and distortional buckling after failure. The web and top flange of the main purlins showed clear continuous medium size half-waves lengths equal to the hat purlin interval, but at the same time the cross-section was clearly twisted and the top flange showed a lateral half-wave with the length of the element span as Figure 4-24 shows. The joint between the hat-section and the main purlin had also failed at several locations, resulting in noticeable rotational deformation, which can also be seen in Figure 4-24.

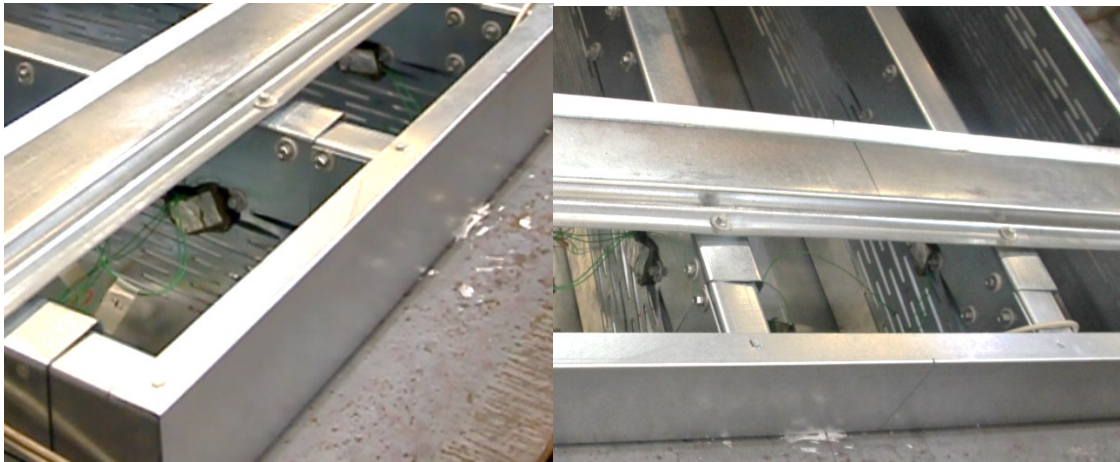


**Figure 4-24.** LTB over the full element span and distortional buckling half-waves between the hat profiles on test specimen 7.2M-B1 after failure.

The braced test specimen 7.2M-B2 did not show signs of LTB, despite the longer span. The test specimen differ from the final product, as the final product as a horizontal diaphragm.

#### **4.5.2.5 Shear deformations at supports**

Shear deformations occurred especially for the 5.4M test specimen. These showed significant deformations at cylinder loads from 15 to 30 kN and can be seen in Figure 4-25. At the supports the small strips between the slotted holes showed that plastic deformations had taken place as shown in Figure 4-26. These occurred due to the high shear forces at the supports of the 5.4M test specimen, but was not visible on the 7.2M test specimen despite the pre-stress on some test specimen. All test specimen showed ductile behaviour and none of the fasteners had failed, nor were there any signs of brittle failure at the supports.



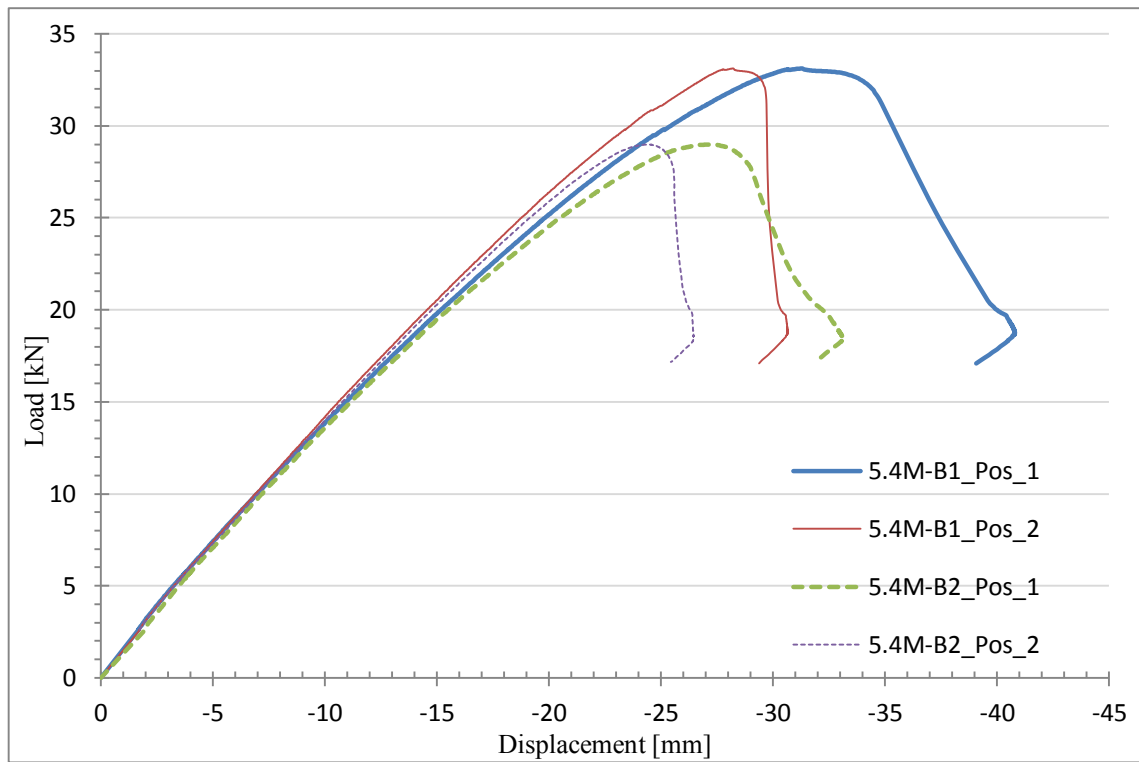
**Figure 4-25.** Shear stress cause big deformations in the web at the support of element 5.4M-B1 during a cylinder load of 15-30 kN.



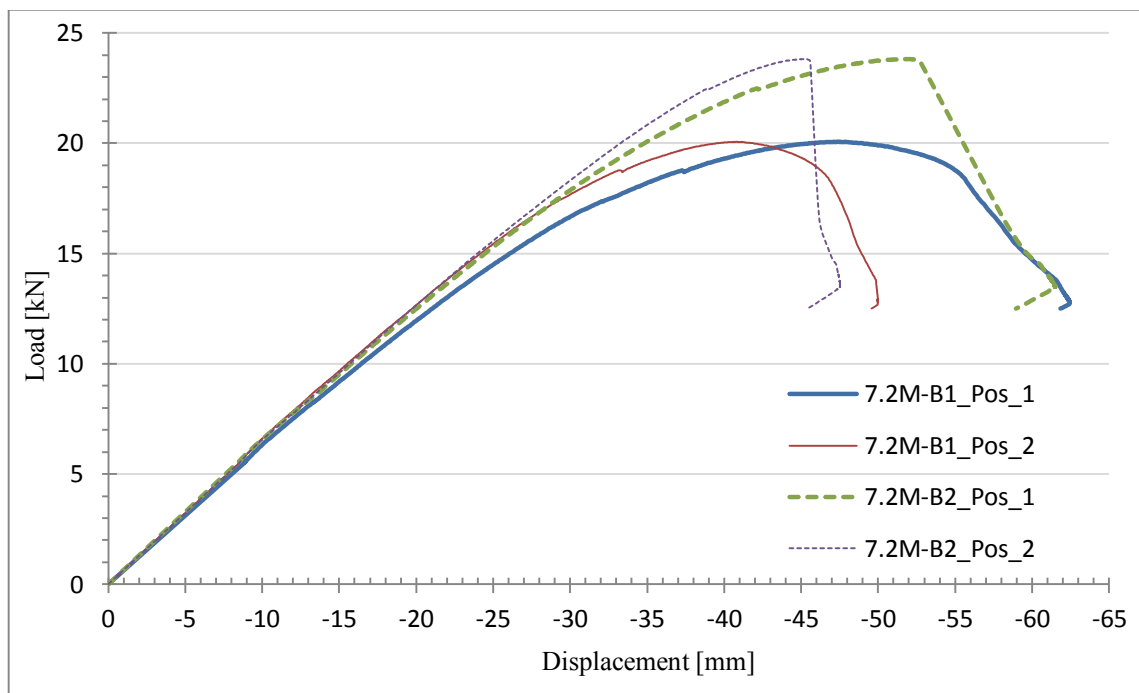
**Figure 4-26.** Plastic deformations at the support after cylinder load removed on test specimen 5.4M-B1.

### 4.5.3 Displacements and strains measured

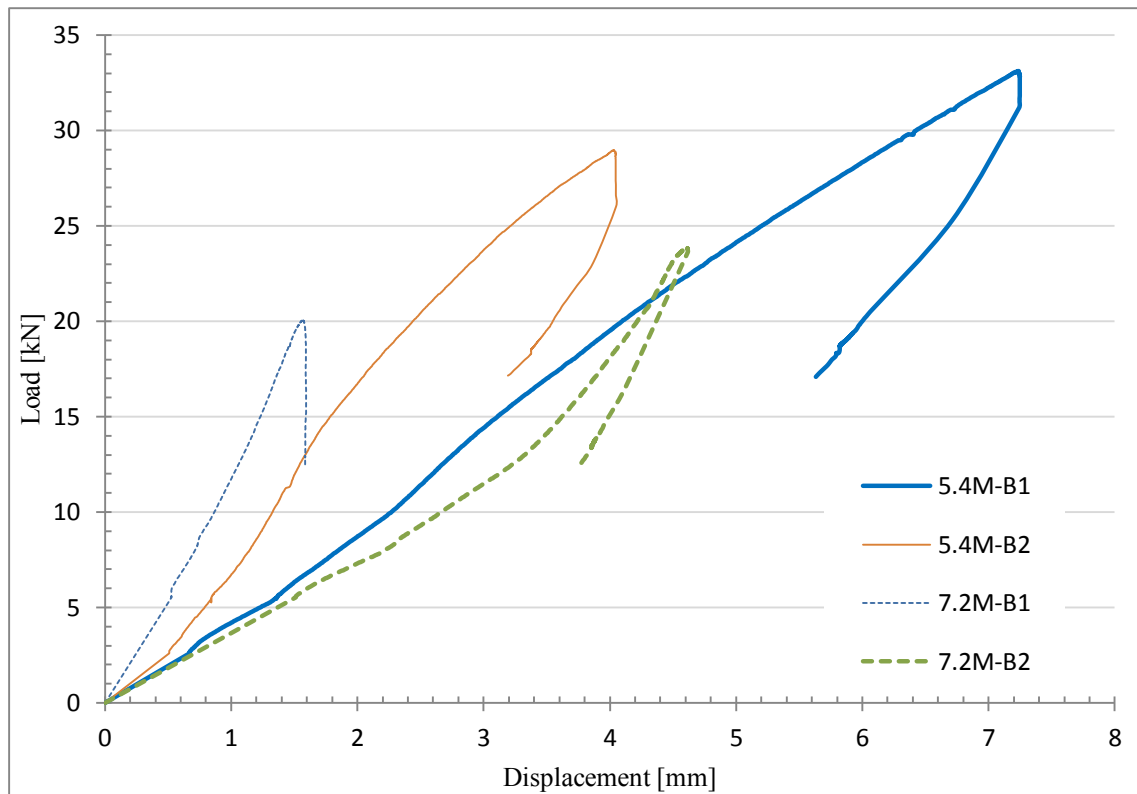
Figure 4-27 to Figure 4-30 show the load-displacement curves, where the x-axis represents the displacement measured at the given transducer position and y-axis represents the total load including the weight of the dividing beams. The displacements are reset before applying dividing beams, but the log was started as the cylinder load was applied. This is why the data is linear up to the load equalling the dividing beams. The self-weight of the test specimen was excluded from the total load in the graphs, as the elements were subjected to it before all the gauges were positioned and reset.



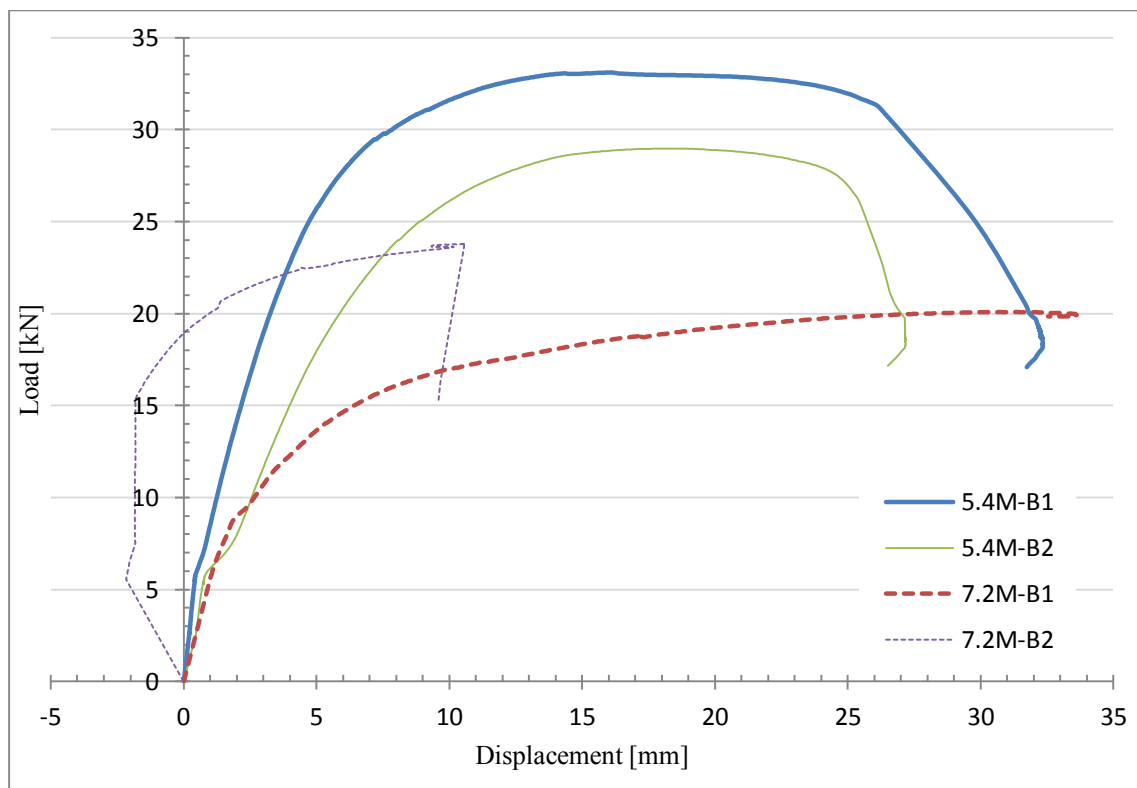
**Figure 4-27.** Load versus vertical displacement at gauges #1 and #2 for roof element type 5.4M.



**Figure 4-28.** Load versus vertical displacement at gauges #1 and #2 for roof element type 7.2M.



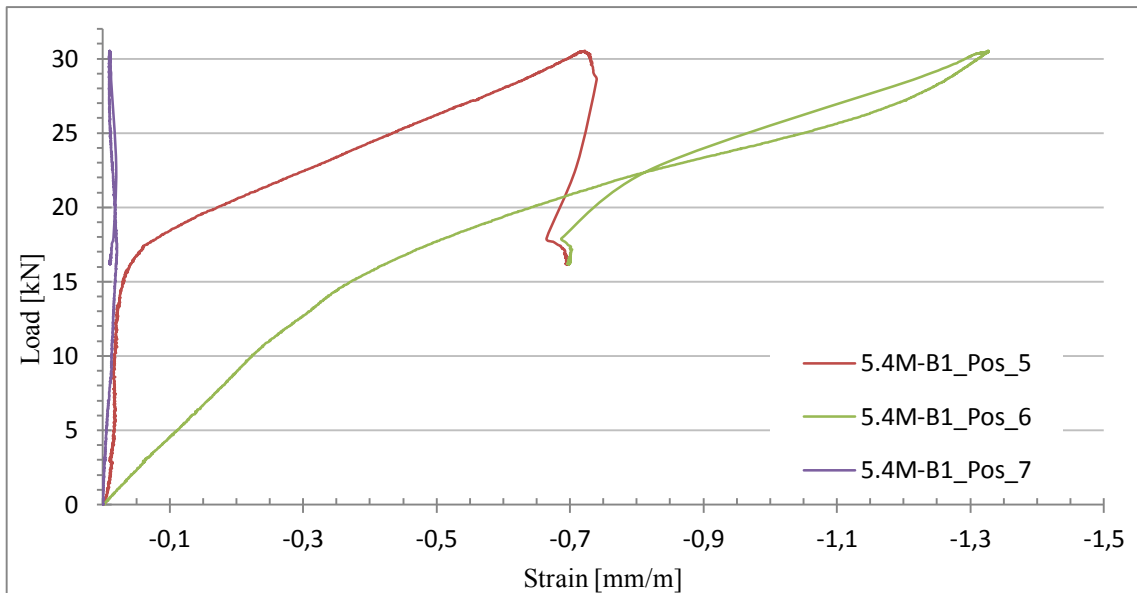
**Figure 4-29.** Load versus horizontal displacement for gauge #3 at the support for all test specimen.



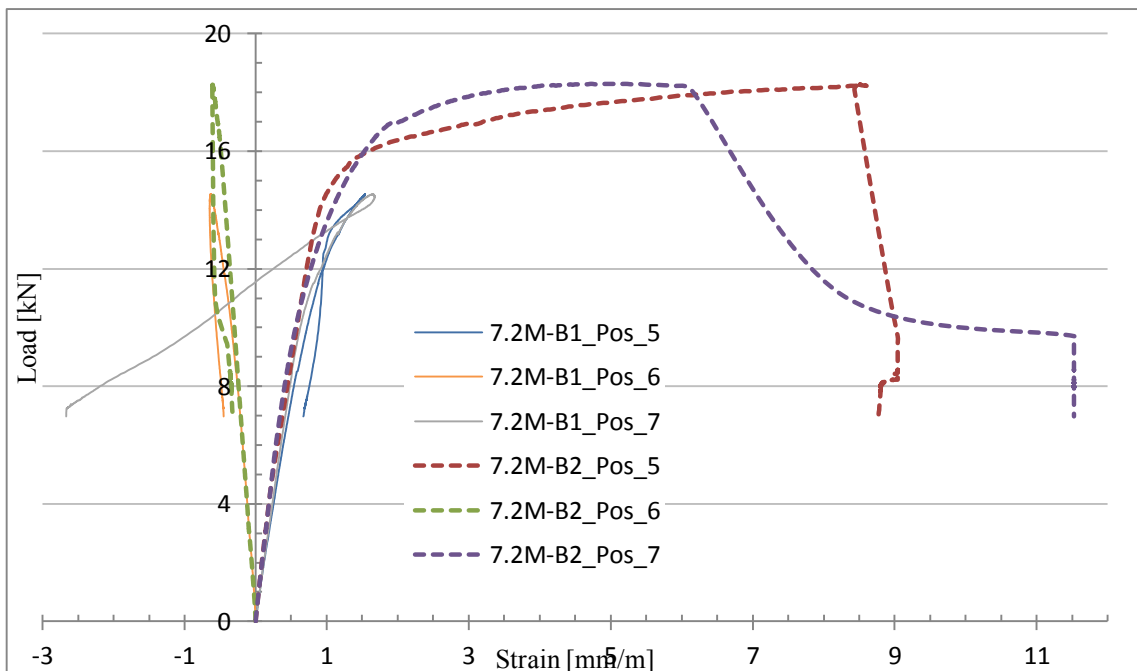
**Figure 4-30.** Load versus horizontal displacement for gauge #4 at mid-span for all test specimen.



As explained earlier the strain gauges were not placed on each element and the locations were changed in between the tests. That is why the positions are not comparable to the same gauge in another test, apart from strain gauge #7 on both 7.2M test specimen, which was placed in the same location on both specimen. The results from these strain gauges can be read from the graphs in Figure 4-31 and Figure 4-32. The deformations in the web due to shear stress can be seen in Figure 4-25 as load is applied.



**Figure 4-31.** Load versus strain at gauges on roof element 5.4M-B1.



**Figure 4-32.** Load versus strain at gauges on roof element type 7.2M.

## **4.6 Discussion of test results**

The experimental tests showed considerably less load capacity than the primary FEM-analysis indicated, but this did not affect the experimental testing. It did however show that the current FEM-model needed to be improved, before it could be used for dimensioning. The most important thing was to analyse the failure modes as this was the main objective. The supports showed ductile behaviour and was not the ultimate failure for any of the test specimen. Below a more detailed discussion on each deformation and failure mode.

### **4.6.1 Effects of deviations and imperfections**

Table 4-5 listed the imperfections and deviations from the manufacturing drawings that were noticed on the test specimen. The main concerns were the missing fasteners and small or in some cases practically no edge distance for fasteners as well as the positioning of the fastener in the joint between the hat-section and the main purlin. The pre-stress in the main purlin at the support was also a concern, but not one of the main concerns. The effects of the pre-stress are discussed in Section 4.6.6 Shear forces at support.

None of the test specimen showed any signs of fasteners tearing, block tearing or shear breaking even where the edge distance was well below the minimum edge distance or in places where there was clearly less fasteners, than specified in the drawings. Neither were there any fasteners that showed signs of tensile breaking or pull through. Some fasteners did however show signs of pull-out failure, as the lower plate showed signs of yielding. This occurred in the connection between the hat-section and the main purlin. More about how this affected the capacity in the following section.

### **4.6.2 Rotational stiffness of top flange joint**

In test specimen 5.4M-B1, 5.4M-B2 and 7.2M-B1, where the compressed upper flange was only restrained at a few points by perpendicularly aligned beams, the execution of the connections at these points became very critical. If the compressed flange is not braced in the horizontal plane, the connections need to have a big enough rotational restraint that reduced the buckling length. Otherwise lateral-torsional buckling (LTB) and distortional buckling will occur at very low loads. The moment capacity of the connections needs to be greater than the moment created by the loads eccentric to the shear centre. The perpendicular beams also need to be able to resist the bending moment, which is transferred onto them through the joint.

In the first two tests the significance of the execution of the joint between the hat purlins and the main purlins was very clear. The rotation of the upper flange in 5.4M-B2 was much bigger than in 5.4M-B1 in the middle of the span after failure. In Figure 4-33 you can see how the fasteners were close to the centre of the top flange in 5.4M-B1 and in 5.4M-B2 they were placed very close to the web of the main profiles. It was also easy to see the difference in the rotation of the top flange between these two tests. The half-wave length of the buckled top flange was also shorter for 5.4M-B1 than for 5.4M-B2.

5.4M-B1 shows a half-wave length that was equal to the hat purlin spacing, when 5.4M-B2 shows a length equal to the element span.

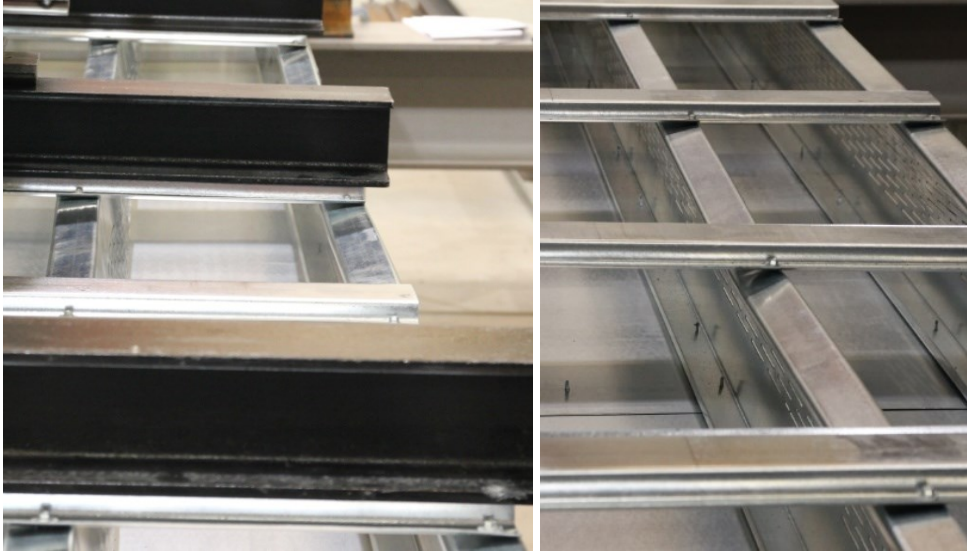
The rotational restraint of a beam can be calculated using a mechanical model based on a torsion spring with the spring stiffness  $C_D$ . The spring stiffness depends on the bending stiffness of the perpendicular beam  $C_{D,C}$ , the distortional stiffness  $C_{D,B}$  of the beam and the stiffness of the connection  $C_{D,A}$ . Assuming that  $C_{D,C}$  is much greater than  $C_{D,A}$  and  $C_{D,B}$ , the total rotational stiffness  $C_D$  can be determined from Equation 4-1. (EN 1993-1-3, 2009).

**Equation 4-1**

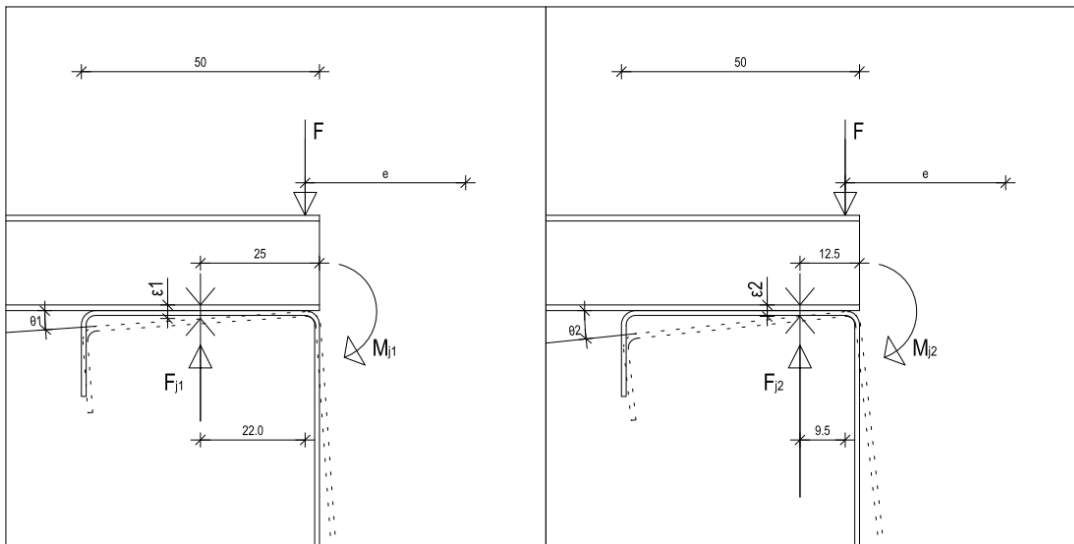
$$C_D = \frac{1}{\frac{1}{C_{D,A}} + \frac{1}{C_{D,B}}}$$

The moment capacity of the joint depends on the position of the fastener, if the plate thicknesses and profiles are the same. Figure 4-34 shows how the imposed load  $F$ , with and eccentricity  $e$  from the shear centre, creates a moment. The imposed load  $F$  is assumed to act in the same location, although there is a contact area between the two profiles, which varies. The moment for the imposed load creates a rotation  $\theta$  of the main purlin. Due to the rotation of the main purlin  $F$  will however be concentrated on to the web. The force in the fastener  $F_j$  is related to the strain  $\varepsilon$  and can be written as  $F_j = E * A * \varepsilon$ , where  $A$  is the cross-section area of the fastener and  $E$  is the modulus of elasticity. When the critical force in the fastener is reached, the rotation  $\theta$  will be much bigger if the fastener is closer to the web. This will also increase the eccentricity  $e$ .

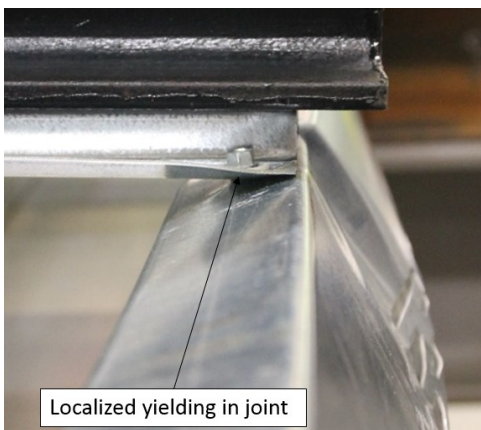
This means that if the distance between the web and the fastener changes from  $\frac{1}{2}$  the width of the flange to  $\frac{1}{4}$  the width it will decrease the maximum imposed load, which the connection can take before failure. When the maximum force of the fastener is reached the rotational restraint will not disappear completely, but the moment from the joint will be less than the imposed moment. This will accelerate the rotational displacement. Figure 4-35 shows how yielding in the joint has occurred after reaching the critical moment capacity.



**Figure 4-33.** Fasteners between hat profile and main purlin in the middle of the span. 5.4M-B1 to the left and 5.4M-B2 to the right. Taken after failure.



**Figure 4-34.** The moment capacity of the joint between the hat purlin and top flange of main purlin depends on the location of the fastener.



**Figure 4-35.** Joint between hat and main purlin has exceeded its moment capacity.

### 4.6.3 Local buckling

Local buckling occurred at an early stage on all test specimen. As the buckling length for local buckling was short and the deformations small in the beginning, it was difficult to determine exactly at which load local buckling started. From the pictures and the video recording, it was still clear that local buckling took place at a load below 13 kN. From the vertical displacement graphs in Figure 4-27 and Figure 4-28 the post-buckling curve was still almost linear, which shows that the local buckling has small influence on the stiffness of the element, but it may have on the loadbearing capacity.

### 4.6.4 Distortional buckling and local transverse load

Distortional buckling was clearly visible on the top flange as medium sized half-wave lengths and a deformed web. The distorted cross-section increased the eccentricities of loads, which lead to the failure of two specimen, 5.4M-B1 and 7.2M-B2. These two specimen also showed signs of buckling under local transverse load.

The point load under the hat section on each main purlin divided equally on each joint was considerably higher on the 5.4M test specimen, than on the 7.2M test specimen, as the 7.2M test specimen had 8 dividing beams placed on the hat sections, when the 5.4M only had 4 dividing beams. The highest point load on the 5.4M-B1 is over 2.7 times higher than the point load on 7.2M-B2 as Table 4-6 shows. This indicates that it was due to the distorted cross-section and the increased eccentricity of the load that the flange buckled.

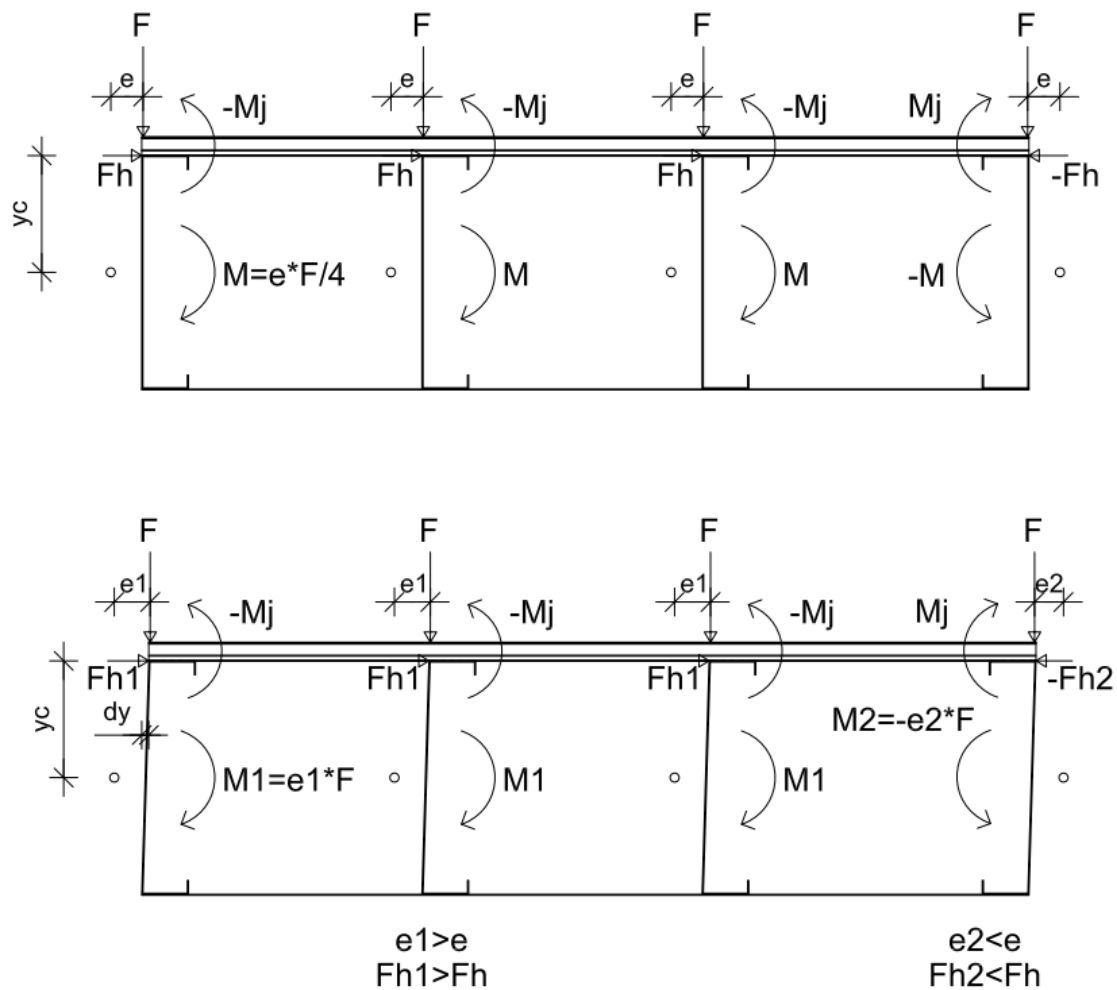
### 4.6.5 Lateral-torsional buckling

LTB occurred only in one direction, as the top flanges are connected with hat-sections. The element was constructed with most of the main purlins facing the same way, only the last edge purlin facing the opposite way. LTB occurred in the direction the most of the flanges were facing. The bottom flange of each main purlin was braced by the bottom plate and this restrains the bottom flange and prevents big horizontal deformation of the lower part of the element. Due to the relatively weak flexural stiffness in the horizontal plane, and the almost unrestrained top flange may buckle laterally while rotating around the length axis. This may be prevented with a sufficient lateral or rotational restraint.

In the horizontal displacement graphs shown earlier in Figure 4-30 it was clear how the horizontally braced element 7.2M-B2 does not show any notable change in horizontal displacement between 7-15 kN load, while the displacement of the otherwise identical, but unbraced element 7.2M-B1 only accelerates. Although the 7.2M-B2 element was not fully braced all over the full length of the element, the bracing reduced the lateral buckling length by approximately 3, as they were placed a third of the span from the support. The accelerated increase in the displacement in 7.2M-B1 was due to the low moment capacity in the joint between hat and main purlin. The equivalent horizontal load components  $F_h$  created by the moment were in this test positive on three purlins and negative on one. The negative one cancels out one of the positive load components,

which leaves two positive load components as long as the element does not have significant horizontal deformation. See Figure 4-36. As the moment capacity in the joint was exceeded, at about 9 kN load, the rotation accelerates and the eccentricity of the load from the shear centre increases.

The positive horizontal load components bend the element horizontally, which increases the eccentricity  $e1$  and the positive load components, but reduces the eccentricity  $e2$  and the negative load component. As a result the acceleration of the horizontal deformation of the element at position 4 in Figure 4-30 was exponential. Only the additional bracings in element 7.2M-B2 are able to transfer the horizontal load components towards the supports to a certain degree, preventing the main profiles from big rotation and lateral displacements.



**Figure 4-36.** Horizontal displacement increases lateral forces as eccentricity increases.

The loading cylinder was fixed, and as the element moves horizontally to the right when looking at section A-A in Figure 4-12 and Figure 4-13, more load may have been applied on the left than on the right side of the element. The bigger vertical

displacements on the left side of the element support this, because the centre of gravity was actually on the left side, which normally would result in more loaded right side.

#### **4.6.6 Shear forces at support**

At the supports of the 5.4M-B1 element, big deformations could be seen already during loading as shown in Figure 4-25. The horizontal displacements were more than 5 mm at the location of gauge #3 as Figure 4-29 shows.

Figure 4-31 showed the strain at the support in the slotted web, but all that could be concluded with certainty from the results was that the stress was not equal on each purlin, because gauges #5 and #6 were positioned at the same location on the two purlins in the middle of the element. There was a slight displacement acceleration after 15 kN load and this might indicate some sort of local buckling of the strips. The other graphs do not show any significant changes at this load, which suggests, that this did not have any significant effect on the stiffness of the element. The shear forces for the 7.2M elements were smaller, due to the smaller total load.

Several supports were also subjected to pre-stress due to the poor manufacturing. This did not however lead to any failure at the support. 5.4M-B2 did not show any signs of plastic deformations, as there were significant pre-stresses that lead to distorted main purlins at the support before any load was applied. See Figure 4-7. It is possible that the closure flashing took the biggest stresses of the main purlins.

Plastic deformations were visible after the load was removed on 5.4M-B1 as shown in Figure 4-26, but no tearing or critical failure occurred. The shear forces from the main purlin were effectively transferred to the thicker C100x38x2.0-section and on to the support. None of the self-drilling screws showed any sign of failure either. The residual deflection was not recorded for full characteristic loading, as the ultimate load was not known. The residual deflection should not exceed 20% of the maximum recorded deflection under full characteristic load. These shear deformations may be critical in reaching this goal.

#### **4.6.7 Discussion of failure modes**

The optimum failure from a load bearing point of view would be yielding of the bottom flange, as this would result in the largest load bearing capacity for the roof element. This failure mode is of course very uncommon among thin-walled cross-sections and other beams with cross-section class 4, where buckling usually is governing. Yielding of the bottom flange did not occur in any of the tests, but buckling occurred in several forms and at different stages. The difficult part was to assess, which type of buckling was the ultimate failure mode.

All test specimen showed signs of local buckling of the upper part of the web at loads below 13 kN. The post-buckling stiffness of the element remained as good as unchanged. As the load was increased, distortional buckling became dominant and local buckling was difficult to observe.

Distortional buckling was visible on all of the specimens. The upper part of the web showed medium length half-waves as the load neared half of the ultimate load. The stiffened top flanges also showed signs of global buckling, but with varying half-wave lengths. For specimens 5.4M-B1 and 7.2M-B2 the half-wave lengths for the top flange was equal to the centre to centre distance of the hat profiles. For the other two specimens, the half-wave length was equal to the element span.

Both specimens 5.4M-B2 and 7.2M-B1 showed clearly less lateral restraint compared to the other element of same span. This indicates that the moment capacity in the joint was exceeded earlier, which lead to an accelerated lateral displacement. The global lateral displacements were over 25 mm for these two unbraced elements at failure. All elements showed an accelerated horizontal displacement as the load neared the ultimate value. The maximum horizontal displacements were still in all cases smaller than the vertical displacements for each element, even though they were close to the same for all but the braced element 7.2M-B2.

For specimens 5.4M-B2 and 7.2M-B1 this ultimate bending moment on each main purlin was clearly less than on the other two test specimen. Failure occurred already at an ultimate moment under 5.0 kNm per purlin. This was because the lateral restraint of the elements was not sufficient to resist the lateral-torsional buckling of the main purlins. The top flange of both elements show a half-wave length equal to the element span, the horizontal displacement and the rotation of the main purlins were signs that lateral-torsional buckling was the main failure for these elements.

There was also localized buckling of flange under the concentrated transverse load from the hat-section along with the distorted cross-section visible for test specimens 5.4M-B1 and 7.2M-B2. See Figure 4-20. The ultimate point load, which was applied on each main purlin on 4 locations for 5.4M test specimens and 8 locations on 7.2M test specimens was much higher for the 5.4M test specimens. See Table 4-6. This indicates that the distortional buckling lead to increased eccentricities for the load, which caused the cross-section to buckle under the concentrated load.

Shear failure was not critical for any of the elements. The support arrangement proved to be very ductile, even though stresses were high enough for the web to show signs of plasticity and shear buckling of strips between perforations. This did not however affect the elements load capacity in any way. If the main profile would have been supported directly on the support without proper strengthening, the web could buckle due to concentrated compressive load and this could lead to a sudden collapse, as the height of the main profile is suddenly reduced.



## 4.7 Conclusions of the test

The experimental tests were not executed perfectly, as there were so many variables. The main reason for this was due to the poor execution at the workshop, which lead to big deviations between elements that should have been identical. The deviations and imperfections mostly affected the global buckling length for the same type of element, leading to different type of failure. Corrections and changes were done along the way to get results, which were important for the objectives of this experimental test. These lead to more variables and less data, which could be directly comparable. It was not possible to follow the testing procedures given in EN 1993-1-3 Annex A.4 to the fullest either, as the characteristic load was not known.

The positive thing was to see how big difference the execution might have on the ultimate capacity of the element. This gave valuable insight, which might not have been achieved if the elements would have been manufactured according to the drawings. The objectives were also achieved, which was the most important thing in these experimental studies.

The test results clearly show two separate categories based on the failure mode and the bending moment capacity of the main purlins. Test specimen 5.4M-B2 and 7.2M-B1 can be categorized by the LTB-failure and under 5.0 kNm bending moment capacity, while test specimen 5.4M-B1 and 7.2M-B2 failed due to distortional buckling in the mid-span, achieving over 5.6 kNm bending moment capacity. The two latter provided better lateral or rotational restraint for the top flange, which was under compression.

It is not safe to assume that the connection between the main purlin and the hat purlins provides sufficient torsional restraint to resist lateral torsional buckling, due to the risk of manufacturing mistakes. It is however possible to achieve sufficient restraint with this type of connection. This would still require more research on the moment capacity of the joint and how it affects the critical buckling length. It would also require extensive quality control during manufacturing. The final product will be manufactured with a horizontal diaphragm, providing the top flange with a sufficient lateral restraint.

## 5 Structural capacity

In this chapter the ultimate load bearing resistance ( $R_d$ ) of the roof element of two modular spans is analysed according to EN 1993-1-3. The project specific design value of the actions ( $E_d$ ) is not known, as the project locations vary. The project specific design value can easily be compared to the load bearing resistance to check if it satisfies Equation 5-1 and in this way check if the specific element is suitable for the project.

Equation 5-1

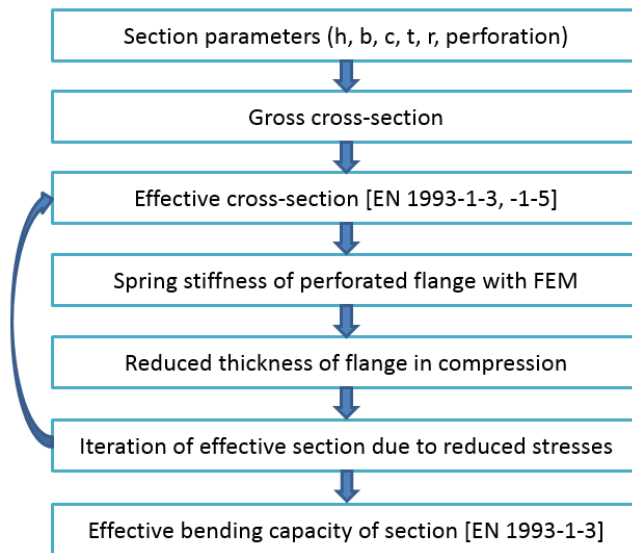
$$E_d \leq R_d$$

In the first Section the boundary conditions will be examined and after that we will follow the workflow shown in Figure 5-1. The effective cross section parameters are calculated analytically according to EN 1993-1-3. The fire resistance is also analysed. Lastly we will take a look at what needs to be taken into account in each project and how the element could be optimized for different projects.

Based on the test results from the experimental tests, it was concluded that lateral-torsional buckling will be critical, if sufficient lateral or rotational restraint is not provided, otherwise distortional buckling will be governing. As a result a diaphragm bracing was added to the upper flange in order to avoid lateral-torsional buckling. The deflection is not analysed, as the experimental tests show deflections less than  $L/200$  for the typical spans with characteristic loads.

EN 1993-1-3 gives design values for thin-walled cold-formed cross-sections, but it does not include thermally slotted cross-sections. The slotted part will mostly be in the ineffective area of the cross-section, with moment about the strong axis, so the bending capacity of the cross-section can be quite accurately calculated according to EN 1993-1-3. It is only the spring stiffness of the web, which cannot be directly determined with the formulas provided in EN 1993-1-3 Chapter 5.5. EN 1993-1-3 allows for the spring stiffness to be inserted, if it is determined through testing or another calculation method.

The elements can be dimensioned based on the ultimate bending moment resistance in the strong axis. Shear failure will not occur for spans over 5 m, with evenly distributed gravitational loads.



**Figure 5-1.** Calculation workflow of a cold-formed thermally slotted cross-section.

## 5.1 Boundary conditions and assumptions

The roof element is supported by steel frames with an external truss. The element rests on the bottom flange of the bottom chord, which is a WQ-section. The steel frame is stiffened by steel bracings, which will take any horizontal forces and none will be transferred to the roof elements.

The dimensional load on the roof element is a surface load, such as self-weight and snow and/or wind load, which is transferred through the hat purlins with a centre to centre distance of 600 mm. This is simplified as an evenly distributed line load on the purlins. The load is project specific, which means that the design capacity will be checked in each project according to local regulations and compared to the design load  $E_d$ . It is important to remember to use design loads, which have been multiplied with specific safety factors and not characteristic loads.

The roof elements are fixed to the bottom flange of the roof truss with single bolts at 3 locations along each support of the element and may be considered hinged in both ends and sliding in one end as the holes have big tolerances.

The main purlins are fully braced in x- and y-direction at the bottom flange by a steel sheet. The bottom steel sheet is only assumed to provide horizontal support, and not take any part in the bending moment capacity. The upper flanges of the purlins are connected by hat purlins placed perpendicular to the main purlins with two fasteners at each joint. The moment capacity in these joints around the x-axis is neglected, as it is very much depending on the manufacturing accuracy. The top flange has been braced with a diaphragm instead to provide horizontal restraint to the top flange.

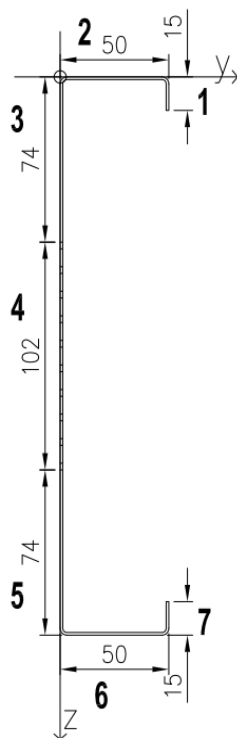
## 5.2 Calculations according to EN 1993

The calculations are based on the results from and conclusions of the experimental. The calculations are according to EN 1993-1-1, -2, -3 and -5. Based on the experimental tests, the effective bending moment capacity will be governing, as it takes into account both local and distortional buckling as long as lateral torsional buckling is prevented. Lateral torsional buckling is not analysed, as the lateral displacement of the top flange is prevented with a diaphragm.

Apart from these things, the C-profiles at the support were checked against local transverse force and the effectiveness of the inside insulation layer as fire insulation was also checked.

### 5.2.1 Section parameters of LPT-C250x50x1.2

The cross-section LPT-C250x50x1.2 is a thermally slotted thin walled cold-formed steel purlin. The slots are 75 mm x 3 mm with a centre to centre distance of 100 mm in 10 intermitted rows in the centre of the web. Figure 5-2 shows the cross-section dimensions and how the parts of the section have been numbered. Origin is in the top left corner. The steel grade used is S350GD+Z and the material properties are presented in Table 5-1.



Thickness:	$t = 1.2 \text{ mm}$
Width:	$b = 50 \text{ mm}$
Height:	$h = 250 \text{ mm}$
Stiffener:	$c = 15 \text{ mm}$
Height of thermally slotted (perforated) web:	$h_{\text{perf}} = 102 \text{ mm}$
Gross area:	$A_{\text{gr}} = 445 \text{ mm}^2$
Net area (perf. reduced $3/4 \cdot t$ ):	$A_{\text{net}} = 416 \text{ mm}^2$
Inner radius:	$r = 1.9 \text{ mm}$
Centre of gravity:	$y_0 = 11.1 \text{ mm}$
	$z_0 = 125 \text{ mm}$

Figure 5-2. Section properties of LPT-C250x50x1.2.

**Table 5-1.** Material properties of steel used in calculations.

Material:	E modulus [N/mm <sup>2</sup> ]	G modulus [N/mm <sup>2</sup> ]	Specific weight [kN/cm <sup>3</sup> ]	$f_{y,k}$ [N/mm <sup>2</sup> ]
Steel S350GD+Z	210 000	81 000	$7.850 \cdot 10^{-5}$	350.00

EN 1993-1-3 takes into account the rounded corners of the cross-section by using notional flat widths. These are used in the calculations. The geometrical proportions of the cross-section do also fulfil the maximum width-to-thickness ratios set in EN 1993-1-3 Table 5.1.

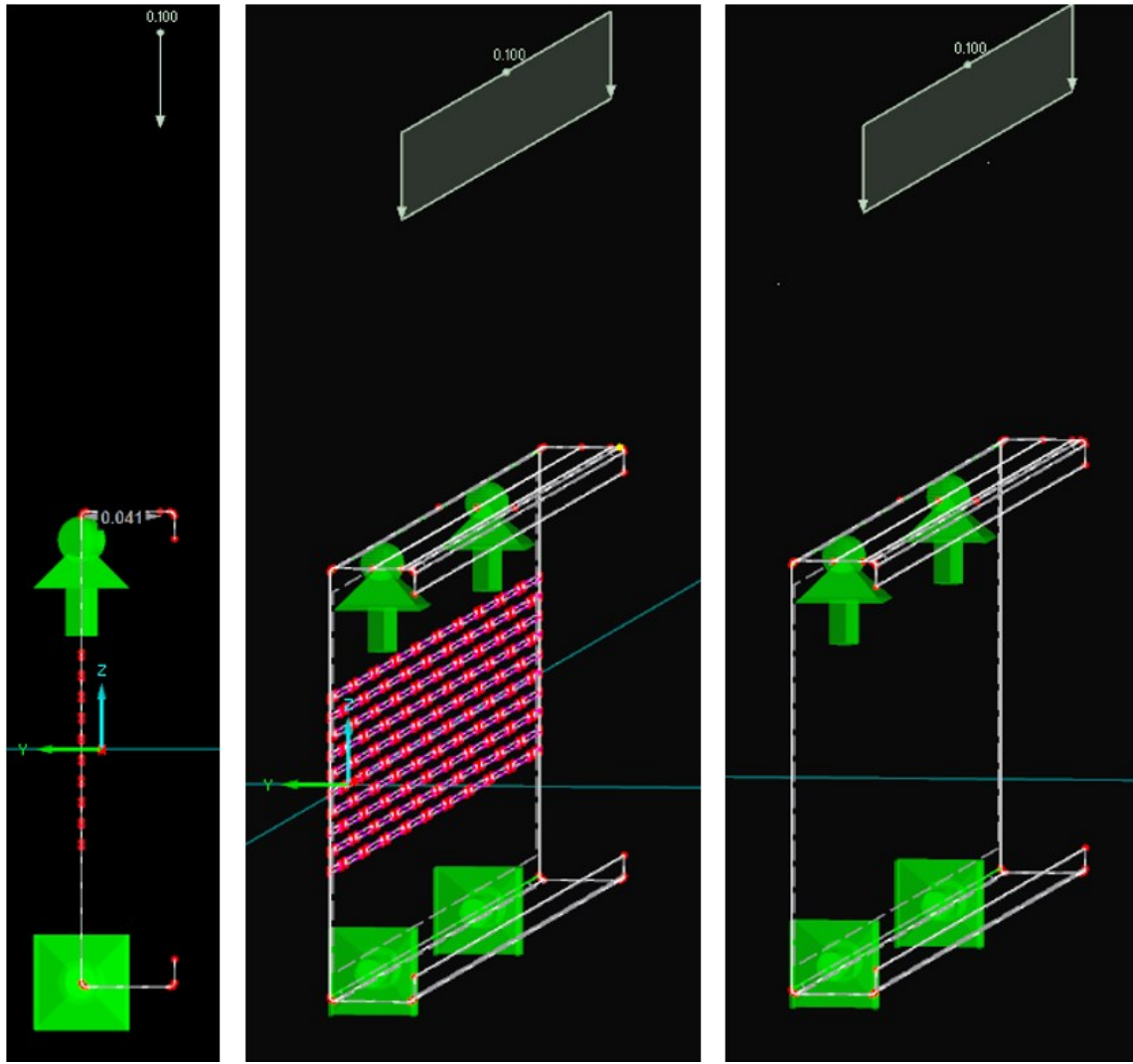
### 5.2.2 Spring stiffness of web

As stated earlier, formula (5.10b) in EN 1993-1-3 Chapter 5.5 is not suitable determining the spring stiffness  $K$  for the flange of a slotted section, as holes in the web alters the stiffness of the web. Determining the spring stiffness  $K$  is fairly simple with a FEM-model. The unit load  $u$ , which is inserted in the model, is divided by the deflection  $\delta$ , and this gives  $K$  according to formula EN 1993-1-3 (5.9). The calculation model should have the same boundary conditions as specified in Figure 3-2.

To determine the spring stiffness  $K$ , an RFEM-model was created of a 1.0 m long section of the LPT-C250x50 purlin using surface thicknesses of 1.2 mm, 1.5 mm and 2.0 mm. Each perforation was cut out of the web surface. The surfaces were supported according to Figure 5-3 with a hinged line support along the upper edge of the web and a hinged line support, which was released in z-axis along the bottom edge of the web as specified in Figure 3-2. A unit line load of 0.10 kN/m was placed at  $b_1=41.3$  mm from the web-to-flange junction.

An isotropic plastic 2D/3D material model was chosen along with second order analysis for the load case. The FE mesh was set to target 10 mm. Mindlin's plate bending theory was chosen for the calculations. Maximum stress reached was clearly below the yield strength of the Steel S 350 GD material. More about the software used in Section 4.1.2.

Due to the inaccuracies in the earlier RFEM models, a comparison model was created without the slots in the web to be able to compare the RFEM results with the spring stiffness calculated according to EN 1993-1-3 (5.10b).



**Figure 5-3.** RFEM-model of spring stiffness calculation for LPT-C250x50x1.2 purlin and comparison model to the right without perforations.

The unite load  $u = 0.10 \text{ N/mm}$  created an average deflection  $\delta_p$  for the slotted section and an average deflection  $\delta_f$  for the non-slotted. The deflection ratio of slotted to non-slotted varied from 4.8-5.1, which means that neglecting the slotted web would have a significant influence on the effective area of the top flange and would lead to higher effective second moment of inertia  $I_{y,eff}$ , than the slotted cross-section realistically can achieve. Table 5-2 presents the deflections calculated with the RFEM-model and the calculated spring stiffness of the non-slotted sections based on the RFEM-results versus the results according to formula (5.10b) in EN 1993-1-3. The table shows that RFEM gives results, which are 8-11 % more conservative than Eurocode in this case. This shows that the spring stiffness of the slotted web calculated with this FE-method can be used in the analytical calculations of the effective cross-section properties.

**Table 5-2.** Comparison of calculations of the spring stiffness of web.

Deflection $\delta$ due to unit load $u=0.1$ N/mm				Spring stiffness $K$ of non-slotted section [N/mm <sup>2</sup> ]			
Thickness	RFEM		Ratio	RFEM		EN 1993-1-3	Ratio
LPT-C250	Slotted	Non-slotted	$\delta_p/\delta_f$	$u/\delta_p$	$u/\delta_f$	(5.10b)	$K_l/K_f$
$t$ [mm]	$\delta_p$ [mm]	$\delta_f$ [mm]		$K_p$	$K_f$	$K_l$	
1,2	2,75	0,57	4,82	0,036	0,175	0,194	1,106
1,5	1,43	0,29	4,93	0,070	0,345	0,379	1,099
2,0	0,62	0,12	5,13	0,163	0,833	0,899	1,079

### 5.2.3 Effective cross-section parameters

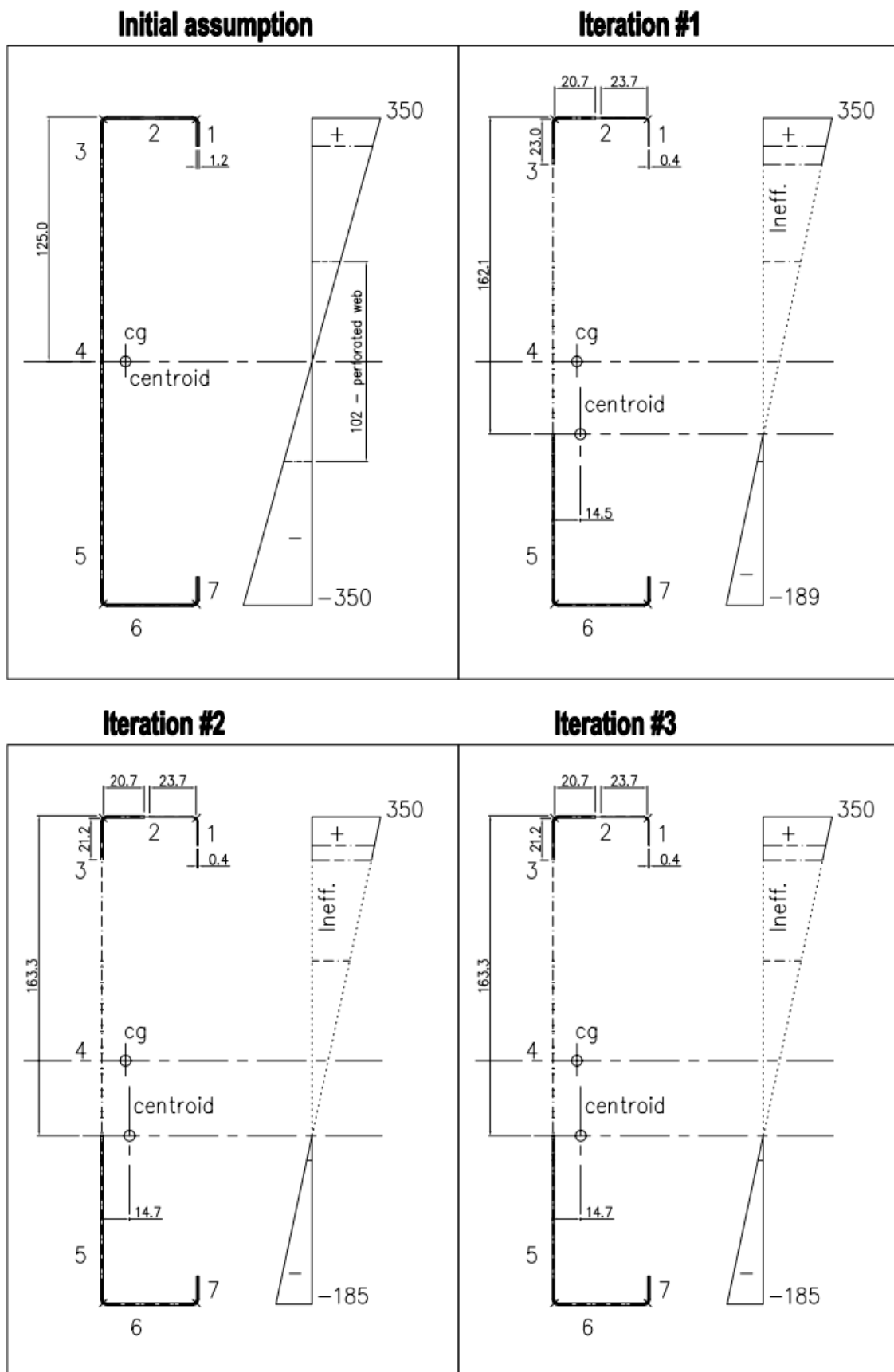
EN 1993-1-3 deals with the fairly complex buckling issues of the slender thin-walled steel cross-sections by neglecting certain parts of the cross-section, where local and distortional buckling may occur. This requires that the loading conditions are known, because it is only the parts that are subjected to compression which normally buckle. In the calculations an initial stress distribution was assumed, where the top flange was subjected to a positive (compressive) stress equal to the yield strength and the bottom flange to an equal negative (tensile) stress, which represents gravitational loading. The stress was initially assumed to be linearly changing over the height of the cross-section as shown in Figure 5-4.

The effective widths were then calculated for each part of the cross-section, which was subjected to compression according to EN 1993-1-5. The effective part of the web under compression was assumed to be an outstanding element, as the perforation has reduced the stiffness of the web so radically.

Distortional buckling is taken into account in EN 1993-1-3 using a reduction factor  $\chi_d$  that reduces the effective area of the flange stiffener  $A_s$ . In the calculations for the reduction factor  $\chi_d$ , the spring stiffness of the slotted web needs to be considered. In the calculations the spring stiffness of the slotted cross-section  $K_l$  from the RFEM-calculations, as described in the previous section, was used.

The effective areas were then calculated and the stress distribution re-evaluated based on the location of the centroid. After this three iterations were done using the newly calculated stress levels to get the exact effective widths for each part of the cross-section. Figure 5-4 shows the initial assumption, where the stress is distributed linearly over the height of the cross-section, with a stress value of 350 MPa at the top flange and -350 MPa at the bottom flange. The centre of gravity and centroid are also in the same location. Iteration #1 shows how the location of the centroid has changed the stress distribution and which areas are now ineffective.





**Figure 5-4.** Initial assumption and iterations due of ineffective areas due to the stress distribution change in the cross-section.

As the iterations were done, the effective cross-section properties were calculated one final time. Using these effective cross-section values the bending moment capacity in the strong axis  $M_{y,Rd}$  was calculated. The calculations of the effective cross-section properties of the main purlin LPT-C250x50x1.2 are found in Appendix 1. Figure 5-1 showed the workflow in determining the effective section properties according to Eurocode.

The ultimate bending moment capacity in the strong axis ( $M_{y,Rd}$ ) of the LPT-C250x50x1.2 purlin was calculated as 5.257 kNm. Table 5-3 lists the other cross-section properties.

**Table 5-3.** Effective cross-section properties of LPT-C250x50x1.2 with 10 rows acc. to EN 1993-1-3.

h	t	b	c	M	A	A <sub>eff</sub>	I <sub>y,eff</sub>	W <sub>y,eff</sub>	M <sub>y,Rd</sub>
[mm]	[mm]	[mm]	[mm]	[kg/m]	[mm <sup>2</sup> ]	[mm <sup>2</sup> ]	[mm <sup>4</sup> ] x10 <sup>6</sup>	[mm <sup>3</sup> ] x10 <sup>4</sup>	[kNm]
250	1,2	50	15	3,055	416,2	237,2	2,453	1,502	5,257

where:

- h is height of cross-section
- t is thickness
- b is width of flange
- c is height of flange stiffener
- M is weight of cross-section per length meter
- A is the area of cross-section with slotted web
- A<sub>eff</sub> is the effective area of cross-section
- I<sub>y,eff</sub> is the effective second moment of area about y-y axis
- W<sub>y,eff</sub> is the effective section modulus about y-y axis
- M<sub>y,Rd</sub> is the design value of resistance to bending moments about y-y axis

## 5.2.4 Support reactions

The smaller C-purlins at the supports were partly added to avoid the cold bridge, but also because the webs of the thermal purlins would have been subjected to a high compression force. This may have resulted in buckling of the web of the thermal purlins at the support, as the stiffness of the web is heavily reduced. By placing the C-purlin below the top flange, the web of the thermal purlin will be mainly subjected to tension and shear forces when subjected to gravitational loads. This prevents the thermal purlin from buckling.

This solution is of course beneficial for the resistance of the thermal purlins, but the same forces are now transferred to the C-purlins. The shear capacity of the C-purlin is however higher, as it is thicker, the height is smaller and the web is not slotted. The Eurocode EN 1993-1-3 contains analytical formulas for calculating the resistance of a thin-walled cold-formed cross-section under local transverse force. These formulas are

however not applicable for a thermally slotted cross-section and can only in this case be used for the support profiles.

With an evenly distributed surface load on the roof, which would equal the ultimate bending moment resistance of the main purlins, the support reactions would be 4.15 kN on each of the 5.4M purlins and 3.06 kN on the 7.2M purlins.

The resistance of a 2.0 mm thick and 100 mm high profile was calculated using the formulas presented in EN 1993-1-3:2006 / AC:2009 in section 6.1.7.2 and they gave a dimensional resistance value  $R_{w,Rd} = 12.10$  kN. See calculations in Appendix 1. This 2.0 mm thick profile was used in the experimental tests, but the calculations show that even a 1.5 mm thick profile would be sufficient, providing a  $R_{w,Rd} = 6.18$  kN. If other main purlins are used, with different bending moment resistance, the shear force needs to be checked again.

### 5.2.5 Fire resistance

The sound absorbing insulation also works also as a thermal insulation and thus reduces the surface temperature of the load bearing purlins. According to EN 1993-1-2 the critical steel temperature,  $\theta_{crit}$ , for a cross-section in class 4 is 350 °C.

In a standard fire situation, with the fire temperature development according to EN 1991-1-2, the 70 mm thick Paroc COS-5 insulation reduces the surface temperature at the steel surface to 318 °C at 60 minutes. This means that the element can withstand a standard fire of 60 minutes. The temperature calculations can be found in appendix 2. The density, thermal resistance and capacity are product dependent and the values used in the calculations are obtained from the manufacturer of this specific insulation.

In a typical Wärtsilä engine hall, there is not much fire load. According to a fire technical report made 2004, the smoke detection system cuts off the fuel feeding, and after this there will be a linear decrease in the rate of heat release. In the report there are two fire simulation cases, where the second is the worst case. In this fire scenario a sizeable leakage was assumed to have occurred, and thus causing a bigger fire load.

In the second fire simulation case the fire will be extinguished after about 420 seconds. According to the report the maximum temperature under the ceiling is approximately 900 °C, when the standard fire is 898.8 °C. This shows that the temperature development in the engine hall is very close to the standard fire case. (Markku Kaurila Ltd, 2004)

This shows that the roof elements can sustain the load bearing capacity in a fire situation. Project specific requirements might still be higher than this and in these cases project specific analysis are required.

## 5.2.6 Discussion and comparison of calculated and test results

The ultimate bending capacity of the roof elements is surely one of the most interesting results from these experimental tests. Table 5-4 shows the ultimate bending moment divided equally on each main purlin before failure along with the calculated capacity and the difference between the tested and calculated values. The table shows roughly two categories, below 5.0 kNm, which is more than 5% lower than the analytically calculated moment capacity  $M_{b,Rd} = 5.257$  kNm, and above 5.6 kNm, which is over 7% more than the calculated capacity. These are not specific to a certain element span. They are related to the lateral and torsional restraints of the main purlins. If we look at the difference between the capacity of the ones exceeding  $M_{y,Rd}$  and the ones below  $M_{y,Rd}$ , it is 12-17%. This indicates that there are some local failures occurring in the joints of the hat section to main purlins, which reduces the lateral torsional restraint. This allows for lateral torsional buckling to occur before the stress reaches its critical value for distortional buckling failure.

**Table 5-4.** Comparison between calculated and tested bending moments.

Element	Max bending moment in test	Calculated $M_{y,Rd}$	Difference		Failure mode
Nr.	[kNm]	[kNm]	[kNm]		Type
5.4M-B1	5,640	5,257	0,383	7,3 %	DistB
5.4M-B2	4,962	5,257	-0,295	-5,6 %	LTB
7.2M-B1	4,977	5,257	-0,280	-5,3 %	LTB
7.2M-B2	5,839	5,257	0,582	11,1 %	DistB

The experimental tests show that it is possible to dimension the main purlins using the effective cross-section properties according to EN 1993-1-3. It also shows that lateral torsional buckling may occur, if the flange under compression is not provided with sufficient lateral or torsional restraint. If LTB occurs, the critical bending moment may be well below the effective cross-section bending moment capacity.

When using FEM-calculation software, it is fairly easy to get results, which look very nice and might seem realistic, but which might differ from the intended structure. It might be due to fairly small thing that have been modelled the wrong way, a boundary condition which is has the wrong releases or some settings in the calculation method. This is why it is very important to have a deep understanding of how the software works and also the theory behind it. In these types of thin plate structures, imperfections may have significant influence on the results.

If there is a way to do some analytical calculations to check if the results are within the plausible range, it is always good to do so. If the structure is very complex and differs from what has been done before, it might be good to do some experimental tests, which can confirm the accuracy of the primary calculation model and give insight on which phenomena have to be analysed more thoroughly. In this Thesis, the secondary model was however skipped in favour of the analytical calculations, which proved to be fairly straight forward.

### 5.3 Optimization for projects

The roof element is designed, so that it is suitable for several different projects. It is of course not known exactly what requirements these projects may have on the roof structure. The 5.4M element can resist a total dimensional surface load of  $5.45 \text{ kN/m}^2$ , which includes the self-weight. In Finland for example, this would be enough to withstand the self-weight of  $0.5 \text{ kN/m}^2$  plus a live load of over  $3 \text{ kN/m}^2$ . This is enough for the snow load of most of Finland. The 7.2M element however can only resist a dimensional surface load of  $2.97 \text{ kN/m}^2$ . This means that the thickness of the profile will most surely need to be increased to achieve a more suitable bending moment resistance of the main purlins. Table 5-5 shows the different allowable loads for each roof element span and profile thickness. If other main purlins are used, the effective section properties can be used to calculate the dimensional gravity load using the same method as long as the boundary conditions and spans remain the same.

In such concept orientated design as this, it is best to keep the variables to a minimum. This type of element gives fairly reasonable flexibility only by changing the thickness of the purlins. This way the assembly details will remain the same and the manufacturing details can be used with only slight updates. It is also possible to adjust the centre to centre distance of the purlins, but this may have a bigger consequence on both details and may affect the element size as well. These also have some impact on the thermal resistance of the roof element.

**Table 5-5.** Maximum allowable design gravity loads on roof elements including self-weight of element.

Element [mm]	$M_{y,Rd}$ [kNm]	Lineload per purlins c/c 300 mm [kN/m]	Surface load [kN/m <sup>2</sup> ]
5.4M t=1.2	5,25	1,64	5,46
5.4M t=1.5	7,12	2,22	7,39
5.4M t=2.0	11,37	3,54	11,80
7.2M t=1.2	5,25	0,89	2,97
7.2M t=1.5	7,12	1,21	4,03
7.2M t=2.0	11,37	1,93	6,43

## **6 Building physical properties**

The envelope needs to protect the engine and other equipment from the sun, rain and wind. It also needs to protect the outside environment from the noise produced by the engines. The noise inside tends to get even louder, if there are only hard reflecting surfaces and no sound absorbing surfaces or material surrounding a sound source.

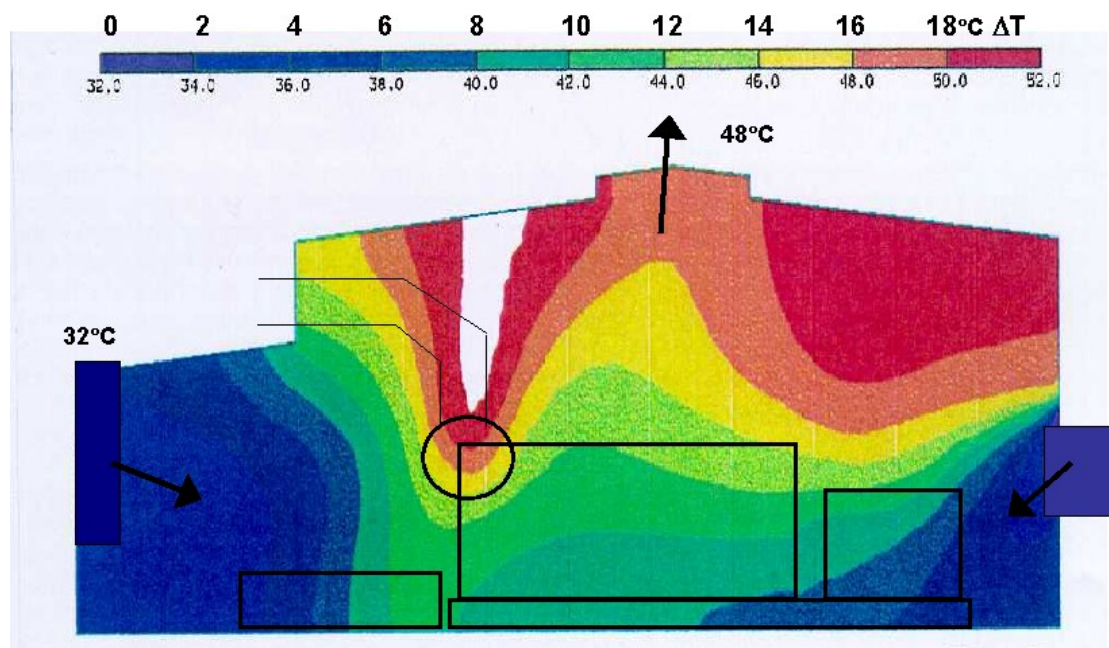
Apart from the more common tropical conditions in Wärtsilä power plants, the arctic conditions require more thorough analysis of the envelope. Due to the low outside temperatures, the envelope needs to have a higher thermal resistance, so that not all heat is lost. High temperature and humidity differences between the outside and inside air also means that the envelope needs to have a vapour barrier layer on the warm side of the structure to prevent condensation inside the insulation. These issues are explained and analysed in the following sections of this chapter.

## 6.1 Boundary conditions

The boundary conditions concerning building physical calculations may vary a lot from project to project, but a reference project was chosen to get some theoretical values. Each country or customer may have individual requirements as well, but in this Thesis we will only focus on the physical properties of the roof element, given some realistic boundary conditions. A project located in Russia in the city of Kurgan was chosen as a reference project. The boundary conditions are listed below and the temperature gradient inside the engine hall is shown in Figure 6-1.

Kurgan:

- Design ambient; ambient air temperature: +25 °C
- Maximum ambient temperature: +39 °C
- Design temperature max: +23,8 °C
- Minimum ambient temperature: -50 °C
- Design temperature: -37 °C
- Dimensioning RH outside warmest month: 69%
- Dimensioning RH outside coldest month: 79%
- Volume: 20 010 m<sup>3</sup>

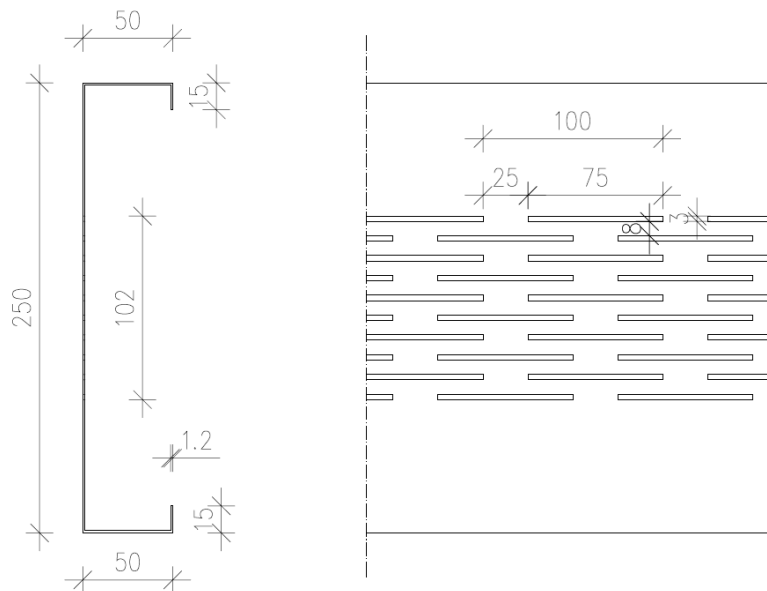


**Figure 6-1.** Result of simulation showing temperature gradients in the engine hall. (Andersson, 2008)

## 6.2 Thermal properties

The improvements from the roof element used in tropical conditions are not only additional insulation. Because of the high thermal conductivity of steel,  $50 \text{ W/(m}\cdot\text{K)}$ , compared to thermal insulation,  $0,034 \text{ W/(m}\cdot\text{K)}$ , the steel forms so called cold bridges through the structure. In Scandinavia it is common to reduce these cold bridges in thin-walled steel structures by introducing slotted holes in the web that are intermitted. The slotted holes increase the distance and reduce the cross-section area which the heat passes through. This results in a steel stud with an increased thermal resistance comparable to a 40 mm wide wooden stud of the same depth that has a thermal conductivity of  $0,14 \text{ W/(m}\cdot\text{K)}$ . (Thöyrä, 2001)

The slots holes in the LPT-C250x50x1.2 have a length of 75 mm and a width of 3 mm, intermitted with a centre to centre distance of 100 mm. The slots are in 10 rows, 11 mm apart in the centre of the web. See Figure 6-2



**Figure 6-2.** Section and arrangement of slotted holes.

To simplify the thermal conductivity calculations, only two-dimensional calculations were used for the roof element taking into account the cold bridges formed by the steel purlins. To achieve more exact calculations, also taking into account the width of the flange and other longitudinal heat transfer a three-dimensional calculation would be required. Two-dimensional calculations are anyhow considered sufficient for cold-bridge analyses.

The thermal resistance of the slotted steel stud was analysed by splitting up the stud into smaller components. The centre to centre distance for the slots was 100 mm, so to begin with only a 100 mm long part of the section was studied. Then the section was split into upper, middle and lower part of the web. The middle or the slotted part of the web was then split into vertical 25 mm wide sections and longitudinal 8 mm cross-sections.

The symmetry of the 100 mm section was noticed, so this was further split in two. This meant that the 25 mm sections became 12.5 mm sections and that the system could be



calculated as a series. Each section with the index  $i$  was considered as a resistor with the thermal resistance  $R$ , where the cross-section area  $A$ , thermal conductivity  $k$  and average length  $L$  resulted in a specific resistance according to Equation 6-1. The air in between the steel parts was not considered in the calculations, as the thermal resistance was so much greater than the thermal resistance of steel.

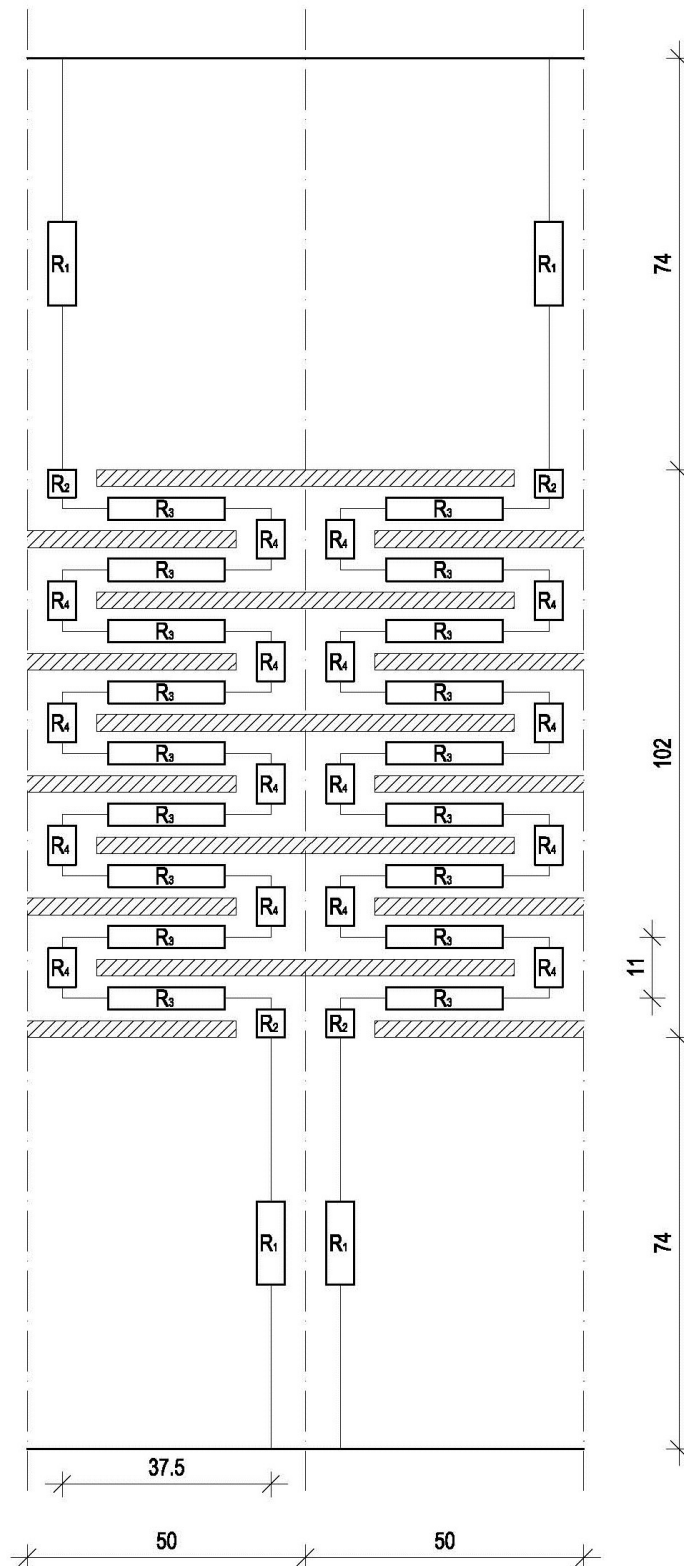
**Equation 6-1**

$$R_i = \frac{L_i}{k_i A_i}$$

As shown in Figure 6-3, the system can be seen as a series of resistances, the sum of them makes up for the resistance of the stud from one side to the other. The resistance of each single part and the calculated total resistance as well as the U-value for the complete structure can be seen in Table 6-1. The U-value for the structure is 0.141. Table 6-2 shows the U-value for the same structure with different thick main profiles. (Çengel, 2008) and (Ahokas, 2003).

The calculation model was also compared to the U-values calculated by HAMK for Ruukki in 2009 using Trisco building physics software for a certain structural type, and the results were the same for the same type of structure. (Fabrín & Martikainen, 2009).

The need of thermal resistance might vary from project to project, in which it is also possible to choose a thermal insulation of lower quality, which is usually also cheaper. These U-values calculated in Table 6-2 to show the best possible values that can be achieved with the products available today. It is also possible to compensate for heat loss of one structure by increasing the thermal resistance of another or decreasing the heat loss through air leakage for example if the structure does not meet the target value.



**Figure 6-3.** The schematic thermal resistance of the LPT-C250x50x1.2 section.

**Table 6-1.** The thermal conductivity for the thermally slotted roof element.

<b>Layers:</b>	<b>Thickness:</b>	<b>Ratio:</b>	<b>Thermal conductivity <math>\lambda_D</math></b>	<b>Thermal resistance R</b>
0.0 Convection, $R_{se}$			-	0,04
1.0 Roofing sheet	20/0.6	1	-	-
2.0 Ventilation gap	20+30	1	-	-
3.0 Breather membrane	0,3	1	-	-
4.0 Insulation + Steel purlin	250	1	-	4,75
4.1 LPT-C250x50x1.2 R10 c/c 300	587,5	0,004	50	13,33
4.1.1 Non-slotted part of web, 2 parts	74	1	50	0,370
4.1.2 First and last row of slots, 2 parts	7	0,25	50	0,140
4.1.3 Horizontal part between slots, 9 parts	37,5	0,16	50	1,172
4.1.4 Vertical part between slots, 8 parts	11	0,25	50	0,220
4.2 Paroc eXtra Plus	250	0,996	0,034	7,38
5.0 Vapour barrier	0,2	1	-	-
6.0 Sound absorber, Paroc COS-5	70	1	0,035	2,00
7.0 Perforated steel sheet	0,7	1	50	0,00
8.0 Convection, $R_{si}$			-	0,10
			<b>R<sub>tot</sub>: 6,891</b>	
			<b>U: 0,145</b>	

**Table 6-2.** Thermal conductivity depending on profile thickness.

<b>Main purlin:</b>	<b>U-value:</b>
LPT-C250x50x1.2	0,145
LPT-C250x50x1.5	0,154
LPT-C250x50x2.0	0,167

There are also some other issues, apart from the actual roof element, which cause some technical difficulties. As the roof truss is external, but the columns and other structures are internal, the columns are penetrating the roof. These cannot be avoided, but will be insulated and tightened at site. In the tropic roof element solution the lower flange of the WQ-beam is in contact with the inner climate. In arctic climate this would also cause a huge thermal bridge, which would most certainly cause condensation along the bottom chord.

To minimize the thermal bridge, the roof structure was lowered 220 mm, so that the bottom of the WQ-beam could be insulated and still keeping the inner surface flat. This will also be carried out with a pre-assembled element, but this element is not in the scope of this Thesis.

### 6.3 Moisture analysis

Increasing the insulation thickness in arctic conditions may lead to water vapour condensation in the insulation, as the heat insulation slows down the heat flow through the wall, if there is no layer resisting the moisture flow. To reduce the moisture flow through the structure, vapour barriers are commonly used. These are usually placed on the inside of the structure or no deeper than 1/3 of the depth of the heat insulation from the inside. In the roof element the vapour barrier is placed almost at 1/3 the depth of the heat insulation to increase the acoustical properties. The risk for condensation is still low, as the relative humidity inside the engine hall will remain low during the cold periods.

The ventilation of the engine hall is usually executed with inlet fans so that the cool air can be directed at the engines and other equipment that need cooling. This produces a controlled over pressure inside the engine hall. The moisture content of the inlet air is not altered, which means that the inlet air has the same moisture content as the air outside.

There are not many additional sources of water vapour inside the engine hall. There is an emergency shower and a sink, but these are rarely used and form a very small moisture load. The concrete slab is the main source adding to the moisture content in the air. The moisture load is of course bigger when the concrete is newly cast. After a while, as it dries, the amount of moisture evaporating from the surface decreases. The moisture load also depends on the temperature of the air and the relative humidity of the air. When the air gets warmer the relative humidity decreases. This increases the potential between the air and the slab and also the evaporation rate.

In the engine hall each engine has its own air ventilation unit(s). The ventilation flow, when the engines are in use, varies from 30 m<sup>3</sup>/s during the warm periods to about 2 m<sup>3</sup>/s during the cold periods. This equals a minimum air exchange rate of about 4 times the volume of each engine module an hour. With such a high exchange rate, the water vapour content in the inside air will be very close to the outside air's water vapour content. The relative humidity will however be lower inside, if the temperature is higher.

When the engines are not running the temperature of the inlet air is still pre-heated to +5 to +10 °C, so that there are not too big deformations in the engines and equipment due to the temperature change. In the Kurgan project the stand-by ventilation was a minimum of 3 times the volume of the engine module per hour. This means that a normal airtight roof structure with a regular 0.2 mm PE-membrane as vapour barrier is enough and there is no significant risk for condensation inside the insulation layer.

It is also important to have a breather membrane like the Tyvek Solid or Tend KM-0 that lets water vapour through, but prevents water from dripping from the water sealing back onto the insulation and soaking it. This may occur on cloud free and windless nights, when the radiation from the steel sheet or other water sealing is high. At such conditions the temperature of the outer steel sheet may drop below the air temperature. As the air from inside passes through the structure with a relatively high humidity, it may condensate when reaching the cold steel sheet. The condensed water may drip back down, but the membrane prevents the water from reaching the mineral wool. It also

directs water from small leaks in the roof sheets towards the eaves preventing it from soaking the insulation.

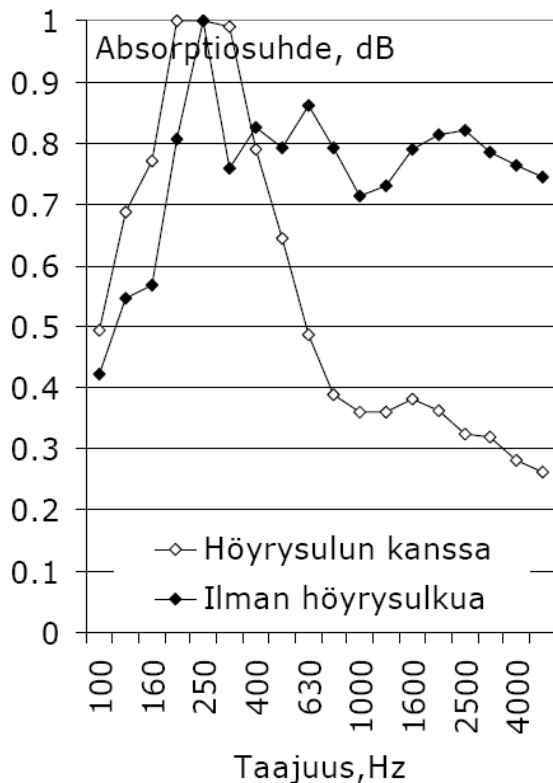
The most important thing however, is to prevent the rain from entering the structure. As the roof elements are installed, the breather membrane can protect the elements from small amounts of rain before the roof sheets are installed. The roof sheets are fully water resistant, but there are a lot of joints and overlaps, where special care needs to be taken to keep the water on the outside.

It is common to think that rain only travels downward, but in reality wind pressure may push water up a vertical wall. In ventilated structures, small drops of water may also easily be transported along with the fresh air into the air gap. It is very hard to prevent this, but the important thing is that the ventilated space can dry quickly. It is also important to use materials that are not too sensitive to moisture in the air gap. (Nevander & Elmarsson, 1994).

## 6.4 Acoustic properties

In the engine hall the sound power level  $L_W$  is very high and all the surfaces are hard, so there are usually no materials that naturally absorb noise. This would normally increase the sound pressure level  $L_p$  in a room. To avoid this Wärtsilä has used a load-bearing steel sheet with 15 % of the web perforated with holes of 3 mm in diameter to allow for the sound waves to pass through the sheet and be absorbed in the roof insulation on top of the load-bearing sheets. This reduces the reverberation time and decreases the sound power level in the engine hall.

When Wärtsilä started to use roof elements, they perforated the inner surface as well, to allow for the sound waves to be absorbed in the insulation. The structure did not need any vapour barriers, as they were only for tropic climate conditions. By adding a vapour barrier between the perforated sheet and the insulation slab, the acoustic absorption ratio would drop at higher frequencies, as the shorter sound waves would not penetrate the vapour barrier as efficiently. See Figure 6-4.



**Figure 6-4.** Absorption ratio with vapour barrier (höyrysulun kanssa) and without vapour barrier (ilman höyrysulkua) for a corrugated steel sheet with 15 %, 3 mm perforation and 100 mm mineral wool per frequency (taajuus). (Hongisto, 2005)

In arctic climate conditions the vapour barrier is needed as explained in the previous section. To maximize the absorption ratio of the structure, the vapour barrier was placed below the load carrying frame of the element and under this the acoustical insulation, which is fastened with self-drilling screws through both the perforated corrugated steel sheet and the insulation. The insulation, which was chosen, is a slab that can withstand 5 kPa compressive stress, which is enough so that no additional studs or purlins are needed in this layer.

In practice the acoustic atmosphere in the engine hall is improved quite dramatically with the increased absorption area. For a W20V34DF engine hall for, the reverberation time would be an average of 2.0 seconds. The sound pressure level average would be 111 dB. The difference between this and if there was for example only 40 m<sup>2</sup>-Sab absorption area, the  $L_p$  would be practically the same as  $L_W$ , which would give a  $L_p = 123$  dB. Even worse, the average reverberation time would be over 30 seconds. If the absorption area would be less than 4 m<sup>2</sup>-Sab, the  $L_p$  would increase. This is because there is practically nothing absorbing the energy from the sound waves. They just bounce back from the surface it hits. In reality there is always some energy lost, so the absorption area is never zero, but with close to no absorption area the sound pressure level would be near 150 dB. This is a huge difference when you consider that this is a working environment for some people.

To give you some idea of how high sound pressure levels we are talking about, 105 dB is the level of a rock concert. The Finnish Federation of Hard of Hearing does not recommend that anyone spends more than 4 minutes in a space with a sound pressure level of 106 dB or 1 minute if the sound pressure level is 112 dB without protecting the ears. The noise threshold of pain is 120 dB so the sound absorbing area is very critical here. Without it the risk for hearing disabilities would be much bigger. Ear protection is necessary in any case, but if for some reason a person loses them or forgets to put them on, he or she could injure him-/herself within minutes. (The Finnish Federation of the Hard of Hearing, 2014).

In Table 6-3 below you can see the sound power level  $L_W$  of the W20V34DF engine hall per frequency. It also shows the absorption ratio from Figure 6-4 per frequency and the calculated reverberation times and sound pressure levels per frequency.

**Table 6-3.** Calculated reverberation times and sound pressure levels per frequency for the W20V34DF engine hall.

Frequency, f [Hz]	125	250	500	1000	2000	4000
Absorption ratio	0.55	1	0.79	0.72	0.82	0.77
Reverberation time, T [s]	2.8	1.5	1.9	2.1	1.9	2.0
Sound power level, $L_{W,A}$ [dB]	109	120	125	129	124	126
Sound pressure level, $L_{p,A}$ [dB]	88.3	96.7	102.7	107.1	101.5	103.8

## 7 Conclusions and discussions

The main objective of this Thesis was to develop a fully functional roof element for arctic conditions. The arctic climate condition put a lot of requirements on the roof element, which affected both structural resistance as well as the structural type. The building physical aspects defined the core of the element, which affected the whole system. The development process has been very long, partly due to the big amount of work involved, but also as this has not been a full time project for most of the time.

It was a very interesting process to see how small ideas developed and some had to be discarded due to some restrictions or as they might not have been applicable. Still, the main objective remained and the development continued. The final result was a roof element type specific for the client and the climate, which still needs some detailed design, but is fully functional as a concept. All the building physical aspects, such as thermal insulation, moisture control and sound absorption have been considered to provide a suitable working environment.

The structural analysis started with preliminary FEM-analysis for the experimental tests. The experimental tests showed that the FEM-results were not accurate and focus was put on analytical calculations according to EN 1993-1-3 instead. The analytical calculations gave results, which were comparable to the experimental tests, as long as the top flange was provided with lateral or torsional restraint to prevent lateral torsional buckling.

The perpendicular hat profile provided sufficient torsional restraint for one of the test specimen, but two of the test specimen failed as a result of lateral torsional buckling. Due to this the fourth test specimen was braced at the top flange. As a result of the experimental tests the roof element was reinforced with a lateral diaphragm at the top flange of the main purlins to prevent lateral torsional buckling even when the hat profile do not sufficient torsional restraint.

The experimental test elements showed how big the deviations from the manufacturing drawings can be. The deviations and imperfections may have a significant impact on the ultimate loadbearing capacity of the element. This stresses the importance of quality control at the workshop. The risk can be minimized by designing such a structure, which does not rely too much on the stiffness of the connections.

There are still some work to do before the first elements can be installed in an engine hall, as detailed design was not part of the scope, but this development work gives the basic principal solutions. The detailed design is something, which needs to be done as part of the project. The dimensioning can however be done based on the bending moment resistance of the main purlins, based on the effective cross-section according to EN 1993-1-3, which will be helpful and speed up the design process.



## **7.1 Further studies**

If one would like to use only the perpendicular hat profile as the main lateral-torsional restraint on cold-formed thin-walled steel structures, further studies would be needed. The experimental tests in this Thesis shows that it may be possible, but there are not enough studies on the subject to provide suitable and safe calculation methods. It also became very clear that the execution in the workshop may be very different from the design and the workshop may not always understand the importance of the connection details in such thin-walled structures. Due to the high risk involved in the execution, sufficient safety factors would be needed in the design.

The design resistance of a thermally slotted purlin against local transverse force is another thing which could be studied more in order to get an analytical calculation model and formulas. The slotted section has significantly lower resistance than an otherwise identical non-slotted section.

## References

- Aalto, J., 2009. *Laattarakenteiden kimmoiset menetelmät - Luentomoniste*. s.l., Aalto university.
- Ahokas, R., 2003. *The National Building Code of Finland - C4*. Helsinki: Ministry of the Environment.
- Andersson, L.-J., 2008. *Design handbook - Ventilation systems*, Vaasa: Wärtsilä.
- Bergamaschi, L. & Putti, M., 1999. Mixed Finite Elements and Newton-type linearization for the solution of Richards' equation. *INTERNATIONAL JOURNAL FOR NUMERICAL METHODS IN ENGINEERING*, 5 January, Issue 3 August 1998, p. 22.
- Çengel, Y. A., 2008. *Introduction to Thermodynamics and Heat Transfer 2nd edition*. Second Edition toim. s.l.:McGraw-Hill Companies Inc.
- Dlubal Software GmbH, 2013. *Program RFEM 5 Spatial Model Calculated Acc. to Finite Element Method*. July 2013 toim. Tiefenbach: Dlubal Software GmbH.
- EN 1993-1-3, 2009. *EN 1993-1-3 2006 + AC 2009 Eurocode 3 - Design of steel structures - Part 1-3: General rules*. Brussels: s.n.
- Fabrin, P. & Martikainen, L., 2009. *The influence of thermal stud to the thermal transmittance of modelled wall structure*, Hämeenlinna: HAMK - University of Applied Sciences.
- Grey, C. N., 2011. *Cold-Formed Steel Behavior*, Blacksburg, Virginia: Virginia Polytechnic Institute and State University.
- Hongisto, V., 2005. *Tuotekehityscaset, ääneneristys*. s.l., Työterveyslaitos.
- Hughes, T. J. R., 2000. *The finite element method : linear static and dynamic finite element analysis*. Courier Corporation toim. Mineola(NY): Dover Publications.
- Ivanyi, M. & Skaloud, M., 2014. *Stability Problems of Steel Structures*. Udine: Springer.
- Karwowski, W. & T. S., 2012. *Advances in Ergonomics in Manufacturing*. Boca Raton, FL: Taylor & Francis.
- Kesti, J., 2000. *Local and distortional buckling of perforated steel wall studs*. Helsinki: Helsinki University of Technology.
- Lindqvist, K. & N. W. M. S., 2009. *Wärtsilä Technical Journal 02.2009. Wärtsilä in Finland*. [Online]  
Available at: <http://www.wartsila.fi/file/Wartsila/1278515174979a1267106724867-The-W%C3%A4rtsil%C3%A4-20V46F-power-plant-solution-.pdf>  
[Accessed 03 01 2015].

Markku Kaurila Ltd, 2004. *Fire Technical Report - Engine hall fire scenarios and function of smoke detectors*, Turku: s.n.

Nevander, L. E. & Elmarsson, B., 1994. *Fukt handbok - Praktik och teori*. Andra toim. Stockholm: AB svensk Byggtjänst.

Rakennustieto Oy, 2010. *RunkoRYL 2010 - Rakennustöiden yleiset laatuvaatimukset. Talonrakennuksen runkotyöt*. 2010 toim. Helsinki: Rakennustietosäätiö RTS.

The Finnish Federation of the Hard of Hearing, 2014. *Kuuloliitto*. [Online]  
Available at: [http://www.kuuloliitto.fi/fin/kuulo/kuulonsuojelu/meluvamman\\_synty/](http://www.kuuloliitto.fi/fin/kuulo/kuulonsuojelu/meluvamman_synty/)  
[Accessed 19 03 2014].

Thöyrä, T., 2001. *Strength of Slotted Steel Studs*. Stockholm: Royal Institute of Technology.

Wärtsilä Corporation, 2014. *Power Plant Technology - Overview*. [Online]  
Available at:  
[http://www.wartsila.com/file/Wartsila/en/1278540642271a1267106724867-Wartsila\\_Power\\_Plants\\_Solutions\\_2014\\_brochure.pdf](http://www.wartsila.com/file/Wartsila/en/1278540642271a1267106724867-Wartsila_Power_Plants_Solutions_2014_brochure.pdf)  
[Accessed 03 01 2015].

Yang, J. & Liu, Q., 2012. *An experimental study into flexural behaviour of sigma purlins attached with roof sheets*, birmingham: School of Civil Engineering, University of Birmingham.

## **APPENDIX 1**

**Analytical calculations of section properties of LPT-C250x50x15x1.2, S350GD+Z  
according to EN 1993-1-3:2006 /AC:2009**

**Section properties of LPT-C250x50x1.2, S350GD+Z according to EN 1993-1-3:2006 /AC:2009 under bending in major axis.**

Material data:

$$f_{yb} := 350 \frac{\text{N}}{\text{mm}^2}$$

$$f_u := 420 \frac{\text{N}}{\text{mm}^2}$$

$$E := 210000 \frac{\text{N}}{\text{mm}^2}$$

$$\nu := 0.3$$

$$\gamma_{M0} := 1.0$$

Cross-sectional dimensions:

$$t := 1.2 \text{ mm}$$

$$b := 50 \text{ mm}$$

$$h := 250 \text{ mm}$$

$$r := 1.9 \text{ mm}$$

$$\phi := 90 \text{ deg}$$

$$c := 15 \text{ mm}$$

$$h_{\text{perf}} := 102 \text{ mm}$$

$$d_{\text{perf}} := 3 \text{ mm}$$

$$t_{\text{perf}} := \frac{25}{100} t = 0.3 \cdot \text{mm}$$

Effects of rounded corners acc. to EN1993-1-3:

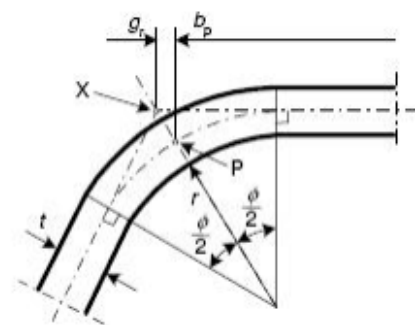
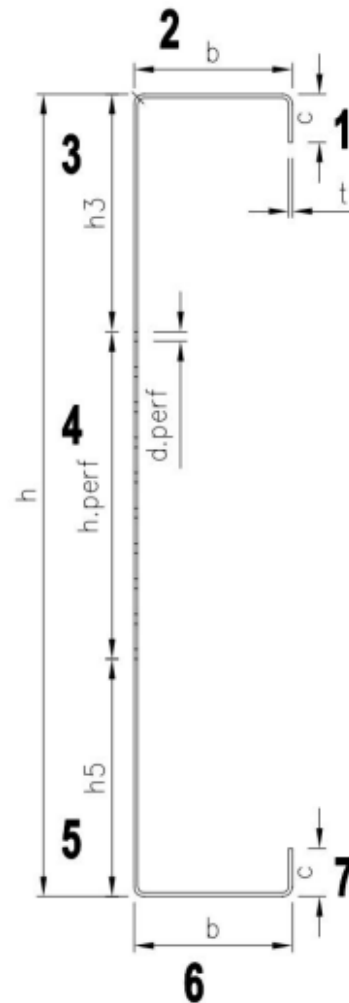
$$r_m := r + \frac{t}{2} = 2.5 \cdot \text{mm}$$

$$r_o := r + t = 3.1 \cdot \text{mm}$$

$$h_p := h - t - \left[ 2 \cdot \left( 1 - \sin\left(\frac{\phi}{2}\right) \right) \cdot r_m \right] = 247.336 \cdot \text{mm}$$

$$b_p := b - t - \left[ 2 \cdot \left( 1 - \sin\left(\frac{\phi}{2}\right) \right) \cdot r_m \right] = 47.336 \cdot \text{mm}$$

$$b_{p,c} := c - \frac{t}{2} - \left( 1 - \sin\left(\frac{\phi}{2}\right) \right) \cdot r_m = 13.668 \cdot \text{mm}$$



The diagram shows a frame structure with the following dimensions and labels:

- Horizontal dimensions:**
  - Top horizontal member: 50 units long.
  - Bottom horizontal member: 50 units long.
  - Vertical offset between horizontal members: 15 units.
- Vertical dimensions:**
  - Left vertical member: 74 units long.
  - Right vertical member: 102 units long.
  - Vertical offset between horizontal members: 74 units.
- Labels:**
  - 1:** Top horizontal member.
  - 2:** Left vertical member.
  - 3:** Right vertical member.
  - 4:** Bottom horizontal member.
  - 5:** Left vertical member.
  - 6:** Right vertical member.
  - 7:** Bottom horizontal member.
- Coordinate System:**
  - y:** Horizontal axis pointing right.
  - z:** Vertical axis pointing down.

$$A_7 := b_{p,c} \cdot t = 16.401 \cdot \text{mm}^2$$

$$z_7 := h - \frac{c}{2} = 242.5 \cdot \text{mm}$$

$$z_0 := \frac{A_1 \cdot z_1 + A_2 \cdot z_2 + A_3 \cdot z_3 + A_4 \cdot z_4 + A_5 \cdot z_5 + A_6 \cdot z_6 + A_7 \cdot z_7}{A_{\text{tot}}} = 125 \cdot \text{mm}$$

### Effective cross-section according to EN 1993-1-5:

Initial assumptions. Correct values will be determined by iteration.

#### Effective web, upper part:

$$\sigma_{c,\max} := f_{yb} \quad \sigma_{t,\max} := -f_{yb}$$

$$h_3 := \frac{h_p - h_{p,\text{perf}}}{2} = 72.668 \cdot \text{mm}$$

$$\psi_3 := \frac{143.5}{350} = 0.41$$

$$k_{\sigma,3} := \frac{0.578}{\psi_3 + 0.34} = 0.771$$

Stiffness of perforated web assumed to be near 0.

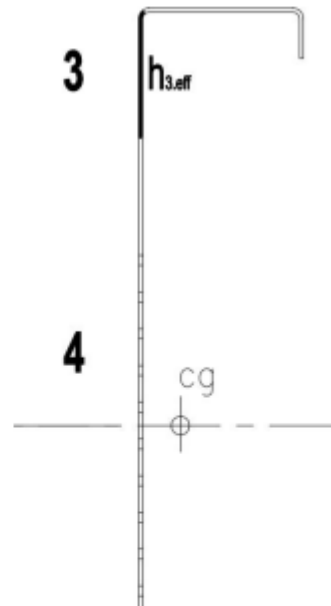
$$\lambda_{p,3} := \frac{\frac{h_3}{t}}{28.4 \cdot \sqrt{\frac{235 \text{ N}}{f_{yb} \cdot \text{mm}^2}} \cdot \sqrt{k_{\sigma,3}}} = 2.964$$

$$\rho_{b,3} := \begin{cases} 1 & \text{if } \lambda_{p,3} \leq 0.748 \\ \frac{\lambda_{p,3} - 0.188}{\lambda_{p,3}^2} & \text{otherwise} \end{cases} = 0.316$$

$$h_{3,\text{eff}} := \rho_{b,3} \cdot h_3 = 22.96 \cdot \text{mm}$$

$$h_{3,\text{ineff}} := h_3 - h_{3,\text{eff}} = 49.708 \cdot \text{mm}$$

$$A_{3,\text{eff}} := h_{3,\text{eff}} \cdot t = 27.552 \cdot \text{mm}^2$$



Perforated area assumed to be completely in compression.

$$A_{4,\text{eff}} := 0 \text{ mm}^2$$

**Effective top flange:**

Initial assumptions. Correct values will be determined by iteration.

$$\psi_2 := 1$$

$$k_{\sigma,2} := 4$$

$$\lambda_{p,2} := \frac{\frac{b_p}{t}}{28.4 \cdot \sqrt{\frac{235N}{f_{yb} \cdot \text{mm}^2}} \cdot \sqrt{k_{\sigma,2}}} = 0.848$$

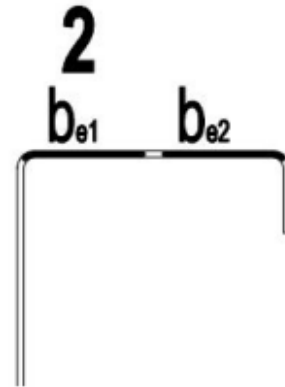
$$\rho_{b,2} := \begin{cases} 1 & \text{if } \lambda_{p,2} \leq 0.5 + \sqrt{0.085 - 0.055 \cdot \psi_2} \\ \frac{\lambda_{p,2} - 0.055 \cdot (3 + \psi_2)}{\lambda_{p,2}^2} & \text{otherwise} \end{cases} = 0.874$$

$$b_{\text{eff}} := \rho_{b,2} \cdot b_p = 41.353 \cdot \text{mm}$$

$$b_{e1} := 0.5 \cdot b_{\text{eff}} = 20.677 \cdot \text{mm}$$

$$b_{e2} := 0.5 \cdot b_{\text{eff}} = 20.677 \cdot \text{mm}$$

$$A_{2,\text{eff}} := b_{\text{eff}} \cdot t = 49.624 \cdot \text{mm}^2$$

**Effective flange stiffener width:**

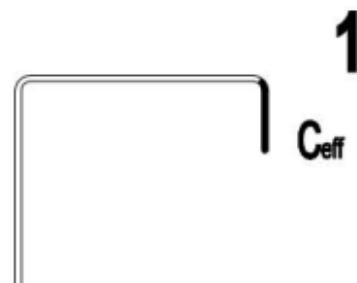
Initial assumptions. Correct values will be determined by iteration.

Spring stiffness of flange and reduction factor for the edge stiffener:

$$\psi_1 := 1$$

$$k_{\sigma,1} := \begin{cases} 0.5 & \text{if } \frac{b_{p,c}}{b_p} \leq 0.35 \\ \left[ 0.5 + 0.83 \cdot \sqrt{\left( \frac{b_{p,c}}{b_p} - 0.35 \right)^2} \right]^3 & \text{if } 0.35 < \frac{b_{p,c}}{b_p} \leq 0.6 \end{cases} = 0.5$$

$$\lambda_{p,1} := \frac{\frac{b_{p,c}}{t}}{28.4 \cdot \sqrt{\frac{235N}{f_{yb} \cdot \text{mm}^2}} \cdot \sqrt{k_{\sigma,1}}} = 0.692$$





$$\rho_{b,1} := \begin{cases} 1 & \text{if } \lambda_{p,1} \leq 0.748 \\ \frac{\lambda_{p,1} - 0.188}{\lambda_{p,1}^2} & \text{otherwise} \end{cases} = 1$$

$$c_{\text{eff}} := \rho_{b,1} \cdot b_{p,c} = 13.668 \cdot \text{mm}$$

$$A_{s1} := t \cdot c_{\text{eff}} = 16.401 \cdot \text{mm}^2$$

$$A_{s2} := t \cdot b_{e2} = 24.812 \cdot \text{mm}^2$$

$$A_s := A_{s1} + A_{s2} = 41.213 \cdot \text{mm}^2$$

$$A_{s0} := A_s$$

$$y_{s,\text{cg}} := \frac{t \cdot b_{e2} \cdot \left( b_p - \frac{b_{e2}}{2} \right) + t \cdot c_{\text{eff}} \cdot y_1}{A_s} = 41.933 \cdot \text{mm}$$

$$z_{s,\text{cg}} := \frac{t \cdot (b_{e2} \cdot z_2 + c_{\text{eff}} \cdot z_1)}{A_s} = 3.346 \cdot \text{mm}$$

$$I_{z,s} := \frac{1}{12} \cdot t \cdot c_{\text{eff}}^3 + \frac{1}{12} \cdot b_{e2} \cdot t^3 + A_{s1} \cdot (z_{s,\text{cg}} - z_1)^2 + A_{s2} \cdot (z_{s,\text{cg}} - z_2)^2 = 728.414 \cdot \text{mm}^4$$

Deformation of flange calculated with RFEM and the unit load  $u$

$$u := 0.1 \frac{\text{kN}}{\text{m}}$$

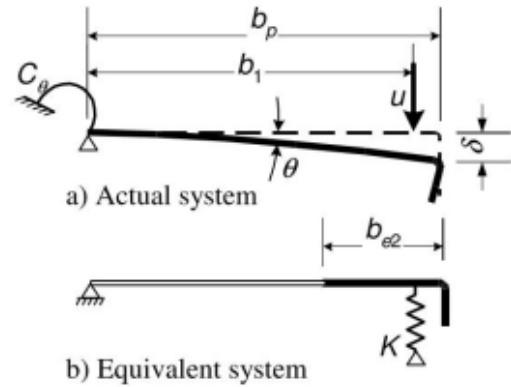
$$\delta := 2.75 \text{ mm}$$

$$K_1 := \frac{u}{\delta} = 0.036 \cdot \frac{\text{N}}{\text{mm}^2}$$

$$\sigma_{\text{cr},s} := \frac{2 \cdot \sqrt{K_1 \cdot E \cdot I_{z,s}}}{A_s} = 114.452 \cdot \frac{\text{N}}{\text{mm}^2}$$

$$\lambda_d := \sqrt{\frac{f_{yb}}{\sigma_{\text{cr},s}}} = 1.749$$

$$\chi_d := \begin{cases} 1 & \text{if } \lambda_d \leq 0.65 \\ 1.47 - 0.723 \cdot \lambda_d & \text{if } 0.65 < \lambda_d < 1.38 \\ \frac{0.66}{\lambda_d} & \text{otherwise} \end{cases} = 0.377$$



Calculating the effective width with reduced compressive stress:

Iteration 1:

$$\sigma_{\text{com.Ed}_1} := \chi_d \cdot \frac{f_{yb}}{\gamma_{M0}} = 132.096 \cdot \frac{\text{N}}{\text{mm}^2}$$

$$\lambda_{p,\text{red.1}} := \lambda_{p.2} \cdot \sqrt{\chi_d} = 0.521$$

$$\rho_{b.1} = 1 \quad c_{\text{eff}} = 13.668 \cdot \text{mm}$$

$$\rho_{b.2} = 1 \quad b_{e2} = 23.668 \cdot \text{mm}$$

$$\chi_{d.1} = 0.365$$

Iteration 2:

$$\sigma_{\text{com.Ed}_2} := \chi_{d.1} \cdot \frac{f_{yb}}{\gamma_{M0}} = 127.782 \cdot \frac{\text{N}}{\text{mm}^2}$$

$$\lambda_{p,\text{red.2}} := \lambda_{p.2} \cdot \sqrt{\chi_{d.1}} = 0.512$$

$$\rho_{b.1} = 1 \quad c_{\text{eff}} = 13.668 \cdot \text{mm}$$

$$\rho_{b.2} = 1 \quad b_{e2} = 23.668 \cdot \text{mm}$$

$$\chi_{d.2} = 0.365$$

$\chi_{d.2} = \chi_{d.1}$ , no further iteration needed.

$$A_{s1} := t \cdot c_{\text{eff}} = 16.401 \cdot \text{mm}^2$$

$$A_{s2} := t \cdot b_{e2} = 28.401 \cdot \text{mm}^2$$

$$A_s := A_{s1} + A_{s2} = 44.803 \cdot \text{mm}^2$$

$$y_{s,\text{cg}} := \frac{t \cdot b_{e2} \cdot \left( b_p - \frac{b_{e2}}{2} \right) + t \cdot c_{\text{eff}} \cdot y_1}{A_s} = 40.59 \cdot \text{mm}$$

$$z_{s,\text{cg}} := \frac{t \cdot (b_{e2} \cdot z_2 + c_{\text{eff}} \cdot z_1)}{A_s} = 3.126 \cdot \text{mm}$$

$$I_{z.s} := \frac{1}{12} \cdot t \cdot c_{\text{eff}}^3 + \frac{1}{12} \cdot b_{e2} \cdot t^3 + A_{s1} \cdot (z_{s,\text{cg}} - z_1)^2 + A_{s2} \cdot (z_{s,\text{cg}} - z_2)^2 = 753.74 \cdot \text{mm}^4$$

$$\sigma_{\text{cr.s}} := \frac{2 \cdot \sqrt{K_1 \cdot E \cdot I_{z.s}}}{A_s} = 107.098 \cdot \frac{\text{N}}{\text{mm}^2}$$

$$\lambda_d := \sqrt{\frac{f_{yb}}{\sigma_{cr.s}}} = 1.808$$

$$\chi_d := \begin{cases} 1 & \text{if } \lambda_d \leq 0.65 \\ 1.47 - 0.723 \cdot \lambda_d & \text{if } 0.65 < \lambda_d < 1.38 \\ \frac{0.66}{\lambda_d} & \text{otherwise} \end{cases} = 0.365$$

$$\lambda_{p.red} := \lambda_{p.2} \cdot \sqrt{\chi_d} = 0.512$$

$$\sigma_{com.Ed} := \frac{h - \left( z_{s.cg} - \frac{t}{2} \right) - z_0}{h - z_0} \cdot \frac{f_{yb}}{\gamma_{M0}} = 342.927 \cdot \frac{N}{mm^2}$$

$$A_{s.red} := \chi_d \cdot A_s \cdot \frac{\frac{f_{yb}}{\gamma_{M0}}}{\sigma_{com.Ed}} = 16.694 \cdot mm^2 < A_s = 44.803 \cdot mm^2$$

$$t_{red} := \frac{t \cdot A_{s.red}}{A_s} = 0.447 \cdot mm$$

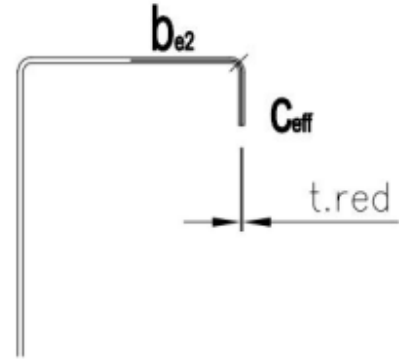
$$A_{1.eff} := \frac{t_{red}}{t} \cdot A_1 = 6.111 \cdot mm^2$$

$$A_{2.eff} := b_{e1} \cdot t + t_{red} \cdot b_{e2} = 35.395 \cdot mm^2$$

$$y_{2.eff} := \frac{b_{e1} \cdot t \cdot \frac{b_{e1}}{2} + b_{e2} \cdot t_{red} \cdot \left( b_p - \frac{b_{e2}}{2} \right)}{b_{e1} \cdot t + b_{e2} \cdot t_{red}} = 17.862 \cdot mm$$

$$z_{3.eff} := \frac{h_{3.eff} + r_m \cdot \left( 1 - \sin\left(\frac{\phi}{2}\right) \right) + \frac{t}{2}}{2} = 12.146 \cdot mm$$

$$A_{eff.tot} := A_{1.eff} + A_{2.eff} + A_{3.eff} + A_{4.eff} + A_5 + A_6 + A_7 = 229.464 \cdot mm^2$$



**Location of centroid:**

$$y_{c0} := \frac{A_{1,eff} \cdot y_1 + A_{2,eff} \cdot y_{2,eff} + A_{3,eff} \cdot y_3 + A_{4,eff} \cdot y_4 + A_5 \cdot y_5 + A_6 \cdot y_6 + A_7 \cdot y_7}{A_{eff,tot}} = 14.091 \cdot \text{mm}$$

$$z_{c0} := \frac{A_{1,eff} \cdot z_1 + A_{2,eff} \cdot z_2 + A_{3,eff} \cdot z_{3,eff} + A_{4,eff} \cdot z_4 + A_5 \cdot z_5 + A_6 \cdot z_6 + A_7 \cdot z_7}{A_{eff,tot}} = 161.766 \cdot \text{mm}$$

$$z_{4,eff} := z_{c0} + \frac{\left( \frac{h}{2} + \frac{h_{perf}}{2} - z_{c0} \right)}{2} = 168.883 \cdot \text{mm}$$

$$A_{4,eff} := \left[ \left( \frac{h}{2} + \frac{h_{perf}}{2} \right) - z_{c0} \right] \cdot t - 2d_{perf} \cdot 0.75 \cdot t = 11.681 \cdot \text{mm}^2$$

$$A_{eff,tot} := A_{1,eff} + A_{2,eff} + A_{3,eff} + A_{4,eff} + A_5 + A_6 + A_7 = 241.144 \cdot \text{mm}^2$$

Effective perforated area not neglectable as  $z_{4,eff} \gg z_{c0}$ .

Iteration needed:

Iteration 1:

$$z_{4,eff} = 169.055 \cdot \text{mm} \quad z_{c0} = 162.111 \cdot \text{mm}$$

Iteration 2:

$$z_{4,eff} = 169.054 \cdot \text{mm} \quad z_{c0} = 162.107 \cdot \text{mm}$$

Iteration 3:

$$z_{4,eff} = 169.054 \cdot \text{mm} \quad z_{c0} = 162.107 \cdot \text{mm}$$

$$z_{c0} := \frac{A_{1,eff} \cdot z_1 + A_{2,eff} \cdot z_2 + A_{3,eff} \cdot z_{3,eff} + A_{4,eff} \cdot z_{4,eff} + A_5 \cdot z_5 + A_6 \cdot z_6 + A_7 \cdot z_7}{A_{eff,tot}} = 162.107 \cdot \text{mm}$$

$$z_{4,eff} := z_{c0} + \frac{\left( \frac{h}{2} + \frac{h_{perf}}{2} - z_{c0} \right)}{2} = 169.054 \cdot \text{mm}$$

$$A_{4,eff} := \left[ \left( \frac{h}{2} + \frac{h_{perf}}{2} \right) - z_{c0} \right] \cdot t - 2d_{perf} \cdot 0.75 \cdot t = 11.271 \cdot \text{mm}^2$$

$$A_{eff,tot} := A_{1,eff} + A_{2,eff} + A_{3,eff} + A_{4,eff} + A_5 + A_6 + A_7$$

$$h_{4,\text{eff}} := \left( \frac{h}{2} + \frac{h_{\text{perf}}}{2} \right) - z_{c0} = 13.893 \cdot \text{mm}$$

$$y_{c0} := \frac{A_{1,\text{eff}} y_1 + A_{2,\text{eff}} y_2 + A_{3,\text{eff}} y_3 + A_{4,\text{eff}} y_4 + A_5 y_5 + A_6 y_6 + A_7 y_7}{A_{\text{eff.tot}}}$$

$$z_{c0} := \frac{A_{1,\text{eff}} z_1 + A_{2,\text{eff}} z_2 + A_{3,\text{eff}} z_{3,\text{eff}} + A_{4,\text{eff}} z_{4,\text{eff}} + A_5 z_5 + A_6 z_6 + A_7 z_7}{A_{\text{eff.tot}}}$$

$$y_{c0} = 14.508 \cdot \text{mm}$$

$$z_{c0} = 162.107 \cdot \text{mm}$$

$$A_{\text{eff.tot}} = 240.735 \cdot \text{mm}^2$$

Distances between center of gravity of effective partial areas and centroid i z-axis.

$$d_1 := |z_{c0} - z_1| = 154.607 \cdot \text{mm}$$

$$d_2 := |z_{c0} - z_2| = 161.507 \cdot \text{mm}$$

$$d_3 := |z_{c0} - z_{3,\text{eff}}| = 149.961 \cdot \text{mm}$$

$$d_4 := |z_{c0} - z_{4,\text{eff}}| = 6.946 \cdot \text{mm}$$

$$d_5 := |z_{c0} - z_5| = 50.893 \cdot \text{mm}$$

$$d_6 := |z_{c0} - z_6| = 87.293 \cdot \text{mm}$$

$$d_7 := |z_{c0} - z_7| = 80.393 \cdot \text{mm}$$

**Effective moments of area:**

$$I_{y1} := \frac{1}{12} \cdot t_{\text{red}} \cdot (c_{\text{eff}})^3 = 95.139 \cdot \text{mm}^4$$

$$I_{y2} := \frac{1}{12} \cdot (b_{e1} \cdot t^3 + b_{e2} \cdot t_{\text{red}}^3) = 3.154 \cdot \text{mm}^4$$

$$I_{y3} := \frac{1}{12} \cdot t \cdot h_{3,\text{eff}}^3 = 1.21 \times 10^3 \cdot \text{mm}^4$$

$$I_{y4} := \frac{1}{12} \cdot t \cdot h_{4,\text{eff}}^3 - (0.25 \cdot t \cdot d_{\text{perf}}) \cdot \left[ \left( h_{4,\text{eff}} - \frac{d_{\text{perf}}}{2} \right)^2 + \left( \frac{d_{\text{perf}}}{2} \right)^2 \right] = 127.888 \cdot \text{mm}^4$$

$$I_{y5} := \frac{1}{12} \cdot t \cdot \left( \frac{h_p - h_{\text{perf}}}{2} \right)^3 = 3.837 \times 10^4 \cdot \text{mm}^4$$

$$I_{y6} := \frac{1}{12} \cdot b_p \cdot t^3 = 6.816 \cdot \text{mm}^4$$

$$I_{y7} := \frac{1}{12} \cdot t \cdot b_{p,c}^3 = 255.325 \cdot \text{mm}^4$$

$$I_{y,\text{eff}} := I_{y1} + I_{y2} + I_{y3} + I_{y4} + I_{y5} + I_{y6} + I_{y7} + A_{1,\text{eff}}(d_1)^2 + A_{2,\text{eff}}(d_2)^2 \dots \\ + A_{3,\text{eff}}(d_3)^2 + A_{4,\text{eff}}(d_4)^2 + A_5(d_5)^2 + A_6(d_6)^2 + A_7(d_7)^2$$

$$I_{y,\text{eff}} = 2.494 \times 10^{-6} \text{ m}^4$$

$$W_{y,\text{eff}} := \frac{I_{y,\text{eff}}}{z_{c0}} = 1.539 \times 10^4 \cdot \text{mm}^3$$

Table 1 shows the iteration steps and corresponding values. The extreme fibre values were assumed in the beginning and later all these values have been re-calculated in each iteration to get the final values.

**Table 1**

Iteration	$\sigma_{c,\text{max}}$	$\sigma_{t,\text{max}}$	$y_{c0}$	$z_{c0}$	$A_{\text{eff}}$	$W_{y,\text{eff}}$	$I_{y,\text{eff}}$	$M_{y,\text{Rd}}$
#	MPa	MPa	mm	mm	mm <sup>2</sup>	mm <sup>3</sup>	mm <sup>4</sup>	kNm
0	350	-350	14,508	162,107	240,735	15390	2494000	5,385
1	350	-189,17	14,713	163,299	237,248	15030	2454000	5,26
2	350	-185,133	14,718	163,326	237,169	15020	2453000	5,257
3	350	-185,133	14,718	163,326	237,169	15020	2453000	5,257

**Results:**

Location of centroid:

$$y_{c0} := 14.718 \text{ mm}$$

$$z_{c0} := 163.326 \text{ mm}$$

Effective cross-section area:

$$A_{\text{eff.tot}} := 237.169 \text{ mm}^2$$

Effective second moment of inertia, y-y axis:

$$I_{y.\text{eff}} := 2.453 \cdot 10^6 \text{ mm}^4$$

Effective section modulus, y-y axis:

$$W_{y.\text{eff}} := 15020 \text{ mm}^3$$


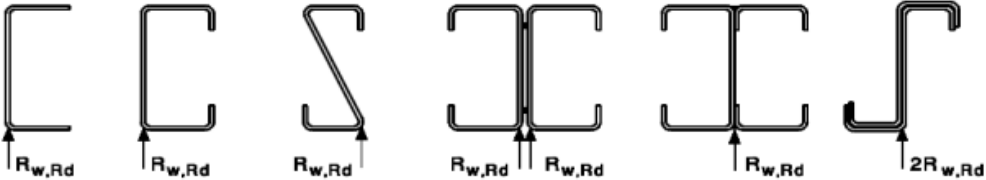
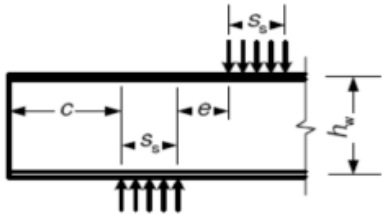
**Bending moment capacity in the strong axis:**


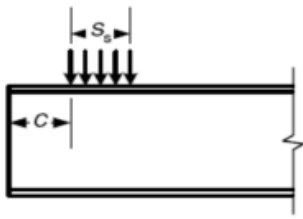
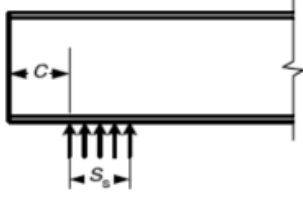
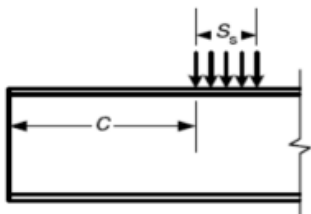
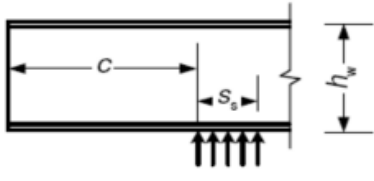
$$M_{y.Rd} := f_{yb} \cdot \frac{I_{y.\text{eff}}}{z_{c0}} = 5.257 \cdot \text{kN} \cdot \text{m}$$


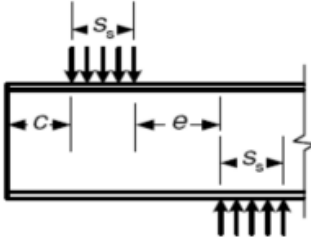
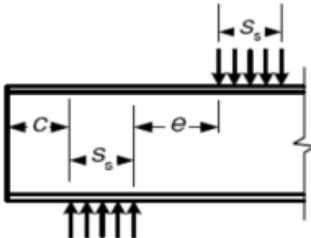
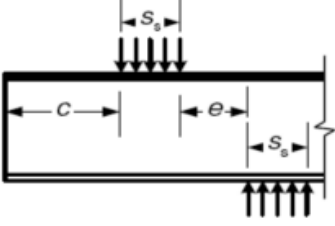
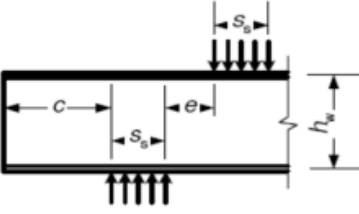
## **APPENDIX 2**


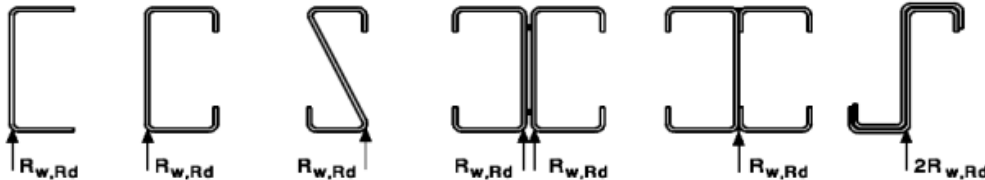
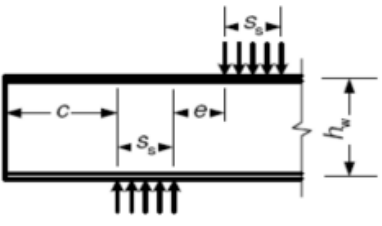
**Local transverse force calculations according to EN 1993-1-3:2006 /AC:2009. For thin-walled cross-sections with a single web**


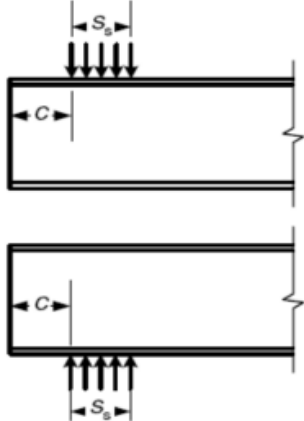
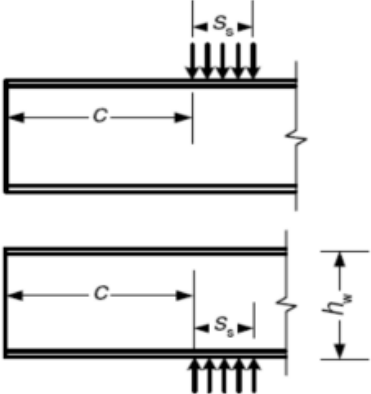



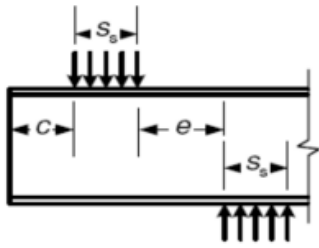
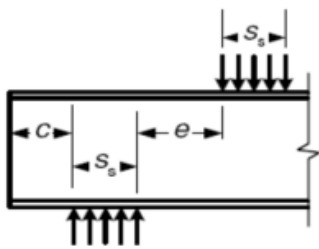
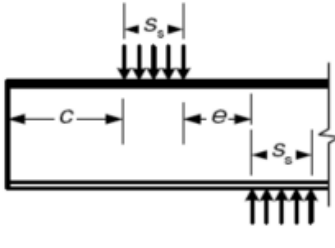
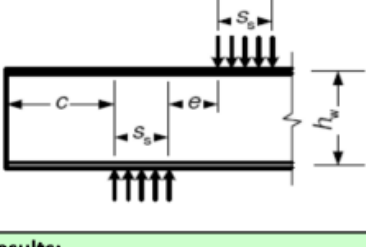
		<b>Input Data</b>	
		Author: Andreas Limnell	Page: 1
		Date: 23.6.2015	
Project: Master's thesis	Work no: #	Contents: Calculation of the support C-profiles of the roof element.	Location: Helsinki
<b>Local transverse force check according to EN 1993-1-3:2006 /AC:2009. For thin-walled cross-sections with a single unstiffened</b>			
Version 0.95			
<b>Input</b>			
<b>6.1.7.2 Cross-sections with a single unstiffened web</b> (1) For a cross-section with a single unstiffened web, see figure 6.6, the local transverse resistance of the web may be determined as specified in (2), provided that the cross-section satisfies the following criteria: <div style="display: flex; justify-content: space-between; margin-top: 10px;"> <div> <math display="block">\frac{h_w}{t} \leq 200</math> <math display="block">\frac{r}{t} \leq 6</math> <math display="block">45^\circ \leq \phi \leq 90^\circ</math> </div> <div>             ... (6.14a)              ... (6.14b)              ... (6.14c)           </div> </div> <p>where:</p> <ul style="list-style-type: none"> <li><math>h_w</math> is the web height between the midlines of the flanges;</li> <li><math>r</math> is the internal radius of the corners;</li> <li><math>\phi</math> is the angle of the web relative to the flanges [degrees].</li> </ul> <div style="text-align: center; margin-top: 20px;">  </div>			
<b>Figure 6.6: Examples of cross-sections with a single web</b>			
<b>Cross-section properties:</b>			
$t = 1,50$ mm $h_w = 100,00$ mm $r = 4,00$ mm $\phi = 90^\circ$	is the thickness of the web and flanges is the height of the web is the internal radius of the corners is the angle between the flange and the web	Criteria (6.14) $h_w/t =$ OK $r/t =$ OK $45 \leq \phi \leq 90$ OK	
<b>Material properties:</b>			
$f_{yb} = 350,00$ N/mm <sup>2</sup> $\gamma_{MI} = 1,00$			
<b>Load input:</b>			
$F_{Ed} = 4150$ N $s_s = 60,00$ mm $c = 0$ mm $e = 20$ mm	is the transverse force is the width of support/force is the distance from a free end is the eccentricity between loads (only if $e < 1.5 \cdot h_w$ )		

		Calculation	
		Author: Andreas Limnell	Page: 2
		Date: 23.6.2015	
Project: Master's thesis	Work no: #	Contents: Calculation of the support C-profiles of the roof element.	Location: Helsinki
Calculations and load case:			
The values of the coefficients $k$ and $k_1$ to $k_5$ :			
$k = 1,54$ $k_1 = 1,33$ $k_2 = 0,75$ $k_3 = 1,00$ $k_4 = 1,22$ $k_5 = 0,90$			
 		<p>a) For a single local load or support reaction</p> <p>i) <math>c \leq 1.5 h_w</math> clear from a free end:</p> <p>Stiffened flanges: <b>Yes</b></p> <p>- for a cross-section with stiffened flanges:</p> $R_{w,Rd} = \frac{k_1 k_2 k_3 \left[ 9,04 - \frac{h_w/t}{60} \right] \left[ 1 + 0,01 \frac{s_s}{t} \right] t^2 f_{yb}}{\gamma_{M1}} \quad (6.15a)$ <p>- for a cross-section with unstiffened flanges:</p> <p>- if <math>s_d/t \leq 60</math>:</p> $R_{w,Rd} = \frac{k_1 k_2 k_3 \left[ 5,92 - \frac{h_w/t}{132} \right] \left[ 1 + 0,01 \frac{s_s}{t} \right] t^2 f_{yb}}{\gamma_{M1}} \quad (6.15b)$ <p>- if <math>s_d/t &gt; 60</math>:</p> $R_{w,Rd} = \frac{k_1 k_2 k_3 \left[ 5,92 - \frac{h_w/t}{132} \right] \left[ 0,71 + 0,015 \frac{s_s}{t} \right] t^2 f_{yb}}{\gamma_{M1}} \quad (6.15c)$	
 		<p>ii) <math>c &gt; 1.5 h_w</math> clear from a free end:</p> <p>- if <math>s_d/t \leq 60</math>:</p> $R_{w,Rd} = \frac{k_3 k_4 k_5 \left[ 14,7 - \frac{h_w/t}{49,5} \right] \left[ 1 + 0,007 \frac{s_s}{t} \right] t^2 f_{yb}}{\gamma_{M1}} \quad (6.15d)$ <p>- if <math>s_d/t &gt; 60</math>:</p> $R_{w,Rd} = \frac{k_3 k_4 k_5 \left[ 14,7 - \frac{h_w/t}{49,5} \right] \left[ 0,75 + 0,011 \frac{s_s}{t} \right] t^2 f_{yb}}{\gamma_{M1}} \quad (6.15e)$	

		<b>Calculation</b>	
		Author: Andreas Limnell	Page: 3
		Date: 23.6.2015	
Project: Master's thesis	Work no: #	Contents: Calculation of the support C-profiles of the roof element.	Location: Helsinki
<b>Calculations and load case:</b>			
 		<p>b) For two opposing local transverse forces closer together than <math>1.5 h_w</math>:</p> <p>i) <math>c \leq 1.5 h_w</math> clear from a free end:</p> $R_{w,Rd} = \frac{k_1 k_2 k_3 \left[ 6,66 - \frac{h_w/t}{64} \right] \left[ 1 + 0,01 \frac{s_s}{t} \right] t^2 f_{yb}}{\gamma_{M1}} \quad (6.15f)$	
 		<p>ii) <math>c &gt; 1.5 h_w</math> clear from a free end:</p> $R_{w,Rd} = \frac{k_3 k_4 k_5 \left[ 21,0 - \frac{h_w/t}{16,3} \right] \left[ 1 + 0,0013 \frac{s_s}{t} \right] t^2 f_{yb}}{\gamma_{M1}} \quad (6.15g)$	
<b>Results:</b>			
<p>Requirement:</p> $F_{Ed} \leq R_{w,Rd}$ <div style="display: flex; justify-content: space-around; align-items: flex-start;"> <div> <math>F_{Ed} = </math> <div style="border: 1px solid black; padding: 2px 10px;">4150</div> N         </div> <div> <math>R_{w,Rd} = </math> <div style="border: 1px solid black; padding: 2px 10px;">6179</div> N         </div> <div> <p>is the transverse force</p> <p>is the local transverse resistance of the web</p> </div> </div> <p>Utilization ratio= <span style="border: 1px solid black; padding: 2px 10px;">0,67</span></p> <div style="text-align: right; margin-top: 5px;"> <span style="background-color: #e0ffff; padding: 5px 15px;">OK</span> </div>			


		<b>Input Data</b>													
		Author: Andreas Limnell	Page: 4												
		Date: 23.6.2015													
Project: Master's thesis	Work no: #	Contents: Calculation of the support C-profiles of the roof element.	Location: Helsinki												
<b>Local transverse force check according to EN 1993-1-3:2006</b> <b>/AC:2009. For thin-walled cross-sections with a single unstiffened</b>															
Version 0.95															
<b>Input</b>															
<b>6.1.7.2 Cross-sections with a single unstiffened web</b> (1) For a cross-section with a single unstiffened web, see figure 6.6, the local transverse resistance of the web may be determined as specified in (2), provided that the cross-section satisfies the following criteria: <div style="display: flex; justify-content: space-between; margin-top: 10px;"> <div> <math display="block">\frac{h_w}{t} \leq 200</math> <math display="block">\frac{r}{t} \leq 6</math> <math display="block">45^\circ \leq \phi \leq 90^\circ</math> </div> <div>             ... (6.14a)              ... (6.14b)              ... (6.14c)           </div> </div> <p>where:</p> <ul style="list-style-type: none"> <li><math>h_w</math> is the web height between the midlines of the flanges;</li> <li><math>r</math> is the internal radius of the corners;</li> <li><math>\phi</math> is the angle of the web relative to the flanges [degrees].</li> </ul> <div style="text-align: center; margin-top: 20px;">  </div> <p><b>Figure 6.6: Examples of cross-sections with a single web</b></p>															
<b>Cross-section properties:</b> <div style="display: flex; justify-content: space-between; align-items: flex-start; margin-top: 10px;"> <table border="1" style="border-collapse: collapse;"> <tr><td><math>t</math></td><td>2,00</td><td>mm</td></tr> <tr><td><math>h_w</math></td><td>100,00</td><td>mm</td></tr> <tr><td><math>r</math></td><td>4,00</td><td>mm</td></tr> <tr><td><math>\phi</math></td><td>90</td><td>°</td></tr> </table> <div> <p>is the thickness of the web and flanges</p> <p>is the height of the web</p> <p>is the internal radius of the corners</p> <p>is the angle between the flange and the web</p> </div> <div style="text-align: right;">             Criteria (6.14)  <math>h_w/t =</math> OK  <math>r/t =</math> OK  <math>45 \leq \phi \leq 90</math> OK           </div> </div>				$t$	2,00	mm	$h_w$	100,00	mm	$r$	4,00	mm	$\phi$	90	°
$t$	2,00	mm													
$h_w$	100,00	mm													
$r$	4,00	mm													
$\phi$	90	°													
<b>Material properties:</b> <div style="display: flex; justify-content: space-between; align-items: flex-start; margin-top: 10px;"> <table border="1" style="border-collapse: collapse;"> <tr><td><math>f_{yb}</math></td><td>350,00</td><td>N/mm<sup>2</sup></td></tr> <tr><td><math>\gamma_{MI}</math></td><td>1,00</td><td></td></tr> </table> </div>				$f_{yb}$	350,00	N/mm <sup>2</sup>	$\gamma_{MI}$	1,00							
$f_{yb}$	350,00	N/mm <sup>2</sup>													
$\gamma_{MI}$	1,00														
<b>Load input:</b> <div style="display: flex; justify-content: space-between; align-items: flex-start; margin-top: 10px;"> <table border="1" style="border-collapse: collapse;"> <tr><td><math>F_{Ed}</math></td><td>4150</td><td>N</td></tr> <tr><td><math>s_s</math></td><td>60,00</td><td>mm</td></tr> <tr><td><math>c</math></td><td>0</td><td>mm</td></tr> <tr><td><math>e</math></td><td>20</td><td>mm</td></tr> </table> <div> <p>is the transverse force</p> <p>is the width of support/force</p> <p>is the distance from a free end</p> <p>is the eccentricity between loads (only if <math>e &lt; 1.5 \cdot h_w</math>)</p> </div> <div style="text-align: right;">  </div> </div>				$F_{Ed}$	4150	N	$s_s$	60,00	mm	$c$	0	mm	$e$	20	mm
$F_{Ed}$	4150	N													
$s_s$	60,00	mm													
$c$	0	mm													
$e$	20	mm													

		<b>Calculation</b>	
		Author: Andreas Limnell	Page: 5
		Date: 23.6.2015	
Project: Master's thesis	Work no: #	Contents: Calculation of the support C-profiles of the roof element.	Location: Helsinki
<b>Calculations and load case:</b>			
The values of the coefficients $k$ and $k_1$ to $k_5$ :			
$k = 1,54$ $k_1 = 1,33$ $k_2 = 0,85$ $k_3 = 1,00$ $k_4 = 1,22$ $k_5 = 0,94$			
		<p>a) For a single local load or support reaction</p> <p>i) <math>c \leq 1.5 h_w</math> clear from a free end:</p> <p>Stiffened flanges: <b>Yes</b></p> <p>- for a cross-section with stiffened flanges:</p> $R_{w,Rd} = \frac{k_1 k_2 k_3 \left[ 9,04 - \frac{h_w/t}{60} \right] \left[ 1 + 0,01 \frac{s_s}{t} \right] t^2 f_{yb}}{\gamma_{M1}} \quad (6.15a)$ <p>- for a cross-section with unstiffened flanges:</p> <p>- if <math>s_s/t \leq 60</math>:</p> $R_{w,Rd} = \frac{k_1 k_2 k_3 \left[ 5,92 - \frac{h_w/t}{132} \right] \left[ 1 + 0,01 \frac{s_s}{t} \right] t^2 f_{yb}}{\gamma_{M1}} \quad (6.15b)$ <p>- if <math>s_s/t &gt; 60</math>:</p> $R_{w,Rd} = \frac{k_1 k_2 k_3 \left[ 5,92 - \frac{h_w/t}{132} \right] \left[ 0,71 + 0,015 \frac{s_s}{t} \right] t^2 f_{yb}}{\gamma_{M1}} \quad (6.15c)$	
		<p>ii) <math>c &gt; 1.5 h_w</math> clear from a free end:</p> <p>- if <math>s_s/t \leq 60</math>:</p> $R_{w,Rd} = \frac{k_3 k_4 k_5 \left[ 14,7 - \frac{h_w/t}{49,5} \right] \left[ 1 + 0,007 \frac{s_s}{t} \right] t^2 f_{yb}}{\gamma_{M1}} \quad (6.15d)$ <p>- if <math>s_s/t &gt; 60</math>:</p> $R_{w,Rd} = \frac{k_3 k_4 k_5 \left[ 14,7 - \frac{h_w/t}{49,5} \right] \left[ 0,75 + 0,011 \frac{s_s}{t} \right] t^2 f_{yb}}{\gamma_{M1}} \quad (6.15e)$	


		Calculation		
		Author: Andreas Limmell	Page: 6	
		Date: 23.6.2015		
Project: Master's thesis	Work no: #	Contents: Calculation of the support C-profiles of the roof element.	Location: Helsinki	
Calculations and load case:				
 		<p>b) For two opposing local transverse forces closer together than <math>1.5 h_w</math>:</p> <p>i) <math>c \leq 1.5 h_w</math> clear from a free end:</p> $R_{w,Rd} = \frac{k_1 k_2 k_3 \left[ 6,66 - \frac{h_w/t}{64} \right] \left[ 1 + 0,01 \frac{S_s}{t} \right] t^2 f_{yb}}{\gamma_{M1}} \quad (6.15f)$		
 		<p>ii) <math>c &gt; 1.5 h_w</math> clear from a free end:</p> $R_{w,Rd} = \frac{k_3 k_4 k_5 \left[ 21,0 - \frac{h_w/t}{16,3} \right] \left[ 1 + 0,0013 \frac{S_s}{t} \right] t^2 f_{yb}}{\gamma_{M1}} \quad (6.15g)$		
Results:				
Requirement:				
$F_{Ed} \leq R_{w,Rd}$		$F_{Ed} =$ <table border="1" style="display: inline-table;"> <tr><td>4150</td></tr> </table> N	4150	is the transverse force
4150				
		$R_{w,Rd} =$ <table border="1" style="display: inline-table;"> <tr><td>12096</td></tr> </table> N	12096	is the local transverse resistance of the web
12096				
Utilization ratio=		<table border="1" style="display: inline-table;"> <tr><td>0,34</td></tr> </table>	0,34	OK
0,34				

## **APPENDIX 3**

### **Insulation thickness for fire resistance - Standard fire**

		<b>Input Data</b>	
		Author: Andreas Limnell	Page: 1
		Date: 29.4.2014	
Project: Master's thesis	Work no: #	Contents: Calculation of the temperature of main purlin of roof element	Location: Helsinki
<b>Insulation thickness for fire resistance - Standard fire</b> <span style="float: right;">Version 0.9</span>			
<b>Input</b>			
<b>Initial data:</b>  $\theta_g(0) = $ <input type="text" value="293"/> K      is the initial temperature before the fire. (0 °C = 273.15 K)			
<b>Requirements:</b>  $R : $ <input type="text" value="60"/> min      is the required fire resistance			
<b>Accuracy:</b>  $\Delta t : $ <input type="text" value="2"/> s      is the time interval. (see Note 1 to the right)			
<b>Insulation parameters:</b>  <div style="display: flex; justify-content: space-between;"> <div> <math>d = </math> <input type="text" value="70,0"/> mm  <math>A = </math> <input type="text" value="1,00"/> m<sup>2</sup>  <math>\rho = </math> <input type="text" value="65,00"/> kg/m<sup>3</sup>  <math>C_p = </math> <input type="text" value="840"/> J/(kg*K)  <math>\lambda = </math> <input type="text" value="0,035"/> W/(m<sup>2</sup>*K)             </div> <div>             is the insulation thickness              is the area              is the density of the insulation              is the thermal capacity              is the thermal resistance           </div> </div>  <div style="display: flex; justify-content: space-between;"> <div> <math>m = </math> <input type="text" value="4,55"/> kg  <math>R_{ins} = </math> <input type="text" value="2,00"/> m*K/W             </div> <div>             is the mass of the inspected insulation              is the thermal resistance of the insulation sheet           </div> </div>			
<b>Calculation formulas:</b>  <div style="display: flex; justify-content: space-between;"> <div> <math>\theta_{gl} = \theta_g(0) + 345 \log_{10}(8 * t + 1)</math>   <math>\dot{Q}_i = (\theta_{gi} - \theta_{ci}) / (R_{ins} * \Delta t)</math>   <math>\theta_{ci} = (Q_{i-1} / (m * C_p)) + \theta_{ci-1}</math> </div> <div>             is the standard fire temperature               is the heat rate through the insulation               is the temperature between the insulation and the steel frame           </div> </div>			



		<b>Calculation</b>						
		Author: Andreas Limnell	Page: 2					
		Date: 29.4.2014						
Project: Master's thesis	Work no: #	Contents: Calculation of the temperature of main purlin of roof element	Location: Helsinki					
<b>Results</b>								
<p><b>Temperatures:</b></p> <div style="display: flex; justify-content: space-between;"> <div> <math>\theta_g(R) = </math> <table border="1" style="display: inline-table;"> <tr><td>1218,3</td></tr> </table> K </div> <div>is the standard fire temperature at t = R</div> </div> <div style="display: flex; justify-content: space-between;"> <div> <math>\theta_c(R) = </math> <table border="1" style="display: inline-table;"> <tr><td>591,2</td></tr> </table> K </div> <div>is the temperature behind the insulation at t = R</div> </div> <div style="display: flex; justify-content: space-between;"> <div> <math>\Delta\theta = </math> <table border="1" style="display: inline-table;"> <tr><td>627,1</td></tr> </table> K </div> <div>is the temperature difference at t = R</div> </div> <div style="display: flex; justify-content: space-between;"> <div> <math>\theta_g(R) = </math> <table border="1" style="display: inline-table;"> <tr><td>945,2</td></tr> </table> °C </div> <div>is the standard fire temperature at t = R</div> </div> <div style="display: flex; justify-content: space-between;"> <div> <math>\theta_c(R) = </math> <table border="1" style="display: inline-table;"> <tr><td>318,1</td></tr> </table> °C </div> <div>is the temperature behind the insulation at t = R</div> </div>				1218,3	591,2	627,1	945,2	318,1
1218,3								
591,2								
627,1								
945,2								
318,1								

## **APPENDIX 4**

**Manufacturing details & drawings for experimental test.**

